Title Page

Title:	Facies and Petrophysical Analysis and Modelling of Sandstone Layers: An Evaluation of the Komso Field
Project period:	01-02-11 to 06-06-11
Date of submission:	06-06-11
Place of study:	Esbjerg Institute of Technology Aalborg University Esbjerg
Supervisor(s):	Svetlana N. Rudyk
Group member(s):	Stephanie Otema Adu
Date:	06-06-11

(Stephanie Otema Adu)

Abstract

The Komso Field located in the West Siberian basin was examined. The purpose of the project included making zonation, in which reservoir rock was separated from non-reservoir rock. From the six wells that were analysed, multi-well correlation was done between them and next, geological analysis was performed in order to identify the oil and gas-bearing layers. Finally, facies analysis of these layers was done and 3-dimensional modelling carried out so as to model these characteristics obtained.

Interactive Petrophysics was first used to find these layers. In total, about 25 layers were found, most of which cut across each of the wells.

Facies analysis[1] is important in the investigation of wells and their log information. It revealed that the predominant facies alternated between transgressive and regressive bars between the sandstone units. There were some deviations occurring at certain points, resulting in mouth bars, breaking currents and deltas. *Petrel* was then used to obtain facies models as well as models of various petrophysical parameters. Correlation and modelling was done for layers cutting across the six wells. Calculations for clay volume, porosity, permeability and water saturation were performed.

The clay volume found was less than 0.2 over all the layers.

Porosity ranged from 5.9% to 51.6%. Seeing that porosity in general cannot exceed 33.3%, those layers that had higher values are possible overestimations. Permeability ranged between 1 and 15mD. Most of the layers, for each of the wells, had hydrocarbon saturations greater than 55%.

The values of the above-calculated parameters suggest that this field is oil-saturated.

Keywords: Reservoir areas, Facies analysis, Clay volume, Porosity, Permeability, Water saturation

Preface

This report has been put together as a final (tenth) semester project report, in partial fulfillment of the Chemical Engineering (Oil & Gas Technology) MSc. programme degree at the Aalborg University Esbjerg Institute of Technology. The report explores sandstone layers of wells of a field, as well as facies analysis. This report may have specific interest for researchers in the oil and gas industry, such as Schlumberger and Senergy. It may also be of interest for any companies and industries interested in facies analysis and modelling.

All references to literature and articles from journals are cited in the references section at the end of this project report – immediately before the Appendices section. Reference may also be made to any one of the five appendices found in the report, especially with respect to charts used for calculations. (For example: [See App. A])

A CD-ROM (attached) contains the entire report.

Acknowledgements

This report is dedicated to the Lord God Almighty who has not only guided me through this tenth semester project but throughout my whole two-year experience at Aalborg University. It is also dedicated to my family and friends for all their support.

Special thanks go to my supervisor Svetlana Rudyk who is constantly helpful. She always gives great advice, not only relating to the project but towards a future career in petrophysics and life in general.

Many thanks also go to Pawel Spirov & Ismaila Adetunji Jimoh for all their help with *Interactive Petrophysics* and *Petrel* and for always making time for me.

Thanks to Senergy for their provision of the software *Interactive Petrophysics*, and Schlumberger, for their provision of the software *Petrel*. These were both was key in analysing the wells and evaluating the well log information.

Tables & Figures

Tables

Figures

Contents

1 Introduction

1.1 Research Objective

This project report seeks to analyse various sandstone layers. A general overview of the various well logging tools available is given as well as an overview of the calculations required to determine various parameters. Facies modelling is done in order to see the distribution of sand and shale throughout each well and the original setting of the rock present, in which the hydrocarbons are found. Important properties of an oil and gas field, such as porosity and water saturation, were also determined.

1.2 Project Method

Six wells were examined and several Cretaceous sandstone units found for each, cutting across each well, determining trends between them. Log plot information was loaded for each using *Interactive Petrophysics* and modelling for several parameters was done in *Petrel*. Various calculations were also performed. Facies analysis helped to gain a deeper understanding into the original depositional formation of the rock strata. The overall investigation and interpretation in this research also helped to gain more knowledge of the Komso field.

2 Well Logging Methods

2.1 Mechanical Methods

2.1.1 Caliper Logging

Fig. 1 The Reeves 2-arm caliper tool[2]

The caliper tool and log is used to determine the shape and size (diameter) of a drilled hole. It measures variations in the borehole diameter.

There are two main types of caliper log, the independent caliper and the attached caliper. The first provides detailed information about the conditions of the drilled hole. It usually has small tips or contact and has a large contact pressure for actual hole diameter determination.

The second type of caliper is attached to other tools and provides information about the size of the hole for tool correcting data. It usually has a large contact and operates under low pressure for the diameter of the fluid column to be found.

As it is being drawn out, after being sent down the borehole, the movement of the caliper arms is converted into electrical signals by use of a potentiometer.

The caliper tool can have from 2 arms to up to several arms. The choice of which caliper tool to use depends on the nature of the borehole, as well as how critical the value must be. The shape of the borehole is not always necessarily perfectly circular. It may sometimes take on an elliptical shape. In this case, a 2-arm caliper tool would give an inaccurate value of the borehole diameter, as it would read according to the longer axis of the oval cross section. If a larger value than expected is obtained, this suggests that a caliper tool with more arms is required.

The caliper log, in addition to providing information on the diameter of the borehole can also give information on the lithology of the well (if used correctly). If there is a weak formation, the washouts can provide this data.

It can also give details of fractures, given that if a pair of the caliper arms locks into a fracture, the tool rotation ceases.[1]

2.2 Acoustic Logging

The acoustic or sonic log measures the travel time of an elastic wave through a formation. In addition, it can be used to derive the seismic velocity of elastic waves through this borehole formation. Mainly, it is used in the determination of the porosity (ϕ) of a formation by first obtaining seismic data.

The acoustic log has many other uses, including the determination of permeability in porous rocks and the identification of lithologies, compaction, over-pressures, source rocks and fractures. The tool works at a higher frequency than seismic waves, therefore one must be careful with the direct comparison and application of sonic log data with seismic data. It has both a transmitter and a receiver mounted on it when it is sent down the borehole. The task is to measure the time taken for either the compressional (P) wave – which can move through both solids and liquids – or the shear (S) wave – which can move only through solids – to travel from transmitter to receiver. The sound waves are generated in all directions by short pulses from the transmitter.

In order to determine the porosity, the interval transit time must be determined, which is the recording versus the depth of time taken for a sound wave to move 1 foot through the formation moving parallel to the borehole wall. It can also be defined as the slowness of the sound wave. The interval transit time is the reciprocal of the velocity of the sound wave.[2,3]

$\phi = (t - t_{ma})/(t_f - t_{ma})$ or $\phi = c[(t - t_{ma})/t]$

; where t is the reading on the acoustic log

t_{ma} is the transit time of the matrix material

t_f is the transit time of the saturating fluid

c is a constant with value approximately 0.67.[4]

2.3 Electrical Methods

The electrical log is used mainly to determine the water saturation (S_w) from a formation. From this, the STOIIP (Stock Tank Oil Initially In Place) can be determined. Since the S_w is derived from the resistivity of the formation water (R_w), it is extremely important to accurately determine R_w, to get a precise value of S_w in order to determine the amount of oil in place correctly.

It can also be used to provide information on the lithology, well correlation, and determination of the shale porosity as well as provide information on source rocks and recognition of hydrocarbon zones.[2]

2.3.1 SP (Spontaneous Potential) Logging

This is a tool used to measure naturally distributed charges. Electricity naturally exists within rock. Two electrodes are placed in the soil, which record the current flow.

The SP can be used to find permeable layers by distinguishing between porous, permeable reservoir rock and non-permeable shale and clay. It is also used for well bed correlation, identification of lithologies, as well as providing information on the shaliness of a formation. It can also be used to confirm the resistivity of drilling mud and formation water after it has been determined in the lab. This resistivity depends on temperature, which can eventually be used to determine the water saturation, S_w.[4,5]

The SP tool consists in general of two electrodes, one within the well and one at the surface of the well, producing a potential reading without the help of any artificially applied current flow. It is also referred to as a self-potential. The electrode within the well is usually made of metal. Ideally it would be made of copper in a copper(II)sulphate solution in a porous ceramic container. Seeing that these electrodes are hard to maintain, lead, bronze or stainless steel electrodes are usually used. Some sources of this spontaneous potential are redox chemical reactions and electrokinetic fluid flow. The main source is the transport of charged ionic species. This generates diffusion potentials – a diffusion of ions due to a concentration gradient. This is due to the fact that positive and negative charges are transported at different rates.

The shale baseline refers to the line in the SP log that can be taken as a static point for 100% shale content, that is, no sand present. It is possible, however, for shale baseline shifts to occur when there is a difference in salinity between formation waters that are separated by a shale bed that is not a perfect cationic membrane.[1,2]

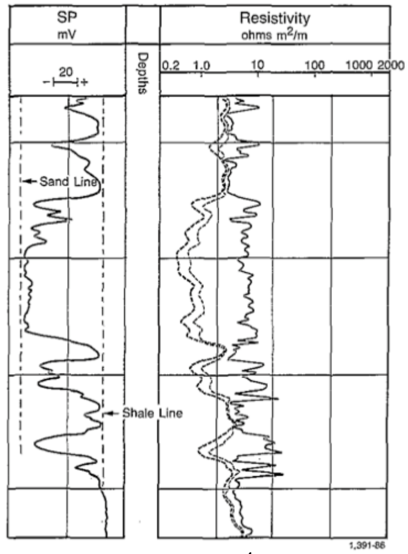

Fig. 2 An example of an SP log in a sand-shale series[4]

In a typical SP log, where the usual case is for the formation water to have a higher salinity than the mud filtrate, there is a deflection from the shale baseline to the left. This deflection indicates the presence of sand.[4]

In order for an SP current to exist:

- the fluid in the borehole must be conductive. This means the drilling mud used must be water-based.
- there must be a porous and permeable bed found between the low porosity, impermeable formation
- for the most part, there must be a difference in salinity between the formation fluid and the borehole fluid. The SP current may however arise due to difference in fluid pressure instead.[2]

There are two main sources of spontaneous potential (current):

2.3.1.1 Electrochemical Influence

Diffusion potential/liquid junction potential – This refers to the spontaneous potential found at the junction between the invaded and uninvaded zones and is an electromotive force. It arises due to the difference in salinity between the formation fluid and the borehole fluid, which in this case is the mud filtrate.

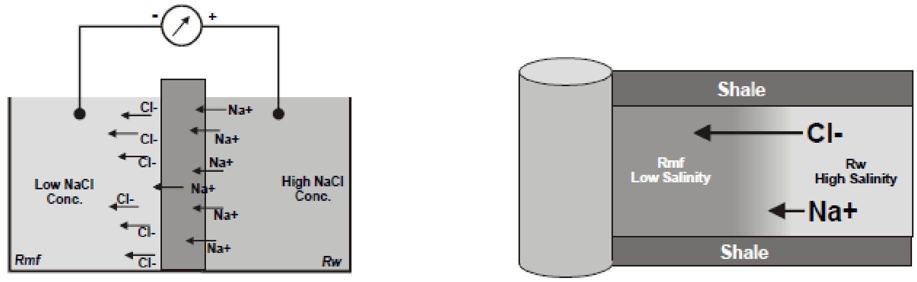

(a) (b)

Fig. 3 Diffusion potential in the lab (a) and in the borehole (b)[2]

Assuming NaCl to be the only source of salinity and the salinity of the formation fluid to be higher than that of the borehole fluid, there is a net movement of negative charge from the uninvaded to the invaded zone – diffusion. This is because the ions move from an area of higher salinity to a lower salinity area and also because the Cl^- ions are smaller and therefore more mobile than the Na^+ ions. This sets up an SP current, due to the charge imbalance, flowing from the invaded to the invaded zone.[2]

$E_d = -11.81*\log(R_1/R_2)$

; where E_d is the diffusion potential

R_1 is the resistivity of the less saline solution

R_2 is the resistivity of the more saline solution

Also, $E_c = -K*\log(a_w/a_{mf})$

; where E_c is the total electromotive force

K is a co-efficient that is proportional to the absolute temperature. Its value is 71 at 25°C [$K = 65 + 0.24T(^oC)$]

a is the chemical activity at formation temperature (of either the formation water or mud filtrate)

Shale/membrane potential – This is the SP found at the junction of the uninvaded and shale zones. Shale has a property of being anionically or electronegatively permselective. They retard the movement of anions – due to the presence of an electrical double layer. This leaves the shale preferentially positive, setting up a potential between the shale and uninvaded zones. This results in a current flow from the uninvaded zone of the formation to the shale zone, and eventually into the borehole.[2]

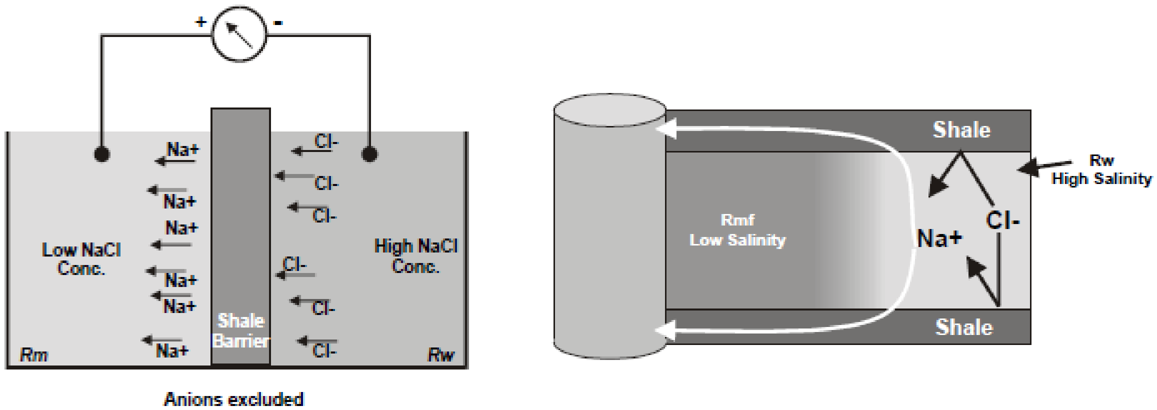

(a) (b)

Fig. 4 Membrane potential in the lab (a) and in the borehole (b)[2]

2.3.1.2 Electrokinetic Influence

Mudcake potential – This is the SP produced by the movement of charged ions through the mudcake and the invaded zones of a permeable formation. Since the mudcake is of low permeability, this is usually as far as the SP gets, hardly ever reaching the invaded zone.

Mudcake, like shale, also has the property of anionic permselectivity. There is therefore a net current flow from the borehole to the mudcake.

Shale wall potential – this arises from the flow of fluid from the borehole to the shale zone. It is usually a small value seeing that the shale is impermeable and fluid flow into it is highly limited.

The *Static spontaneous potential (SSP)* refers to the total voltage obtained from the diffusion of ions across the liquid and membrane junctions. This arises due to the fact that there is now mud filtrate in the well formation that was not there at the time the well was drilled. This value decreases as the contrast in resistivity between the formation water and the mud filtrate decreases. It also switches sign if the resistivity of formation water is found to be higher than the resistivity of the mud filtrate.[2]

The SSP opposite a permeable bed is found if the current is prevented from flowing, which may be due to the presence of strong insulators, such as insulating plugs.

SP current flows through the borehole, the invaded zone, the uninvaded zone and the surrounding shale, with the largest fraction of the current – and therefore the largest SP deflection – travelling through the borehole. Because of this, there is a very large potential drop, seeing that the borehole's cross-sectional area is relatively small as compared with the formation and its resistance would therefore be high.

The total potential drop in this case would therefore be the total electromotive force, the SP deflection ideally opposite a thick, clean formation. In this case there is a lower resistance and the SP would be very close to the actual SSP. Shaliness in the bed is ignored in this case, as well as other sources of potential. It is also assumed that the shale is a membrane that is perfectly cationic.[4,6]

Its value can be determined directly from the SP curve as the difference between the SP maxima opposite the permeable bed and the shale baseline. This can be done as long as the bed is porous, permeable, non-shaly, clean, thick, has saline formation water, drilling mud that is not too resistive and moderate invasion. If the beds meet all these requirements but are thin, corrections can be made for bed thickness using correction charts.

A clean, non-shaly bed is required in order to accurately obtain the resistivity of the formation water, R_w from SP.

In cases where different salts other than NaCl predominate or are found, it affects the value of the SSP. This needs to be taken into consideration. $CaCl_2$ and $MgCl_2$ are the usual salts that are found in addition to NaCl. The SSP is therefore:

$SSP = -K*\log [a_{Na} + (a_{Ca} + a_{Mg})^{1/2}]_w / [a_{Na} + (a_{Ca} + a_{Mg})^{1/2}]_{mf}$

The ionic activities of Na, Ca and Mg, knowing their concentrations, are found from a chart. It is important to find the respective *K* values where other salts predominate.

Several assumptions are made for SP including the ionic activity being inversely proportional to the resistivity. Another assumption is that the mud filtrate and formation water have properties of an ideal sodium chloride solution.

For conditions that do not conform to these assumptions, the equivalent resistivity and ionic activity are introduced. This would be for cases where the concentration of the NaCl solution is very high.

$R_{weq} = A/a_w$

; where $R_{weq} \equiv$ equivalent resistivity of formation water

$a_w \equiv$ activity of formation water

$A \equiv$ constant chosen so that $R_w = R_{weq}$ in dilute solutions

The static SP can then be determined using these equivalent resistivities:

$SSP = -K(T)\log(R_{mfeq}/R_{weq})$

2.3.2 *Resistivity, Induction Logging*

The resistivity of fluids within a well refers to the amount of electrical resistance the fluid has to the passage of current through it. It is said to be the reciprocal of conductivity and is measured as:

Resistivity = (Resistance * Area)/Length; R = (r*A)/L

Its unit is the ohm-m. (ohm-meter or Ω-m)

Sedimentary formations are capable of transmitting an electric current only by means of the interstitial and adsorbed water they contain, and if entirely dry would be non-conductive. The electrical resistivity of a fluid-saturated rock is its ability to impede the flow of electric current through that rock. Dry rocks exhibit infinite resistivity.

The resistivity log is extremely important in the characterisation and evaluation of an oil & gas field because it is the only reliable method for hydrocarbon detection.

The neutron log method can also be used, however, this method is based on a hydrogen index and the values for oil and water are very close. The value for gas is quite different though and hence the neutron method is useful for gas detection.

There are several different logs that constitute the resistivity log, each having their specific method of determining resistivity and their own corrections.[2]

2.3.2.1 Conventional Electrical Logs

The normal device has measuring electrodes far apart whereas the lateral device has its measuring electrodes close together.

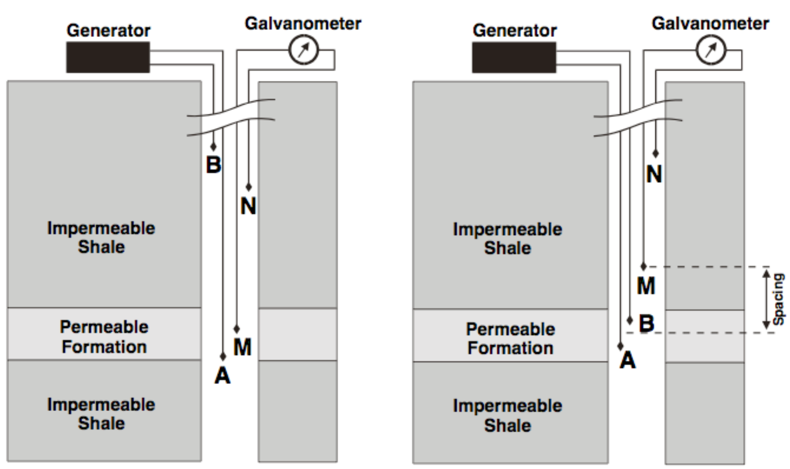

Fig. 5 The normal (left) and lateral (right) configurations of the electrical log[2]

2.3.2.2 Dual Laterologs

This is made up of two tools, one run in deep penetration and the other in shallow penetration.

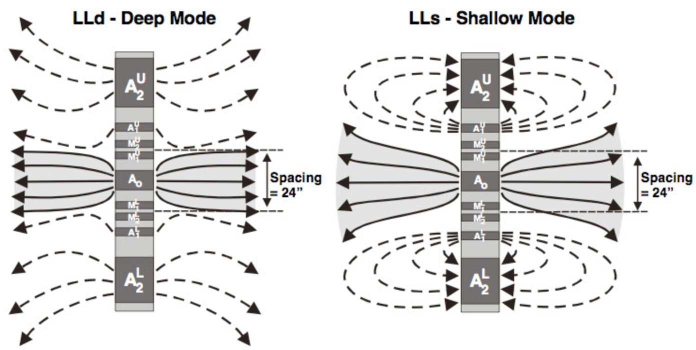

Fig. 6 The DLL electrode configuration in both the deep (LLd) and shallow (LLs) modes[2]

2.3.2.3 Induction Logs

These were initially made for oil-based drilling muds but can now be used in high salinity water-based or fresh water-based drilling muds.

The sonde is made up of a transmitter, a receiver and two wire coils. An alternating magnetic field around the sonde arises due to the high frequency alternating current applied to the transmitter. This induces a secondary current and consequently an alternating magnetic field in the formation, which in turn induces current in the receiver of the sonde. The signal is measured and is proportional to the conductivity of the formation. An induction log's peaks therefore always deflect in an opposite direction to the resistivity curves.

The induction log is usually coupled with the SP log in the same track of the log plot. This gives an idea of hydrocarbon presence in a layer. If their deflections are in the same direction, this is an indication of the presence of oil, whereas if their deflections are in opposite directions, this suggests the presence of water.

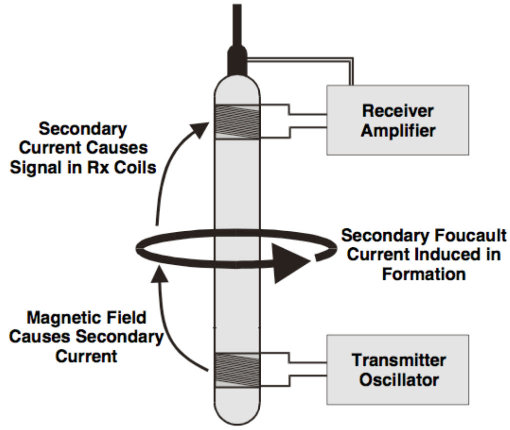

Fig. 7 The mode of operation of induction tools[2]

2.3.2.4 Microresistivity Devices

These have similar electrode setups as the modern resistivity logs, but the electrode spacings are much smaller – only a few inches. The penetration of these tools is therefore only to a small degree and usually does not even go through the mudcake. The sonde of these devices is pressed against the borehole wall.

Microlog – this additionally provides extra caliper readings, known as the microcaliper log.

Microlaterolog – this is a micro scale version of the laterolog.

Proximity log – this is focused only a short distance from the formation. It is larger than the microlaterolog and is an improvement of it, dealing with issues of mudcakes thicker than 3/8 of an inch. It therefore has minimal influence from the mudcake or, in ideal cases, the undisturbed zone. It measures the resistivity of the flushed zone, R_{xo}.

Microspherically focused log – this is usually run together with the dual laterolog. It also measures R_{xo}. The resistivity is considered to be most accurately calculated when the current flows spherically around the current-emitting electrode.[2,4]

2.3.2.5 Proximity Logs

The proximity log (referred to as microsondes here) is used together with the shallow microlateral log to determine the resistivity of the flushed zone [area completely taken over by drilling mud or mud filtrate]. This is why only the shallow microlateral log is considered, since the deep microlateral log has not yet been affected by the drilling mud to affect this measurement.

This determination can be done in several combinations:

Microlateral microsonde vs. Micronormal microsonde [Figure A2, App. A]

From the logging plot, the apparent resistivity, R_{app}, for each microsonde is found.

This is divided by the resistivity of the mudcake, R_{mc}.

The resistivity of the drilling mud, R_m, is typically given from a measurement done at the well site. The resistivity of the mud filtrate, R_{mf}, and the resistivity of the mudcake, R_{mc}, can be found from a chart [Figure A1, App. A]. In general, the relationship $R_{mf} = 0.8R_m$ can be used to determine the resistivity of the mud filtrate.

The R_{app}/R_{mc} values for both microsondes are read off on the microlateral versus micronormal graph.

It is ensured that this intersection matches with the height of the intermediate layer, *l* (in mm) '*l*' is measured as the distance between the borehole wall and the well logging tool. It can sometimes be referred to as the thickness of the mudcake, h_{mc}.

$l = [d_{bit} - d_{caliper}]/2$

The corresponding value for R_{xo}/R_{mc}, is read off the graph and the flushed zone resistivity, R_{xo}, is determined.

Microlateral [shallow] [Figure A3, App. A]

From the logging plot, the apparent resistivity, R_{app}, is determined. It must be noted that the plot is in logarithmic scale and must be measured accordingly.

The apparent resistivity is divided by the resistivity of the mudcake, R_{mc}

The intersection of the R_{app}/R_{mc} value and the height of the intermediate layer, *l*, is found.

From this intersection, the corresponding value for R_{xo}/R_{mc} is determined and the flushed zone resistivity, R_{xo}, calculated.

Microsondes vs. Microlateral [shallow] [Figure A4, App. A]

From the logging plot, the apparent resistivity, R_{app}, for each microsonde is found as well as R_{app} for the shallow microlateral log.

The values for R_{app}/R_{mc} are found for each.

The intersection of the R_{app}/R_{mc} value for each microsonde (separately) with the R_{app}/R_{mc} value for the shallow microlateral is found.

This intersection for each is matched with the height of the intermediate later, *l*, the corresponding R_{xo}/R_{mc} value found and the flushed zone resistivity, R_{xo}, determined.

There are, however, some limitations to applying this method:

The height of the intermediate layer, *l*, must be less than 15mm (l<15mm) in order for the resistivity (of the flushed zone) read to be accurate. If *l*>15mm, then the dependence is on resistivity ratios.[7]

Table 1 Dependence of intermediate layer on resistivity ratios

l, mm	10	15	20	30
R_{xo}/R_e	1 – 1500	1 – 250	1 – 100	1 – 35

; where R_e is the resistivity of the intermediate layer area.

The thickness of the mudcake should be less than 15mm. If the thickness exceeds this, the intermediate layer would not be able to be used for quantitative interpretation.

High distortions of the resistivity values occur when the resistivity of the drilling mud is low. Distortions occur when R_m < 0.50ohm-m.

2.3.2.6 Resistivity of formation water

Formation water, also known as interstitial water, is that which occurs naturally within the rock pores. It is found in the undisturbed zones surrounding the wellbore. Drilling mud and other fluids injected or introduced into the borehole during production do not constitute formation water.

Its resistivity, as well as other properties, can be used for interpretations of measurements made within the well and on the surface.[4,6]

The resistivity of formation water, R_w, is most commonly calculated from the SP log:

The standard SP response equation can be expressed as:

$$SSP = -K_c * \log[R_{mfeq}/R_{weq}] \qquad (1)$$

Re-arranging Equation 1 and solving for R_{weq} ;

$$R_{weq}=[R_{mfeq}/(_{10}(SSP/-K_c))]$$

; where

SSP	is Static SP (mV) measured from a shale baseline,
$\mathbf{R_{mfeq}}$	is equivalent resistivity of mud filtrate at formation temperature,
$\mathbf{R_{weq}}$	is equivalent resistivity of formation water,
$K_c = 61 + .123*T(^oF)$	or,
$K_c = 65 + .24*T(^oC)$	

Analysis Procedure

The SP deflection from the shale baseline, preferably from a thick, clean water sand, is measured. If the mud filtrate resistivity (R_{mf}) at 75^{o}F is higher than 0.1, R_{mf} is corrected to the formation temperature using:

R_{mf} = [R_{mf} at surface temp * (Surface temp + 6.77)]/ (Bottom hole temp + 6.77)

The Schlumberger General Chart can also be used with $R_{mfeq} = 0.85R_{mf}$.

If R_{mf} at 75°F is lower than 0.1, R_{mf} is corrected to formation temperature and a chart, such as Schlumberger's Sp-2, used.

Equation (1) is used to calculate $R_{weq.}$

Formation water resistivity (R_w) is estimated using Chart SP-2.

Water salinity is estimated using a Schlumberger general chart [see Fig. 27] [10]

R_w can also be obtained from resistivity ratios:[9]

$$F \equiv \frac{R_o}{R_w} \qquad (1)$$

$$F \equiv \frac{R_{xo}}{R_{mf}} \qquad (2)$$

F	is Formation Factor
R_w	is the resistivity of the formation water
R_o	is the resistivity of a reservoir rock fully saturated with brine,
R_{mf}	is the resistivity of the mud filtrate
R_{xo}	is the resistivity of the filtrate saturated reservoir

Combining and rearranging equations (1) and (2), R_w can be solved for:

$$\frac{R_o}{R_w} = \frac{R_{xo}}{R_{mf}}$$

$$R_w = \frac{R_o}{R_{xo}} \bullet R_{mf}$$

Both **R_o** and **R_{xo}** measurements must be corrected for borehole environmental effects using appropriate service company charts. **R_{mf}** is corrected to formation temperature using;

$$R_2 = R_1 \bullet \frac{(T_1 + 6.77)}{(T_2 + 6.77)}$$ for Fahrenheit, or,

$$R_2 = R_1 \bullet \frac{(T_1 + 21.5)}{(T_2 + 21.5)}$$ for Celsius.

T_1	is the mud filtrate surface temperature read from the log header,
R_1	is the measured mud filtrate resistivity from the log header,

T_2	is formation temperature,
R_2	is mud filtrate resistivity at formation temperature.

2.3.2.7 Resistivity of drilling mud

Also referred to as drilling fluid, drilling mud refers to the fluid that is used in hydrocarbon drilling operations. These drilling muds can be water-, oil-, gaseous-, or synthetic-based. They typically contain large amounts of suspended solids as well as emulsified oils and water. It is injected into a drilled borehole's injection well with the aim of displacing hydrocarbons found in porous space towards the production wells. R_m, as mentioned above, is usually obtained from measurements done at the well site.[6]

2.3.2.8 Resistivity of mud cakes

Once drilling fluid has been injected into the injection wells of a drilled borehole, it forces its way, under pressure, through the permeable parts of the reservoir. This leaves behind a residue, which is deposited on the borehole wall and is known as the mudcake. The liquid that passes through the permeable area is known as the mud filtrate. Mudcake properties such as its thickness, toughness, slickness and permeability are important because the mudcake that forms on permeable zones in the wellbore can cause a choked pipe amongst other drilling problems. Reduced oil and gas production can result from reservoir damage when a poor filter cake allows deep filtrate invasion. A certain degree of cake buildup is desirable to isolate formations from drilling fluids. In open-hole completions in high-angle or horizontal holes, the formation of an external filter cake is preferable to a cake that forms partly inside the formation. The latter has a higher potential for formation damage.

The resistivity of the mudcake, R_{mc} is found from R_m and the formation temperature.[6] [(10,11,12,13,14)] [see Figure A 1, App. A]

2.3.2.9 Resistivity Profile

This is based on drilling mud that has a fresh water base and is formed from the flushed zone through the invaded zone to the uninvaded zone (from shallow to deep).

Flushed zone: this is the shallow part of the well. This zone has been completely overcome by drilling mud filtrate. It is made up of this drilling mud filtrate and rock.

Invaded zone: This is a type of transition zone and is made up of a mixture of rock, drilling mud as well as oil, gas or water.

Uninvaded zone: as the name suggests, this is the zone where no drilling mud has yet infiltrated. This zone may be made up of a mixture of rock, oil, gas and water in various combinations. This is the deep part of the well.

Measurements are usually done for just the shallow and deep parts of the well. These would give more accurate values for resistivity than the invaded zone, since it is much harder to determine the amount of drilling mud in this zone.

Different resistivity profiles are obtained for zones primarily containing oil and those containing water.

For oil:

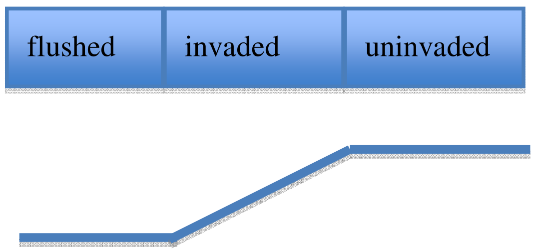

Drilling mud has a higher conductivity than oil, implying that it has a lower resistivity. Therefore, in the flushed zone, where only drilling mud filtrate is found, there would be a low resistivity. In the invaded zone, where there is a decrease in the amount of mud filtrate and increased amounts of oil, the resistivity gradually increases. In the uninvaded zone, where no drilling mud is found, there is only oil and therefore high values for the resistivity. This is shown in the resistivity profile above.

For water:

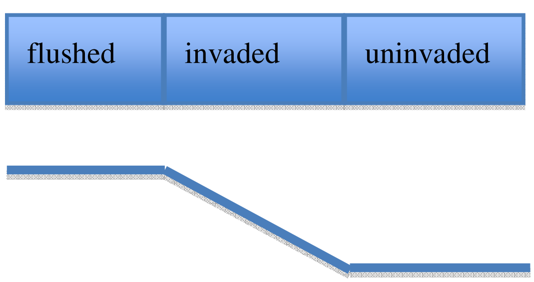

Drilling mud has a lower conductivity than water, implying that it has a higher resistivity. In the flushed zone, there is high resistivity. In the invaded zone, where there is a decrease in the amount of mud filtrate and increased amounts of water, the resistivity gradually decreases. In the uninvaded zone, with no drilling mud and only water, there are low values for the resistivity, as seen in the resistivity profile above.

The Archie equations are of extreme importance for the resistivity log. They provide a relationship between the resistivity of the formation and the resistivity of the fluids saturating the formation.

Conductivity and resistivity are inversely proportional:

C(mS/m) = 1000/R(ohm–m)

Reservoir rocks can be made up of the following with their respective resistivity.

Table 2 Resistivities of various components of reservoir rock[2]

Matrix material	High resistivity
Oil	High resistivity
Gas	High resistivity
Formation water	Low resistivity
Water-based mud filtrate	Low resistivity
Oil-based mud filtrate	High resistivity

In the *uninvaded zone* of a formation, the resistivity of the formation depends on the amounts and resistivities of the formation fluids. The rock in this formation comprises oil, gas and formation water.

The resistivity of a formation in the uninvaded zone depends on the porosity, the resistivity of the formation water and the water saturation. It is known as the true resistivity and can only be calculated using deeply penetrating electrical logging tools.

The *invaded zone* has been (partially) overcome by drilling fluid. The resistivity of the formation in this zone depends on the porosity, the saturation and resistivity of the mud filtrate and the saturation and resistivity of the formation water if present.

The bulk resistivity of rock, R_o, is directly proportional to the fluid resistivity, R_w, when the rock is fully saturated with this aqueous fluid.

The constant of proportionality here is the formation factor and arises due to the effect of the presence of the rock matrix.

The formation factor, F, is 1 where there is no rock matrix and is greater than 1 in porous media such as rock.

$R_o = F*R_w$

Relating the formation factor to the porosity, it is found that:

$F = \phi^{-m}$; which is Archie's first law.

Substituting the second equation into the first:

$R_o = R_w\phi^{-m}$

; where *m* is the cementation factor and describes the increase in resistivity due to the presence of insulating mineral grains (rock) that force the current to take a winding path through the conducting fluid. This value usually ranges between 1 and 3.

If however, there is only partial water saturation of the rock, then the bulk resistivity of the rock, R_t, partially saturated with aqueous fluid of resistivity R_w, is directly proportional to the resistivity of the rock fully saturated with the same fluid. This partial water saturation gives:

$R_t = I*R_o$

; where I is the resistivity index and arises due to the effect of partial desaturation of the rock. Fully saturated rock has I=1 and rock that is full of dry air has I approaching infinity (∞).

Relating the resistivity index to the fractional water saturation of the rock:

$I = S_w^{-n}$

Substituting the second equation into the first:

$R_t = R_{o*}S_w^{-n}$

; where *n* is the saturation exponent and ranges usually between 1.8 and 2. This value is determined from lab experiments on core samples.

Combining both laws and rearranging for S_w determination:

$S_w = n[(R_w\phi^{-m} /R_t)^{1/2}] = n[(R_wF/R_t)^{1/2}] = n[(R_o/R_t)^{1/2}]$

The saturation of the mud filtrate, $S_{xo} = n[(R_{xo,mf}/R_{xo,or})^{1/2}]$;

; where $R_{xo,mf}$ is the resistivity of the flushed zone that is 100% filled with mud filtrate

$R_{xo,or}$ is the resistivity of the flushed zone containing residual oil

The saturation of the mobile oil is therefore found to be $S_{xo} – S_w$.

The volume of the mobile oil per unit volume of the rock is $\phi(S_{xo} – S_w)$.

2.4 Radioactive Methods

The radioactivity log, also known as the nuclear or radiation log records the natural or induced radioactive properties of wellbore formations. It is typically made up of the gamma ray and neutron logs. Below, the density log is also discussed. These logs help in the determination of the type of rock formation and the nature of the fluid found in these rocks.[6]

All atoms consist of a nucleus, containing a certain number of uncharged neutrons and a fixed number of positively charged protons. Some atoms have varying neutron numbers, which leads to the existence of different isotopes of atoms.

Surrounding the nucleus are negatively charged electrons. There are the same number of electrons and protons in a neutral atom.

If an isotope is considered unstable, with high energy, there are several ways it can release this energy to become stable. One such method is through the emission of gamma rays, which have no mass and no charge, a process of spontaneous decay.

The gamma ray log measures the natural radiation from a formation whereas the neutron and density logs measure the radiation generated by the particular tool used.[2]

2.4.1 Natural Gamma Ray Logging

Gamma ray logging can be divided into total and spectral gamma ray logs. The total gamma ray log measures the total natural radiation from a formation with the use of a gamma ray detector. Its use is mainly for the determination of the lithology of the formation, shale content and depth matching. The spectral gamma ray log measures the natural radiation from a formation separated into its contribution from each gamma-emitting source. It is also used in the determination of the lithology as well as in uncertainty detection and inter-well correlation.

The gamma ray penetrations are the highest of all radiations, with the exception of neutrons. The most important isotopes that involve gamma ray emission can be found in gamma ray emitting sources. These are the potassium (K) isotope, the Thorium (Th) series isotopes and the Uranium-Radium (U-Ra) series isotopes.

Potassium gives a distinct peak at 1.46MeV and has the highest radioactivity recording, followed by shales.

Shale is the lithology that most commonly emits gamma rays. It is made up of igneous rock, containing feldspars and micas, which are gamma ray emitting sources.[2]

Table 3 Gamma radiation from common minerals and lithologies[2]

Mineral or Lithology	Composition	Gamma Radiation (API Units)
Pure Mineral		
Calcite	$CaCO_3$	0
Dolomite	$CaMg(CO_3)_2$	0
Quartz	SiO_2	0
Lithology		
Limestone	-	5-10
Dolomite	-	10-20
Sandstone	-	10-30
Shale	-	80-140
Evaporites		
Halite	$NaCl$	0
Anhydrite	$CaSO_4$	0
Gypsum	$CaSO_4(H_2O)_2$	0
Sylvite	KCl	500
Carnalite	$KCl\,MgCl_2(H_20)_6$	220
Langbeinite	$K_2SO_4(MgSO_4)_2$	290
Polyhalite	$K_2SO_4MgSO_4(CaSO_4)_2(H_2O)_2$	200
Kainite	$MgSO_4KCl(H_2O)_3$	245
Others		
Sulphur	S	0
Lignite	$CH_{0.849}\,N_{0.015}\,O_{0.221}$	0
Anthracite	$CH_{0.358}\,N_{0.009}\,O_{0.022}$	0
Micas	-	200-350

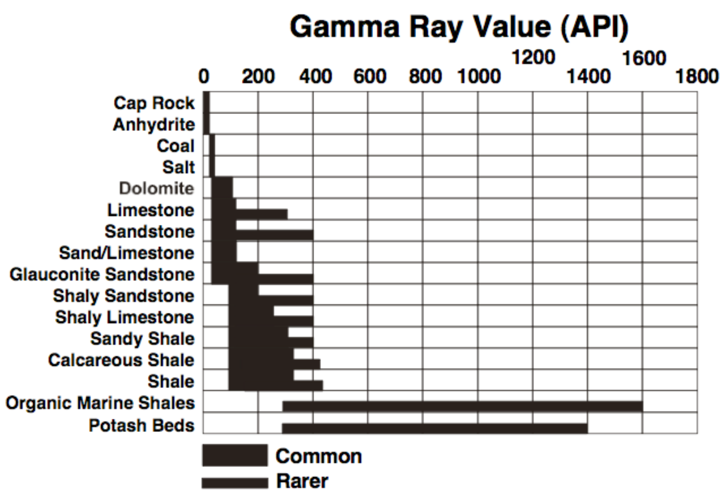

Fig. 8 Gamma ray values from common lithologies[2]

The gamma rays that are emitted can undergo different processes depending upon the amount of energy they have.

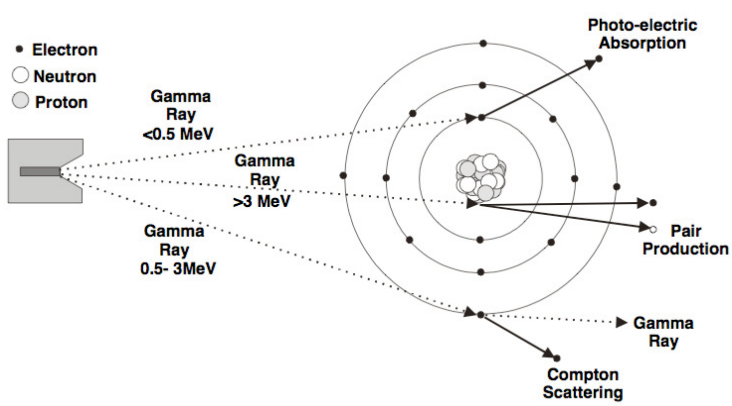

Fig. 9 Processes of gamma ray scattering and absorption[2]

From Fig. 9 it can be seen that:

- If the amount of energy exceeds 3MeV, the gamma rays collide with the nucleus of the atom of the material through which they are passing, resulting in pair production – the conversion of the gamma rays to an electron and a positron.
- If the amount of energy lies between 0.5MeV and 3MeV, the gamma rays collide with the atom of the material through which they are passing and eject an electron from the atom. The gamma rays, in turn, lose energy. This is known as Compton scattering.
- If the amount of energy is less than 0.5MeV, the gamma rays collide with the atom of the material through which they are passing and are absorbed. The energy from the gamma rays is then used to eject an electron or promote it to a higher energy level. This is known as photoelectric absorption.

Therefore, step 2 occurs until the energy is low enough for step 3 to occur.

The density of the material through which the gamma ray is traveling – whether the formation, the fluids, the mudcake or the drilling mud – affects the count rate. The higher the density, the more attenuation will occur and the lower the signal will be, and vice versa. This is sorted by the borehole correction.

The GR log is particularly useful for defining shale beds when the SP is distorted (in very resistive formations), when the SP is featureless (in freshwater-bearing formations or in salty mud; i.e., when $R_{mf} \approx R_w$), or when the SP cannot be recorded (in nonconductive mud, empty or air-drilled holes or cased holes). The bed boundary is picked at a point midway between the maximum and minimum deflection of the anomaly.[4]

2.4.2 Neutron Logging

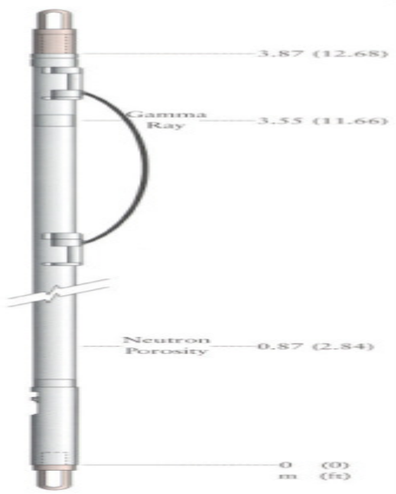

Fig. 10 The neutron logging tool[2]

The neutron log depends mainly on the number of hydrogen atoms in a formation.

It can be used in the determination of the porosity of a formation and in the identification of the lithology of a formation.

In the determination of porosity, there are several effects to be aware of:

The Hydrocarbon effect – The hydrogen index of oil and fresh water are relatively equal. However, the hydrogen index of hydrocarbon gas is much lower than that of fresh water. This is due to the low density of the gas. This therefore gives an underestimation of the porosity.

The Chloride effect – Chlorine is a very good absorber of (thermal) neutrons. They may give an overestimation of the porosity if chlorine is found in the mud filtrate or the formation fluid.

The Shale effect – The bound water molecules found on the surface of clays in shale increase a formation’s hydrogen index. This is because, even for low porosity shale, these bound waters cause an increase the porosity.

The main zone of investigation for the neutron log tool is the flushed zone. It therefore mainly deals with the mud filtrate and any residual hydrocarbons and/or formation water.

There are three main processes involved in neutron logging:

Neutron Emission – High speed and high-energy (about 4.5MeV) neutrons are made to bombard the formation. The source of these neutrons is usually a mixture of beryllium-9 and an alpha radiation source (Radium, Plutonium or Americium)

$$^{9}_{4}Be + ^{4}_{2}He \Rightarrow ^{12}_{6}C + ^{1}_{0}n + \gamma$$

The equation above shows that fast neutron Carbon-12 and gamma rays are produced.

Neutron Scattering – Elastic scattering occurs due to the collision of these fast neutrons with the nucleus of the atom in the formation. Since the size of the neutron and the hydrogen atom are similar, the most effective scattering (resulting in a loss of energy of the neutron) occurs between these two, and less efficiently for larger atoms. The high-energy neutrons lose energy and become low energy neutrons or high-energy gamma rays.

Neutron Absorption – Eventually, after several collisions, the lowest energy thermal neutrons are absorbed by the nucleus of the atom of the formation. Hydrogen and chlorine are two elements with relatively high neutron absorbing characteristics. The effectiveness of neutron absorption depends on the element involved.

The partial concentration of hydrogen per unit mass can be defined as:

(mass of hydrogen atoms in the material) / (mass of all elements in the material)

Hence, the partial conc. of hydrogen per unit vol = (partial conc./unit mass) * density

The Hydrogen Index can be defined as the partial concentration of hydrogen per unit volume relative to water.

When the Hydrogen index = 1, it implies that the porosity = 1

Types of Neutron Logging Tool

Gamma Ray/Neutron Tool

This has a neutron source and a single detector. It can be used in open or closed holes and the tool is centered within the borehole. It is sensitive to borehole conditions such as borehole quality, temperature, drilling mud type and mudcake thickness. It is also sensitive to thermal neutrons and therefore also sensitive to hydrogen and chlorine. Correction curves therefore exist to account for these effects.

Sidewall Neutron Porosity Tool

This also has a neutron source and a single detector. It can, however, only be used in open holes and the tool is pressed against the borehole wall. It is not affected by drilling mud. Neither is it affected by chlorine or hydrogen since it is only sensitive to epithermal neutrons. These have higher energy and are not yet at the stage for absorption by elements.

Compensated Neutron Log

This is made up of a neutron source and two detectors and is pressed up against the borehole wall. It is sensitive to thermal neutrons and therefore also chlorine and hydrogen. The larger detector is found close to the source to ensure an accurate count rate. The two detectors help to compensate for the chloride effect – from chloride-rich mudcake and mud filtrate.

The neutron log, in responding to the presence of these hydrogen atoms, deals mainly with liquid-filled pore space of the formation, where the response is generally a measure of the porosity, ϕ.

2.4.3 Density Logging

The formation density log measures the bulk density of a formation. This is done in order to determine the total porosity. It is also used to detect gas-bearing formations and evaporates.

The density logging tool is made up of:

- a radioactive source of either Cs-137 or Co-60 which releases gamma rays with energy ranging from 0.2-2MeV.
- a short range detector which is found closer to the source
- a long range detector

There are two detectors to help correct for the effects of the mudcake.

The gamma rays released from the source undergo Compton scattering in which the energy of the rays reduces in a stepwise fashion and the rays are scattered in all directions. The collisions occurring depend on the number of electrons in the formation.

Once the energy is low enough, ie. below 0.5MeV, photoelectric absorption occurs upon collision with atomic electrons.

A high bulk density means a high number density of electrons, which indicates a high attenuation of the gamma rays and a low count rate of these gamma rays recorded by the detectors. The vice versa conditions also apply.

A high-density mud affects the readings of the detector. This is because as stated before high density leads to high rates of absorption of the gamma rays. These effects are accounted for by the spine and rib corrections.

There are many uses of the density log in addition to the main ones mentioned above. It can also be used to identify the lithology and detect fractures as well as shale compaction, age and unconformities in the formation. It is used in the identification of minerals in evaporite deposits, for gas detection as well as hydrocarbon density determination.[2]

The density tool, in responding to the electron density [number of electrons per cubic centimetre of formation] of the particular material in the formation, can determine the porosity from the bulk density:

$\phi = (\rho_{ma} - \rho_b)/ (\rho_{ma} - \rho_f)$

; where ρ_{ma} is the density of the formation or rock matrix

ρ_b is the bulk density

ρ_f is the density of the pore fluid[1,4]

Table 4 Common open-hole tools and their uses[2]

Tool	Physical Measurement	Use	Comments
Logging conditions			
Temperature (BHT)	Temperature	Borehole temperature for resistivity calculations.	Corrected with Horner plot
Pressure (PRESS)	Fluid pressure	Fluid pressure for formation volume factor calculations.	Incorporated in RFT
Caliper (CAL)	Borehole diameter	Data quality, in situ stress tensor, lithology and permeability indicator	Available in 2, 4, or multi-arm versions.
Lithology			
Gamma Ray (GR)	Natural radioactivity of the formation.	Shale indicator and depth matching	Can read through casing.
Spontaneous Potential (SP)	Sand/shale interface potential.	Permeable beds Resistivity of formation water	Does not work in conductive muds, or offshore.
Porosity			
Sonic (BHC, LSS)	Velocity of an elastic wave in the formation.	Effective (connected) porosity	Compaction, gas and vugs, calibration of seismic data.
Density (FDC, LDT)	Bulk density of the formation.	Total porosity	Used to calculate synthetic seismograms.
Neutron (SNP, CNL)	Hydrogen concentration in the formation.	Total porosity (shale increases measured porosity, gas reduces measured porosity)	Can read through casing.
Resistivity			
Simple electric log (SN, LN, Lat)	Resistivity of flushed, shallow and deep zones respectively.	Used in water saturation calculations.	Now obsolete, not focussed, can't be used in oil based muds, prone to invasion.
Induction Logs (IES, ISF, DIL, DISF, ILm, ILd)	Conductivity of the formation.	Conductivity and resistivity in oil based muds, and hence calculation of water saturation.	Focussed devices. Use in oil based and fresh water muds. Range of depths of investigation. (Vertical resolution 5-10 ft.)
Laterologs (LL3, LL7, DLL, LLs, LLd)	Resistivity of the formation.	Resistivity in water based muds, and hence calculation of water saturation.	Focussed devices. Use in salt water based muds. Range of depths of investigation. (Vertical resolution 2-4 ft.)
Microlog (ML)	Resistivity of mudcake and flushed zone.	Indicator of permeability. Detector of thin beds.	(vertical resolution about 1 ft.)
Micro-laterolog (MLL)	Resistivity of flushed zone.	Measures R_{XO}	Not good with thick mudcakes.
Proximity Log (PL)	Resistivity of flushed zone.	Measures R_{XO}	Not good if invasion is small.
Micro-spherically focussed log (MSFL)	Resistivity of flushed zone.	Measures R_{XO}	Part of DLL-R_{XO} tool.
Imaging Logs There is a range of imaging logs based upon sonic, visual, electrical and NMR measurements that are beyond the scope of this course.			

3 Stratigraphy & Sedimentology

3.1 Stratigraphy

Stratigraphy refers to the study of strata or layers. It deals with the analysis of rock successions over time and through changing environments.

There are three main types of rocks – sedimentary, igneous and metamorphic rocks. Seeing that sedimentary rocks follow a more predictable pattern, stratigraphy is usually associated with this type of rock. Deposition of igneous and metamorphic rock is less predictable and hence is hardly used.

This is of much use in the oil and natural gas or petroleum industry seeing that the majority of oil and gas reserves for the most part occur in stratified sedimentary rocks. It is therefore advantageous to know which type of rocks to focus on.[15]

Stratigraphic signatures and stratal patterns in sedimentary rock record are a result of the interaction between tectonic activity, eustasy and climate.

The effect of tectonics and eustasy is that they determine the available space that will be filled with sediment. The three together control the sediment supply and determine actually how much of this available space will be filled.[16]

3.1.1 *Absolute & Relative Dating*

Absolute Dating is also referred to as chronometric or calendar dating. This form of dating seeks to determine an approximate computed age of rock strata: Radiometric Dating [Radiocarbon dating, Potassium-Argon dating], Thermoluminescence dating. Chronostratigraphy, defined below, deals with the absolute dating of rock strata.

Relative Dating, also known as internal industry, does not find an approximate age, but determines the relative order and sequence in which certain events took place. Biostratigraphy, described more below, stems from this. The Law of Superposition, as well as the Law of Faunal Succession, also explained below, was derived from, and sums up, the theory of relative dating.

Different types of rocks repeat themselves over time. It is, therefore, usually very hard to determine the exact age of rocks. Analysis of the fossils that make up these rocks, however, can help with this.

There are many types of stratigraphy studied today. The more classical forms of stratigraphy are:

3.1.2 Lithostratigraphy

This refers to the study and correlation of strata to determine information about the Earth's history. The information is based on their lithology, or the nature of the well log response, mineral content, grain size, texture and color of rocks.[6] It is the characterisation of rock strata by the kind and/or arrangement of their mineralogical constituents. Therefore, it is the physical characteristics of the layered rock strata that are studied. Similar lithologies are usually diachronous and therefore have no time significance. Some uses of lithostratigraphy, however, include placing specific geological units in a particular geologic framework, establishing a stratigraphic relationship with geological units above and below and aiding in the correlation between other lithologic units.[15]

3.1.3 Chronostratigraphy

This can be referred to as the characterisation of rock strata based on their temporal relations. It seeks to find the ages of rocks based on when they were formed. Chronostratigraphic units are bodies of rock that were formed within a specific geological period of time. It is the basis for the time scale of the Phanerozoic eon. Chronostratigraphic units are very closely linked to geochronological units, though the latter units represent the actual interval of time. Chronostratigraphic units measure how much sediment was deposited in that time and cannot be defined as actual time. The table below shows the geochronological and chronostratigraphic unit equivalents.[15,17]

Table 5 Chronostratigraphic and geochronologic unit equivalents with an example[15]

Chronostratigraphic Units	Geochronologic Units	Example
Eonathem	Eon	Phanerozoic
Erathem	Era	Mesozoic
System	Period	Cretaceous
Series	Epoch	Upper Cretaceous
Stage	Age	Maastrichtian
Chronozone	Chron	*Belemnella occidentalis* Zone

3.1.4 Biostratigraphy

This deals with the study of the temporal and spatial distribution of fossil organisms. The correlation and dating of rocks is usually found through this method, and may be done on a global scale, between basins, within a basin or within an oil field.

Therefore, once two particular types of rock made up of the same fossils, regardless of their location at the present time and though sedimentary rock changes over time, they can be thought to have been deposited or formed at the same time. There are many different types of fossil assemblages that are used in this type of stratigraphy. Some of them include ammonites, index fossils and trilobites and some microfossils such as chitinozoans, foraminiferans, pollen and spores.[18]

3.1.5 Magnetostratigraphy

Magnetostratigraphy gives relatively precise chronology in strata independent of fossil content. This type of stratigraphy correlates magnetic reversals found in a stratigraphic column with reversal ages derived from sea-floor magnetihc stripes. Magnetostratigraphic geochronometry works best in fine-grained neogene, siliciclastic strata, but it can be used effectively in rocks as old as Middle Jurassic. In rocks that predate the oldest modern sea-floor, magnetic reversal patterns can still be used as correlative tools.

Natural Remanent Magnetisation (NRM) is the basis of magnetostratigraphy. It represents a rock or sediment's permanent magnetism. It can also preserve a record of the Earth's field and the tectonic movement of the rock or sediment for millions of years.[19]

3.1.6 Seismic Stratigraphy

This process seeks to utilise seismic data in the interpretation of stratigraphic information. Though there may be some exceptions, it is generally accepted that within the resolution of the seismic method, the seismic reflections follow gross bedding, and can be considered as timelines. These timelines represent time surfaces in three-dimensional space and can separate and distinguish older rocks from younger ones. Seismic stratigraphy helps give chronostratigraphic as well as lithostratigraphic information from the reflection characteristics at impedance contrasts.[16]

Where there is a difference in density or velocity between physical structures, seismic reflections are generated. They follow stratal surfaces or bedding planes, and not gross lithostratigraphic boundaries, and these stratal surfaces separate the various processes of sedimentation. Together with unconformities, they are the two interfaces that are generated at the time of deposition in a sedimentary section. Changes in the deposition that may have occurred in a basin, and subsequent geological subdivision into stratal units or depositional sequences, can be found through this method, together with the law of superposition. This is done through the recognition of unconformity surfaces. Unconformities, though they do not directly provide chronostratigraphic information, always have younger rock or strata above and older rock below. There are several other useful features of seismic stratigraphy. The seismic reflections are helpful in paleogeology reconstruction, and from that, also paleogeography and paleoenvironmental reconstruction, which seeks to reconstruct the initial and original conditions of the environment. Once depositional units have been determined, an estimation of the reservoir rock content can be done, as well as facies predictions made. It is also very useful as a chronostratigraphic tool, in addition to finding stratigraphic traps.[20]

A more integrated form of stratigraphy, which incorporates several aspects of the aforementioned types of stratigraphy, is:

3.1.7 Sequence Stratigraphy

This stems mainly, however, from seismic stratigraphy. This type of stratigraphy subdivides sedimentary basin fills into genetic packages bounded by unconformties and correlative conformities. It can therefore provide correlation and mapping of sedimentary facies and stratigraphic prediction from a chronostratigraphic framework. It is the analysis of genetically related depositional units within a chronostratigraphic framework. This process seeks to correlate strata and predict stratigraphy, based on analysis of depositional sequences (basin-filling sedimentary deposits). It helps in the understanding of the evolution of basins, and also in the interpretation of potential source rocks and reservoir rocks in frontier areas and in more mature hydrocarbon provinces. Through this method, it is possible to compare widely-separated sediment that occur in correlatable unconformities.

It refers to the study of sediment and sedimentary rocks in terms of repetitive facies and associated strata geometry. This type of stratigraphy is based on the fact that physical unconformities permeate sedimentary layers. No matter the type of unconformity formed, as with seismic stratigraphy, they are able to distinguish between older and younger rock, thereby separating these sedimentary deposits into geological units. They therefore offer time-stratigraphic as well as a genetic significance.[6,16,21,22]

Others also include facies stratigraphy, soil stratigraphy and event stratigraphy.

Stratigraphic Categories	Principal Stratigraphic Unit-terms	Equivalent Geochronologic Units
Lithostratigraphic	Group Formation Member Bed(s), Flow(s)	
Biostratigraphic	Biozones: Range zones Interval zones Lineage zones Assemblage zones Abundance zones Other kinds of biozones	
Magnetostratigraphic polarity	Polarity zone	
Other (informal) stratigraphic categories (mineralogic, stable isotope, environmental, seismic, etc.)	-zone (with appropriate prefix)	
Chronostratigraphic	Eonothem Erathem System Series Stage Substage (Chronozone)	Eon Era Period Epoch Age Subage (or Age) (Chron)

Fig. 11 Summary of categories and unit-terms in stratigraphic classification[23]

The ages of layers can be found by applying three main laws of Nicholaus Steno:

The Law of Original Horizontality: unconsolidated sediments deposited on a solid base must have originally formed horizontal layers since the sediment particles would have been deposited at the lowest point, due to the laws of gravity. Thus, consolidated strata inclined at some angle must have become tilted after consolidation.

The Law of Original Lateral Continuity: layers of unconsolidated sediments deposited on a solid base would have formed continuous sheets of material in open basins. Thus, bands of consolidated sediments whose ends have been broken must have experienced this breakage and erosion after consolidation.

The Law of Superposition: Since each layer of unconsolidated sediment deposited on a solid base must form after the basal layer has been deposited, upper layers of sediment are younger than the lower layers.

William Smith later came up with *The Law of Faunal Succession*, an extension of the Law of Superposition, which states that the youngest fossilized fauna and flora are found in the highest layers and older fossils will be found in progressively lower layers.[15]

Stratigraphy gives information on post-depositional processes. These processes affect soil deposition. It can completely be reversed or changed drastically by various phenomena – hole digging or mud slides for example. To avoid misinterpretation, long profiles or profiles form several units are required.

Cores, samples of these rock strata, must always be taken in order to effectively analyse particular sequences of events as well as interpret how rock strata was initially laid down.

3.2 Sedimentary depositional environments

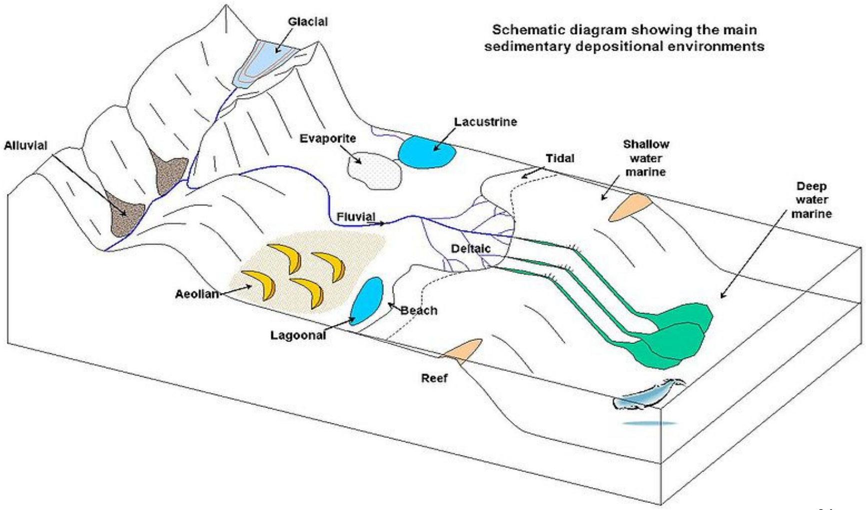

Fig. 12 Schematic diagram showing the main sedimentary depositional environments[24]

A sedimentary depositional environment refers to a depiction of the area within which sediment is deposited and the physical conditions occurring at the site of deposition. The above diagram shows a schematic of the main sedimentary depositional environments that arise. The three main types of depositional environments are continental or terrestrial, transitional or marginal marine and marine. Various factors may lead to sediment being deposited at a particular place or in a particular way.[25]

Below shows each type of depositional environment, together with their subdivisions.

3.2.1 Continental (Terrestrial [land])

Alluvial, Aeolian, fluvial, lacustrine

Table 6 Sedimentary Depositional Environment data – Continental[26]

	ALLUVIAL FAN	FLUVIAL	LACUSTRINE	DESERT (DUNES)	PALUDAL
Rock Type	Breccia, conglomerate, arkose	Conglomerate, sandstone, siltstone, shale	Siltstone, shale, limestone, or evaporites (gypsum)	Quartz arenite (sandstone) or gypsum	Peat, coal, black shale, siltstone
Composition	Terrigenous	Terrigenous	Terrigenous, carbonate, or evaporite	Terrigenous or evaporite	Terrigenous
Color	Brown or red	Brown or red	Black, brown, gray, green	Yellow, red, tan, white	Black, gray, or brown
Grain Size	Clay to gravel	Clay to gravel (Fining upward)	Clay to silt or sand (Coarsening upward)	Sand	Clay to silt
Grain Shape	Angular	Rounded to angular	---	Rounded	---
Sorting	Poor	Variable	Variable	Good	Variable
Inorganic Sedimentary Structures	Cross-bedding and graded bedding	Asymmetrical ripples, cross-bedding, graded bedding, tool marks	Symmetrical ripples, lamination, cross-bedding, graded bedding, mudcracks, raindrop prints	Cross-bedding	Laminated to massive
Organic or Biogenic Sedimentary Structures	---	Tracks, trails,burrows	Tracks, trails, burrows, rare stromatolites	Tracks, trails	Root marks, burrows
Fossils	---	Rare freshwater shells, bones, plant fragments	Freshwater shells, fish, bones, plant fragments	---	Plant fossils, rare freshwater shells, bones, fish

3.2.1.1 Alluvial fans

Alluvial fans are formed where unconsolidated sedimentary deposits accumulate due to the slowing down of a fast-flowing stream, leading to the cessation of the transport of these deposits. As the name suggests, they are fan-shaped and form at the mouth of mountain canyons onto a flatter plain. As the gradient of the stream decreases, sedimentary material is deposited, causing the channel to change direction. This over time, and after continual deposition, leads to the fan shape.

Though they are able to form under several different climatic conditions, they are most common and prominent in arid and semi-arid regions and are thought to be desert landforms.

Several alluvial fans close to one another may converge to form a compound alluvial fan, or bajada.[27]

Fig. 13 An alluvial fan in China's XinJiang province[28]

3.2.2 Transitional (Marginal Marine [coastal])

Deltaic, tidal, lagoonal, beach, paludal

Table 7 Sedimentary Depositional Environment data – Transitional[26]

	DELTA	BARRIER BEACH	LAGOON	TIDAL FLAT
Rock Type	Sandstone, siltstone, shale, coal	Quartz arenite, coquina	Siltstone, shale, limestone, oolitic limestone or gypsum	Siltstone, shale, calcilutite, dolostone or gypsum
Composition	Terrigenous	Terrigenous or carbonate	Terrigenous, carbonate, or evaporite	Terrigenous, carbonate, or evaporite
Color	Brown, black, gray, green, red	White to tan	Dark gray to black	Gray, brown, tan
Grain Size	Clay to sand (Coarsening upward	Sand	Clay to silt	Clay to silt
Grain Shape	---	Rounded to angular	---	---
Sorting	Poor	Good	Poor	Variable
Inorganic Sedimentary Structures	Cross-bedding, graded bedding	Cross-bedding, symmetrical ripples	Lamination, ripples, cross-bedding	Lamination, mudcracks, ripples, cross-bedding
Organic or Biogenic Sedimentary Structures	Trails, burrows	Tracks, trails, burrows	Trails, burrows	Stromatolites, trails, tracks, burrows
Fossils	Plant fragments, shells	Marine shells	Marine shells	Marine shells

3.2.2.1 Deltas

These are complex depositional landforms that develop at the mouths of rivers. They are formed when sediment (alluvial material) is deposited, as a river enters a standing body of water and therefore loses momentum. This standing body may be a lake, sea or ocean.

The sediment deposition occurs according to the grain size. The loss of momentum of the river indicates that it is no longer able to carry the sediment. Depending upon the amount of current the river is able to maintain over time, the deposition may be extensive causing the shoreline to prograde. On the other hand, if the river has a very weak current, it may be stopped almost immediately, not allowing much of a delta to form at all.

In delta formation, the heaviest sediment is dropped first, for example, sand. Further away from the mouth of the delta, finer sediment such as fine sand, silt and clay are found. Because of this, distinct layers – topsets, foresets, bottomsets – are formed.[29]

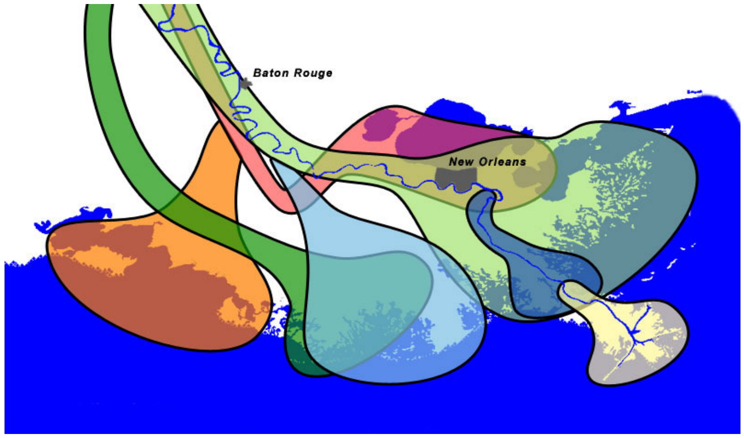

Fig. 14 The shifting nature of the dynamic Mississippi River Delta over the last 4600 years[30]

3.2.3 Marine (Marine [open ocean])

Shallow & deepwater marine: reef, shelf, floodplain

Table 8 Sedimentary Depositional Environment data – Marine[26]

	REEF	CONTINENTAL SHELF	CONTINENTAL SLOPE AND RISE	ABYSSAL PLAIN
Rock Type	Fossiliferous limestone	Sandstone, shale, siltstone, fossiliferous limestone, oolitic limestone	Litharenite, siltstone, and shale (or limestone)	Shale, chert, micrite, chalk, diatomite
Composition	Carbonate	Terrigenous or carbonate	Terrigenous or carbonate	Terrigenous or carbonate
Color	Gray to white	Gray to brown	Gray, green, brown	Black, white red
Grain Size	Variable, frameworks, few to no grains	Clay to sand	Clay to sand	Clay
Grain Shape	---	---	---	---
Sorting	---	Poor to good	Poor	Good
Inorganic Sedimentary Structures	---	Lamination, cross-bedding	Graded bedding, cross-bedding, lamination, flute marks, tool marks (turbidites)	Lamination
Organic or Biogenic Sedimentary Structures	---	Trails, burrows	Trails, burrows	Trails, burrows
Fossils	Corals, marine shells	Marine shells	Marine shells, rare plant fragments	Marine shells (mostly microscopic)

3.2.3.1 Continental shelves

These refer to the gently sloping and extended perimeter of a continent that is submerged under relatively shallow seas – shelf seas – as well as gulfs, and occupies about 7% of the total ocean floor.

Sedimentary material from the continent flows down the continental slope and accumulates at the base of the slope, resulting in the continental rise.

Continental shelves have gentle slopes and are relatively flat due to erosion and the deposition of sediment during the periodic rise and fall over time of the sea covering the shelf.

Continental shelves contain valuable resources, such as oil, gas and minerals. Organic material accumulates on the continental shelf and over time is buried and transformed by heat and pressure into oil and gas, which rises and is concentrated beneath geologic traps. Oil and gas can be found on the continental shelf off the coasts of California and Louisiana. Rocks on land, containing minerals, are carried to the ocean by rivers. The minerals, after deposition in river channels and beaches on the exposed continental shelf, are concentrated and sorted based on their density by waves and river currents.[31,32]

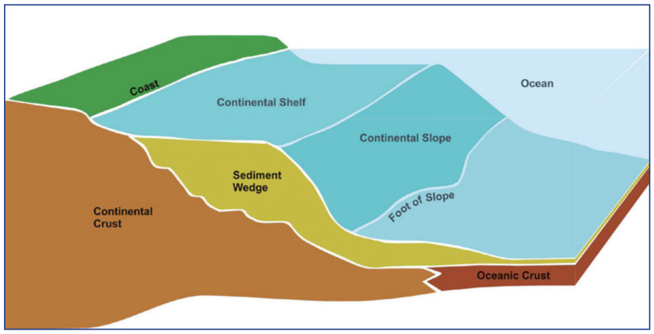

Fig. 15 Diagram showing a continental shelf[33]

Other types also include evaporite and glacial depositional environments.

Sedimentary structures arise from these depositional environments. These physical structures give an idea of the conditions that gave rise to them.

Bedding Planes are formed due to an interruption in bed formation – layers of sediment. This is caused by erosion or a lack of deposition.

Channels are rivers that flow in elongated depressions.

Submerged bars and *Dunes* are formed from water and wind currents respectively. The water currents carry sand or gravel along the bottom and the wind carries sand along a beach or desert. Bar or dune migration occurs based on the direction in which the water or wind is moving.

Ripples form from a water current or wave passing over sand or silt in shallow water. These ripples can be considered to be mini bars or dunes.

Mudcracks are formed when water slowly evaporates from a muddy pool. This leaves behind moist clay, which dries up and eventually cracks.

These structures give an idea about the conditions under which they were formed; mudcracks, for example, tells that this is an area of alternating wet and dry periods.

When considering clastic and organic sediments, two processes may occur.

First, there may be deposition and accumulation of sediment in the depositional environment. This is followed by burial of these by more sediment. Then, lithification [cementation and compaction] of the accumulated sediment occurs leading to the formation of sedimentary rock.

Also, there may be deposition, accumulation and burial of the sediment. However, before lithification can occur, there is erosion and re-exposure of the buried sediment. It, therefore, then goes through one or more new cycles of weathering: erosion – transport – deposition – burial.[25]

4 The Reservoir

In order for oil and/or gas to be detected and subsequently produced, it must be trapped. A trap consists of source rock, reservoir rock and a seal and these three components comprise an oil/gas field.[34]

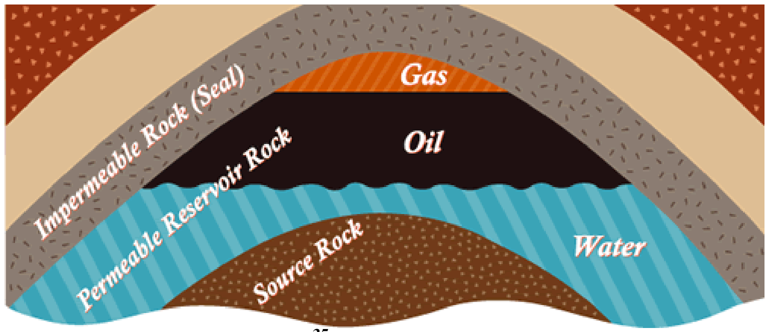

Fig. 16 Components of an oil and gas field[35]

The source rock, made up usually of shale and coals, under the right conditions of temperature, causes hydrocarbons to rise. These light hydrocarbons are able to penetrate the permeable reservoir rock. They then reach the impermeable seal and hence get trapped within the reservoir rock. An example of this seal is caprock (shale) There are two main types of reservoir rock – sandstone and carbonate. These two types of reservoir rock make up almost 99% of all reservoirs. They are formed from sediments found at the earth's surface.[36]

Sandstone: This is the most common type of reservoir, making up about 80% of all reservoirs and 60% of all oil reserves. Cemented grains of quartz (SiO_2) and feldspar ($KAlSi_3O_8$, $NaAlSi_3O_8$, $CaAl_2Si_2O_8$) form sandstone. There is hardly ever 100% clean sandstone, as it is usually mixed with shale, clay or carbonate.[36]

Carbonate: These reservoirs are formed from calcite from biological activity. This is changed chemically to dolomite. Hence they are made up of dolomite ($CaCO_3$, $MgCO_3$) or limestone ($CaCO_3$). This type of rock is also usually mixed with shale. If the amount of shale is high enough, however (above 35%), the permeability of the rock is decreased so drastically that this rock is no longer considered a reservoir.[36]

These reservoir rocks have both inter- and intragranular porosity.

4.1 Permeability

Within a formation, the ease with which fluids are able to travel is the permeability. This characteristic depends on the interconnectedness of the pore spaces.

The permeability that is parallel to a layer is usually higher than the permeability perpendicular to the layer, with anisotropy ratios being very large. This holds for reservoirs that had layers forming flat like blankets or pancakes. The anisotropy refers to the difference in shape, make-up of physical characteristics of a formation. Its unit is the mD (millidarcy) and its symbol is *k*. It can be calculated from Darcy's formula:

$Q = [kA(P_i - P_o)]/\mu L$

; where $Q \equiv$ the (volumetric) flow rate measured in cm^3/s or m^3/s

$P_o \equiv$ the outlet fluid pressure measured in Pa

$P_i \equiv$ the inlet fluid pressure measured in Pa

$\mu \equiv$ the dynamic viscosity of the fluid measured in centipoise (cP)

$L \equiv$ the length of the tube measured in cm or m

$k \equiv$ the permeability of the sample measured in milliDarcy (mD)

$A \equiv$ the area of the sample measured in cm^2 or m^2

The conditions required for the Darcy formula to be able to be used include a laminar flow, steady state, incompressible fluids and a homogeneous formation.[5]

The permeability is measured in the laboratory on core samples obtained from the reservoir. The process is carried out by passing a fluid of known viscosity through the core sample of known dimensions at a set rate, and measuring the pressure drop across the core. It can also be carried out by setting the fluid to flow at a set pressure difference, and measuring the flow rate produced.

The *absolute permeability, k* is derived when there is only one fluid found in the rock, and the rock permeability is at its maximum.

Where there are two or more fluids found within the rock, their flow rates and therefore individual permeabilities in the rock would differ. The individual permeabilities depend on the saturation of the particular fluid in the rock. This is the *effective permeability,* k_w, k_o, k_g for water, oil and gas respectively. The value for all effective permeabilities is always less than the absolute permeability of the rock.

The effective permeability can be written as a fraction of the absolute permeability of the rock of any of the present fluids at 100% saturation. This is referred to as the *relative permeability,* k_r. Here, $k_{rw}=k_w/k$, $k_{ro}=k_o/k$, $k_{rg}=k_g/k$ for water, oil and gas respectively.[2]

Grain size, grain sorting, fluid characteristics and porosity all affect the permeability.[5,37,38]

4.2 Porosity

This refers to the pore volume per unit volume of formation.

It is calculated as:

ϕ = Pore volume/Total bulk volume = $(V - V_s)/V = V_p/V$

; where V_s represents the volume occupied by the matrix.

The porosity within the main types of rock found in a reservoir differs greatly:

Dense carbonates – These are made up of limestones and dolomites. They usually have very low porosity, if any.

Evaporites – These are salt, anhydrite, gypsum and sylvite. They also have very low porosity.

For both dense carbonates and evaporites, the low porosity is due to the fact that the pore space is very small, since the particles are well compacted.

Well-consolidated sandstones – These have porosity of between 10 and 15%.

Unconsolidated sandstones – Since these sandstones are unconsolidated, the pore space is larger and therefore these have porosity of about 30% or more.

Shales/Clays – These have high porosity, usually of about 40%. This porosity is usually water-filled however and due to the small size of the pores, they typically have very low permeability.

Vugs and *caves* are known to be produced due to secondary porosity. This pore space does not arise naturally in the rock but may occur due to the action of tectonic activity or formation water movement on the rock matrix after deposition. It may also arise due to the interaction between the drilling mud and shale.

Fractures, fissures and cracks may also increase porosity slightly. The larger the porosity of the formation, the greater the amount of formation water found in the pore space and consequently, the lower the resistivity.

The *absolute porosity* refers to the ratio of total pore space in the rock to that of the bulk volume.

The *effective porosity* is the absolute or total porosity minus the clay volume.

There are several factors that affect the porosity. These include grain size, grain size distribution, grain packing, grain shape, compaction and cementation.[5]

The sonic, neutron and density logs are the most common well-logging methods used to determine the porosity of the rock being analysed, once the formation lithology is known. The symbol for porosity is ϕ and it is measured as a percentage.

4.3 Water saturation

The saturation of the formation is the fraction of the volume of pore fluid that is filled with a specific fluid.

It is not possible to remove 100% of oil or water from a reservoir. There is always some amount of each fluid that remains within the formation.

The *irreducible water saturation, S_{wi}*, is the fraction of water in the pore space that cannot be removed. It is known as the connate water and this arises due to capillary forces that cause water to cling to the rock.

The *residual oil saturation, S_{or}*, is the fraction of oil in the pore space that cannot be removed by ordinary fluid drives or recovery techniques.

There is a transition zone that occurs between the areas of 100% water saturation, S_w and 100% oil saturation, S_o.

The longer the transition zone is, the lower the permeability and conversely a shorter transition zone has a higher permeability.

The saturation of the residual hydrocarbons in the flushed zone can be calculated by:

$S_{hr} = (1 - S_{xo})$

; where S_{xo} is the saturation of the flushed zone

The saturation of hydrocarbons in the formations is calculated by:

$S_h = (1 - S_w)$;

S_w being the saturation of the formation water

Therefore, the bulk volume of moveable oil = $\phi(S_{xo} - S_w)$[5]

5 Well Correlation

5.1 Introduction

Once sandstone layers have been determined in various wells, it is important to find a correlation between wells. The six wells analysed – 335R, 360R, 333R, 313R, 338R, 312R – were put together in a multi-well correlation to examine trends between them. This also enabled a comparison between the layers found from the correlation and the facies analysis, discussed in the next chapter.

Based on the multi-well correlation performed in *IP*, a general idea of the placement of the wells was found. Seeing that no map was readily available, the wells were given arbitrary coordinates in *Petrel*, and positioned accordingly, as seen in Fig. 18 Various modelling and imaging was then done in *Petrel* using the log information in IP to generate models for the parameters being analysed.

5.2 Geological Description of the Komso Field

The Komso field is located in the Purovskoe region of the Yamalo-Nenets Autonomous District in the Northern West Siberian Plain, on the left bank of Pyakupur – a tributary of the river Pur – along the highway of Surgut-Urengov.

North-east of the field, at a distance of about 15 km, is the town of Gubkinsky, with a population of 20,000 people. About 37 km away is the village of Purpe. On the oilfield site, there are only settlements for rotating staff.

In 1966, gas deposits were found in the Cenomanian, and deposits of oil were found further down in 1982. Test operation began in 1988, after appraisal drilling was conducted in 1986.

Of the 195 wells of the Komso field, 9 of which are injection wells, 120 wells are currently engaged in hydrocarbon production.

16 of the productive reservoirs in this field have production rates of exploration wells to date ranging between 5-30%.

The climate of the area is continental, and is characterised by a negative average annual air temperature of about -6.7°C, and a short 87-day frost-free period. There is uneven precipitation, mainly during the warmer seasons, during periods of high relative humidity and during winter.

The field is a part of the Nadym Pur oil and gas province, which, structurally and tectonically, forms the central zone of the regional uplift. The geological section is represented by the terrigenous-sedimentary Mesozoic-Cenozoic age, with a depth of 3600m, which are allocated complexes of Jurassic, Cretaceous, Paleogene and Quaternary sediments.

There are 2 domes located within the Komso field – the East (15 - 20 km) and West (10 - 15 km) domes. There are potential petroleum deposits associated with the Upper Cretaceous (Cenomanian reservoir, containing free gas) and the Lower Cretaceous (Valanginian-Albian oil-and gas-bearing reservoir) deposits.

The Komso field has quite a complex geological structure with a large number of oil and gas reservoirs in a small margin. It contains 52 productive reservoirs, 10 of which are gas-bearing, the others containing oil, gas and condensate. Geological oil reserves of the Komso field are contained in 13 basic and 8 additional operating units.[39]

5.3 Description of the Core Sample

The sandstone found in this field is made up of small, dark-grey grains with feldspar, quartz, mica and some amount of clay cement. Fissures and claystone nodules are found along the contact line between the shaly and carbonised sandstones.

Fig. 17 Core sample – sandstone[40]

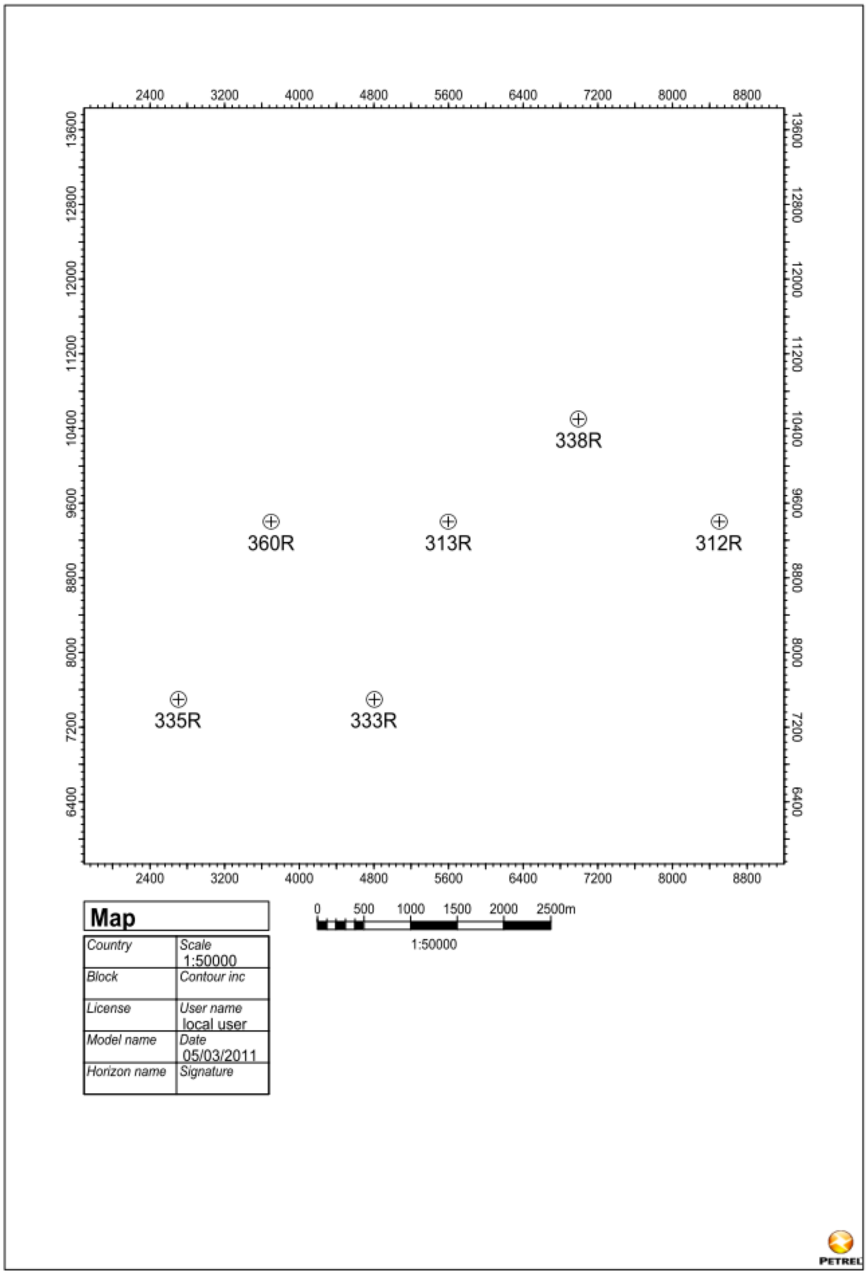

Fig. 18 Mapping of the six wells using arbitrary coordinates for positioning in *Petrel*

5.4 Interactive Petrophysics

Six wells were analysed side by side in a multi-well correlation plot in the Senergy *Interactive Petrophysics* (IP) program. This was to see where certain trends occurred and where the similarities lay between them. Common sandstone layers within the various wells were marked in IP in the correlation plot. The wells were added one at a time, beginning with 2 wells. The addition of more wells changed and updated some of the trends between them, taking into consideration each extra well that was added.

At some particular depth ranges, the matching of sandstone layers is better than at other depth ranges. This helps to give an idea of where the wells are placed in relation to one another in the actual field, as well as the general shape of the layer throughout the six wells. There also seemed to be better correlation further towards the top and towards the bottom of the wells. In the middle, there was a less clear correlation and usually requires more careful analysis.

Below outlines the various sandstone layers found for each of the six wells and their depth ranges.

Table 9 Top and base depths of each layer for each of the six wells

Well →	335R		360R		333R		313R		338R		312R	
Zone → Depth (m)	**Top**	**Base**	**Top**	**Base**	**Top**	**Base**	**Top**	**Base**	**Top**	**Base**	**Top**	**Base**
Layer ↓												
A2	–	–	–	–	–	–	1138.4	1162.2	1152.6	1167.4	–	–
A3	–	–	–	–	–	–	1171.0	1187.2	1167.5	1180.0	–	–
A4	–	–	–	–	–	–	1322.6	1347.6	1324.3	1347.0	–	–
A5	1426.2	1455.6	1400.6	1427.0	1393.8	1424.0	1420.6	1442.2	1414.0	1433.7	1395.0	1408.4
A6	–	–	–	–	1444.4	1463.0	1462.2	1486.0	1462.4	1486.2	–	–
A7	–	–	–	–	1532.2	1550.2	1559.0	1574.0	1537.0	1554.5	–	–
A8	1601.6	1635.4	1598.0	1626.0	1583.4	1613.8	1613.6	1641.0	1609.3	1638.6	1603.4	1624.4
A9	1669.4	1690.6	1630.0	1660.4	1637.8	1659.8	1652.0	1674.6	1647.8	1673.7	1642.0	1660.0
B1	1720.0	1724.0	1693.8	1703.2	1689.0	1700.0	1691.0	1710.0	1685.1	1700.0	1672.4	1682.6
B2	1756.2	1781.6	1740.4	1766.8	1748.4	1774.0	1742.0	1792.2	1742.3	1782.4	1742.0	1752.0
B4	1882.0	1920.4	1872.0	1905.0	1863.6	1896.0	1855.0	1896.0	1854.0	1888.5	1835.0	1879.6
B5	1969.4	2021.2	1953.0	2012.0	1970.6	2017.4	1963.0	2021.0	1957.1	2036.4	1924.0	2007.4
B6	2069.6	2096.6	2039.8	2064.0	2032.0	2056.0	2036.2	2064.8	2037.1	2053.0	2019.4	2033.0
B7	2119.0	2124.8	2079.0	2093.0	2083.0	2093.4	2095.0	2120.0	2102.0	2124.1	2081.4	2094.8
B8	2207.8	2237.4	2184.0	2208.6	2158.8	2181.6	2164.6	2195.4	2184.8	2206.6	2173.4	2203.6
B9	2265.8	2305.8	2223.4	2277.0	2219.4	2271.0	2236.0	2290.6	–	–	2229.2	2266.4
C1	2319.4	2331.2	2276.6	2304.6	2293.0	2306.0	2290.6	2305.0	2284.7	2293.1	2267.2	2289.0
C2	2342.8	2356.2	2306.0	2326.2	2325.4	2342.4	2321.4	2340.0	2320.2	2339.0	2305.0	2331.0
C4	2391.6	2443.4	2360.4	2405.0	2358.8	2397.0	2355.0	2409.0	2369.5	2416.5	2360.6	2410.0
C5	2459.0	2466.4	2427.0	2433.4	2424.0	2433.4	2431.0	2442.0	2431.0	2441.8	2414.2	2422.4
C6	2476.6	2525.8	2443.6	2487.8	2433.6	2489.6	2454.6	2489.0	2451.0	2486.4	2427.4	2447.4
C7	2530.2	2556.2	2487.8	2512.4	2494.0	2520.0	2504.0	2537.6	2508.7	2537.8	2468.6	2499.4
C8	2582.8	2596.6	2538.0	2554.4	2541.4	2555.4	2542.0	2560.6	2548.0	2559.5	2514.0	2539.0
C9	2614.6	2646.0	2571.8	2610.0	2577.4	2608.6	2577.0	2598.0	–	–	2581.4	2606.2

5.5 Petrel

5.5.1 Mapping

The six chosen wells were first shown in a map window [Window–New Map window] in *Petrel*. A <u>New Well Folder</u> [Insert–New Well Folder] was inserted and the six wells inserted into this folder [Insert–New Well]. According to the scale of the map in the map window, arbitrary *x*- and *y*-coordinates were given accordingly for each well, so they each had their own position in the map. These coordinates were based on the positioning of the wells in IP. It is important to also add the Bottom MD value at this point to denote the length of the well's pipe.

5.5.2 *IP Log Data*

The log data for each well from IP was then imported into *Petrel* [Right-click on well–Import (on Selection)–Select relevant file with File type: Well logs (ASCII) (*.*)]. The various wells can now be seen in a 3D window [Window–New 3D window]. The log information can now be displayed in a Well Section window [Window–New Well Section window]

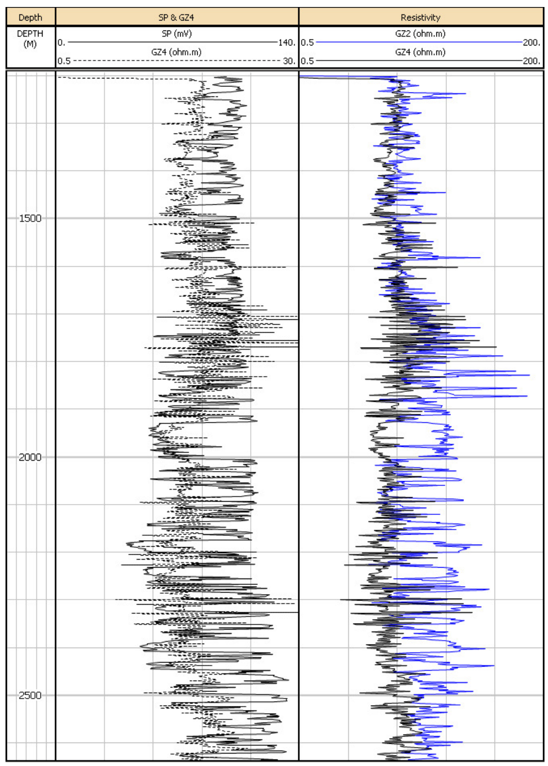

Fig. 19 Initial log plot data for Well 312R showing depth, SP and resistivity curves

5.5.3 *Sections*

In the models pane, a skeleton of the top, mid and base reservoirs is inserted by choosing the Make Simple Grid process [Processes Pane–Utilities Folder–Make Simple Grid]. In the Input tab, the top and base limits were chosen to coincide with the length of the pipe created. A *Z*-value (Bottom MD) of -3000 was chosen for the length of the pipe so the top and base limits chosen were -500 and -2500 respectively. In the Geometry tab, *Xmin,max* and *Ymin,max* values were chosen according to the positioning of the wells in the map window. The minimum values are chosen to be slightly lower than the lowest *x*- and *y*-values for each well and the maximum values chosen to be slightly higher.

5.5.4 Horizons

The top and base horizons for each layer were made in the well section window by creating a Well tops folder in the Input pane [Insert–New well tops]. By expanding the Well tops folder, horizons were created within the Stratigraphy folder, by clicking on the Add new well top surface in the function bar. A top and base was made for each layer (from A2 to C9) and these were connected throughout all six wells. In order to change the depth of a particular layer in a particular well, ensuring the Create/edit well tops button was selected in the function bar, the top or base layer in the well section window was right-clicked, and the depth changed.

5.5.5 Models

Surfaces

Horizons were again made for each layer – top and base – this time in the Models pane [Processes pane–Structural Modelling–Make horizons]. The top and base horizons previously created in the Input Pane [Input pane – Well tops – Stratigraphy] were then placed into the Make horizons dialog box that opens, by clicking the Append item in the table button to insert a row. The layers were entered one by one, inserting the top and base for one layer, before moving on to the next.

Once all these horizons have been created, the horizons folder in the Models pane can be expanded and the horizons selected. In the Models pane, the Edges button can be selected in order to view the connection between a top and base layer. The Zone filter button can be expanded and different zones turned on or off in order to see either all the horizons, as well as their top and base connections, or perhaps the top and base connection for one particular layer only.

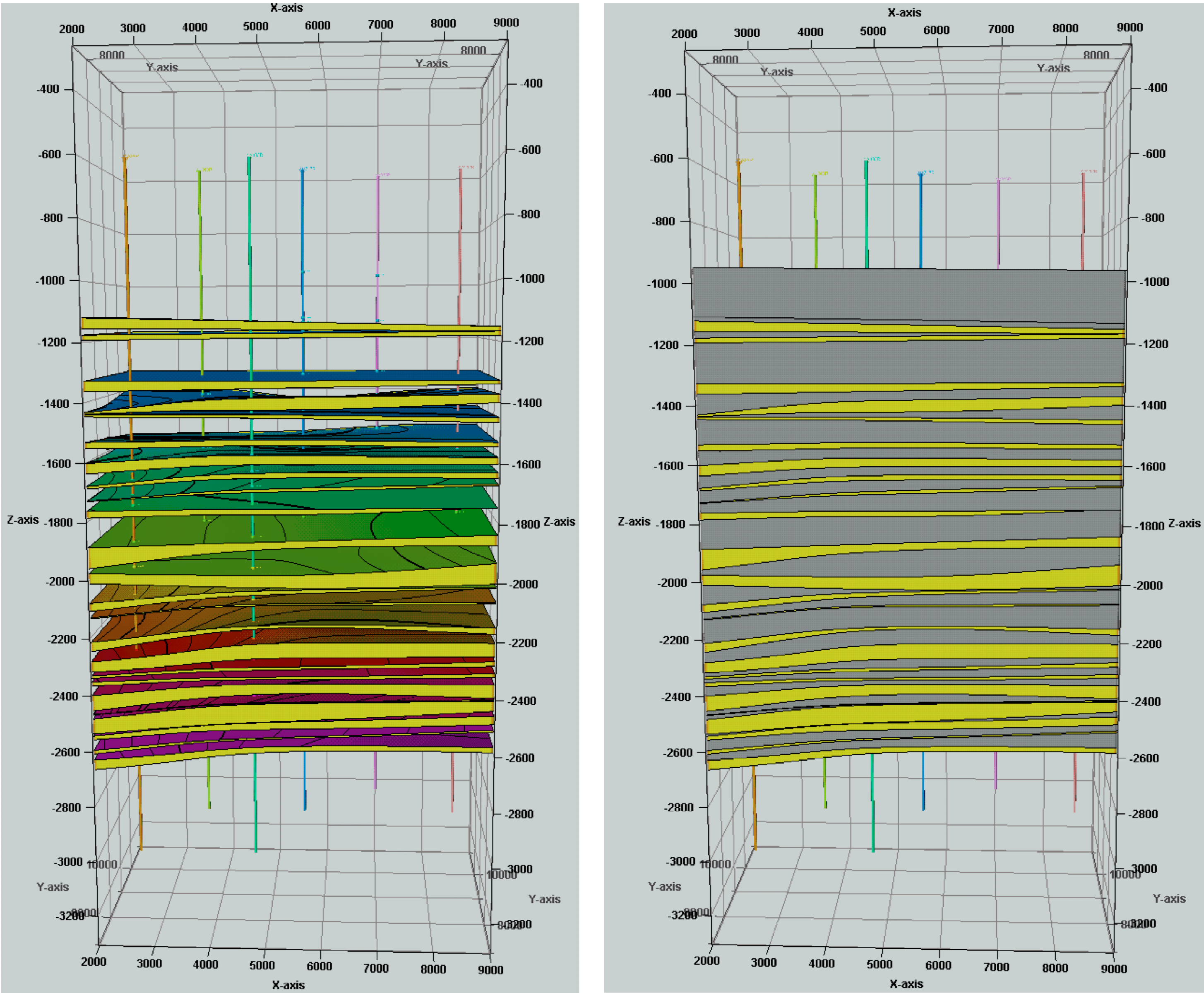

(a) (b)

Fig. 20 Model of various sandstone layers without(a) and with(b) shale layers across the six wells

Below shows the multi-well correlation of each of the sandstone units through the six wells generated in *Petrel.*

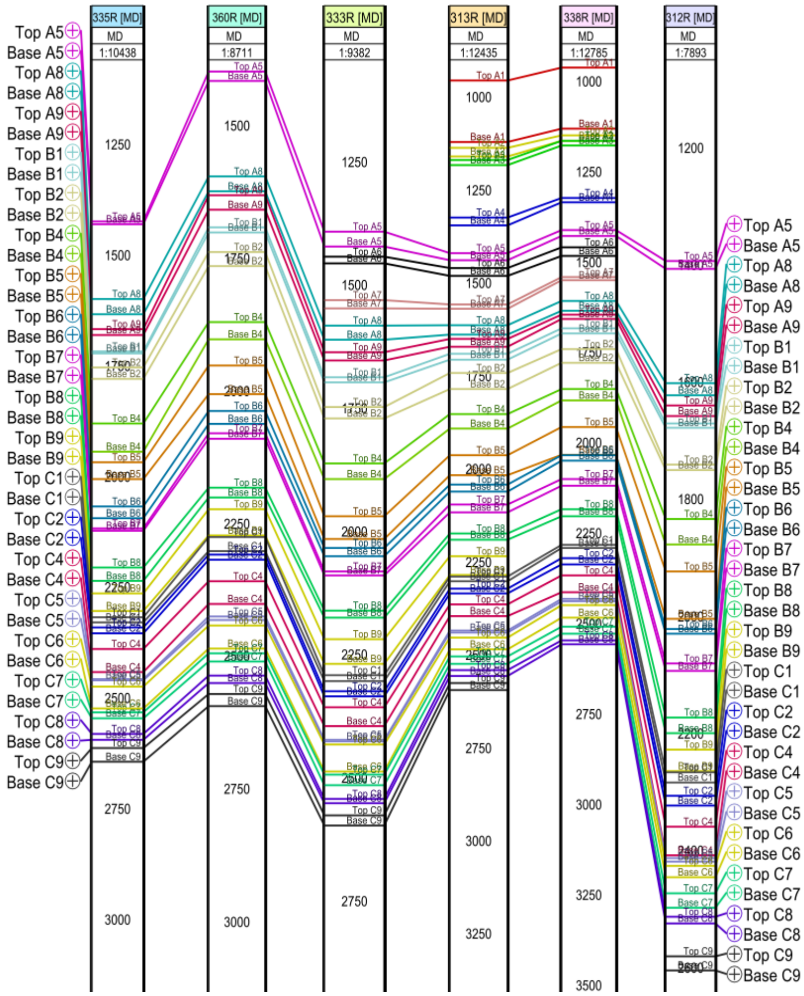

Fig. 21 Multi-well correlation generated in *Petrel* showing various sandstone layers

6 Facies Analysis & Modelling

The term *facies* refers to the depositional setting of the rock.[1] It encompasses all of the characteristics of a particular rock unit. For example, there may be a "tan, cross-bedded oolitic limestone facies". The characteristics of the rock unit come from the depositional environment. Every depositional environment puts its own distinctive imprint on the sediment, making a particular facies. Thus, a facies is a distinct kind of rock for that area or environment.[41]

Facies refers to a body of rock that has specific, distinctive characteristics and forms under certain conditions of sedimentation, reflecting a particular process, set of conditions, or environment. It should differ from those bodies of rock above, below and laterally adjacent to it. Facies can be grouped into facies associations or subdivided into subfacies. The idea of facies has been used for centuries in order to analyse and determine areas of oil, coal and mineral ores.[21]

6.1 Types

Facies are distinguished based on the various types of characteristics the sedimentary rock possesses. Once a core of the rock is taken, or an outcrop is analysed, facies can be defined based on the dominant aspect of the rock.

Biofacies – this is the term to refer to the sedimentary rock that has its biological content as the dominant aspect

Ichnofacies – this is the facies that is defined based on the presence of trace fossils

Lithofacies – if the physical and chemical characteristics of the sedimentary rock are its dominant attribute

Microfacies – this term is used, especially with carbonates, where the major attributes are seen in a very small section of the rock

A = Sandstone facies (beach environment)

B = Shale facies (offshore marine environment)

C = Limestone facies (far from sources of terrigenous input)

Each depositional environment grades laterally into other environments. This is known as facies change when analyzing rock record.[41]

6.2 Modelling

Facies analysis refers to the interpretation of rocks and sediments for the purpose of reconstructing the processes that were responsible for the original deposition.

Facies models can be created based on various classifications. They may be formed based on direct descriptive classifications, from actual observable and measurable features. They may be formed in an attempt to determine the original processes that led the rock to be formed and deposited in the way that it was initially. They may also be based on an attempt to regenerate the environment in which the rock was formed and deposited.

Several facies models have also been formed to take into account external features such as changes in tectonics, climate, type of sediment and sea level.

Advances in technology over time have allowed more sophisticated and intricate facies models to be developed.[21]

There are several types of facies models:

Lithofacies model (Descriptive classifications): These are divided into classes, groups and individual facies. Each classification is based upon different attributes. The classes are distinguished based on grain size, internal organisation and composition, the groups are based on internal structure and texture organisation and the individual facies are based on internal structure, bed thickness, texture and composition. Common lithofacies models were created for deep-water facies and alluvial facies.

Process facies model: This model is based on the generation of information about how the sediment was originally formed and deposited – the formative processes that led to how rock strata are positioned today. The names of these models have an *–ite* ending, an example being the turbidite model, which helped in distinguishing between descriptive and genetic characteristics of facies. It is based on the generation of a turbidity current which explained the co-existence of shallow water containing shallow water fossils and shales containing deep water pelagic fossils. Debrites are massive sandstones formed as sandy debris flows. Other examples include tidalites, which are the facies that arise from tidal currents due to the twice-daily rise and fall of tides. They have a distinctive pattern of cross beds. Contourites are the facies that arise from contour currents that parallel contours on the continental slope and rise. These can range from fine terrigenous sand, to silt, to clay, to biogenic sediment.

Contourites made up primarily of biogenic sediment are extremely similar to pelagites.

Environmental facies model: The type of environment in which facies were formed is just as important as the way in which they were formed. Similar formative processes may occur in completely different types of environments. It is therefore easier for facies analysis, if facies are grouped into facies associations as opposed to being analysed separately. These facies associations are based on some genetic or environmental similarities.

Allocyclic sequence stratigraphic model: It is always possible that facies models may arise due to external factors and forces. Tectonic activity has been highlighted as one of the most common of these external forces.

6.3 Transgression & Regression

Transgression means that water depths are increasing. In a transgressive sequence the energy and sediment grain size will decrease higher up in the stratigraphic column - also known as fining or deepening upward.

Regression of ocean waters indicates that water depths will get shallower so grain size will increase and energy will increase - known as coarsening or shallowing upward.

Transgression - sea level rise

Regression - sea level drop

Fluctuations in sea level are caused by conditions such as:

1. Changes in the size of the polar ice caps, due to climatic changes

- Melting of ice caps leads to sea level rise (transgression) - it has been calculated that the complete melting of the Antarctic Ice Sheet would cause a sea level rise of 60 - 70 meters.

- Growth of ice caps leads to a drop in sea level (regression) - calculations show that sea level was as much as 100 meters lower than at present at the height of the last Ice Age glaciation. Much of the Continental Shelf area would have been exposed and dry.

2. Rate of sea floor spreading - during times of rapid sea floor spreading and submarine volcanism, the ocean ridge system is enlarged by the addition of lava, displacing water onto the edges of the continents (transgression).

3. Localized subsidence or uplift of the land - In the 8000–10,000 years since the melting of the last glacial ice sheet over North America, parts of Canada have risen due to isostatic uplift by up to 300 meters.[41]

6.4 Sandstone Units – Komso Field

Below shows the table of all the wells analysed and the various sandstone layers selected for each. These represent layers that cut across all six wells and facies analysis is done for each layer. The particular facies selected for each well's layer is shown in its horizontal image. This is chosen based on the shape of the SP curve for that particular layer for each well. Trends between the layers are explained below and the full table of all the facies as well as their vertical and horizontal images can be found in App. B

Table 10 Facies analysis for each sandstone unit over the six wells

Well →	**335R**	**360R**	**333R**	**313R**	**338R**	**312R**
Layer ↓						
A1	No info	No info	No info	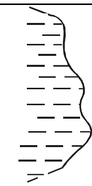	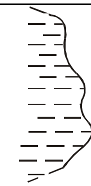	No info
A2	No info	No info	No info	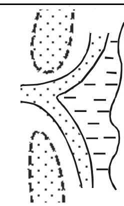	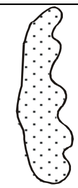	No info
A3	No info	No info	No info	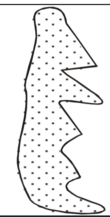	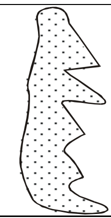	No info

A5	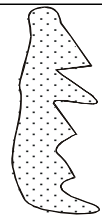	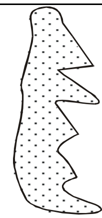	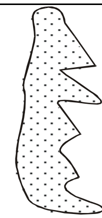	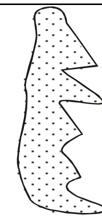	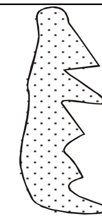	
A8	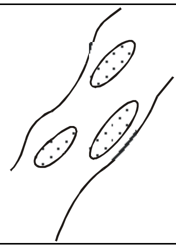	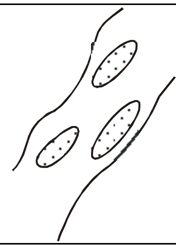	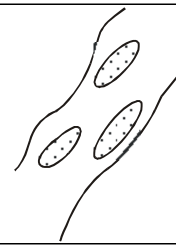	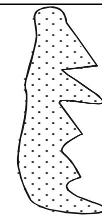	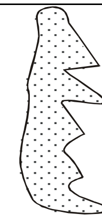	
A9	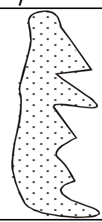	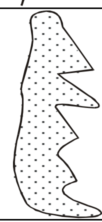	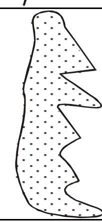	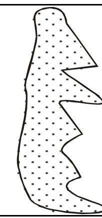		
B1		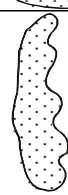	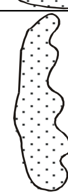			

B2	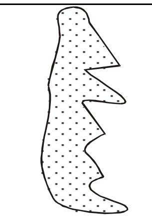	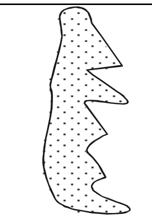	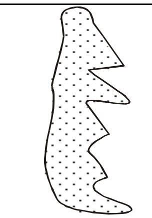	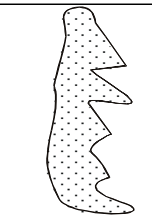	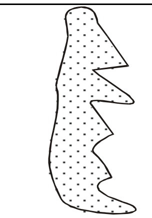	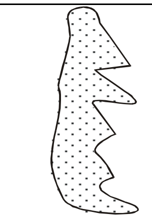
B4	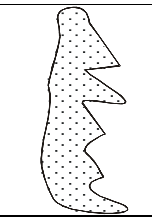	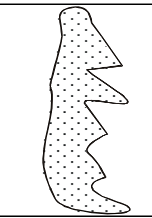	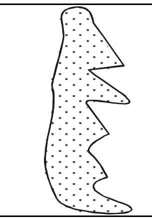	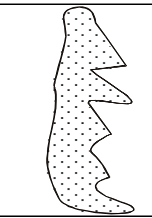	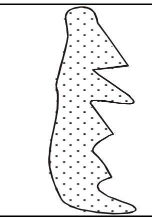	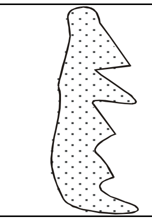
B5	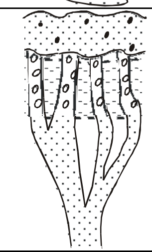	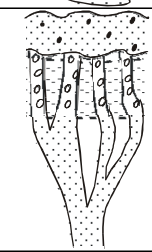	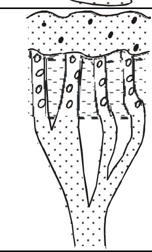	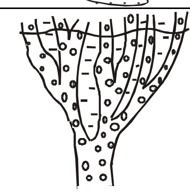	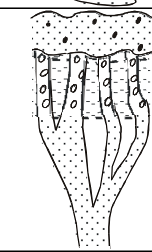	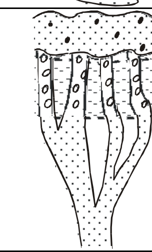
B6	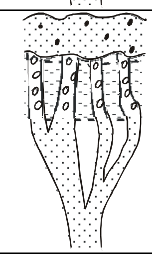	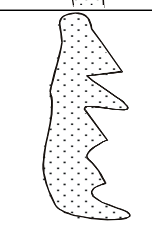	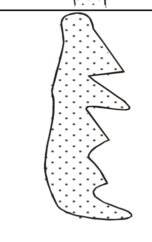	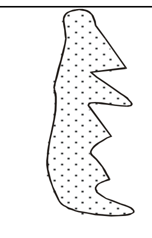	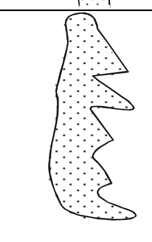	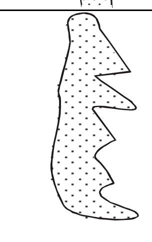

B7	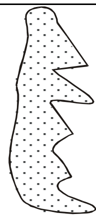	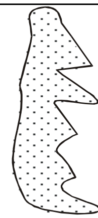	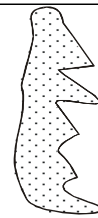	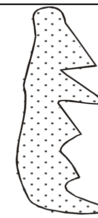	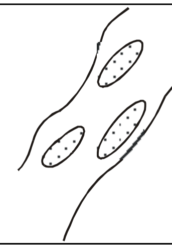	
B8	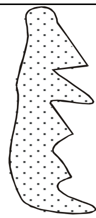	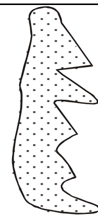	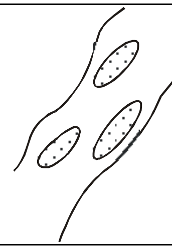			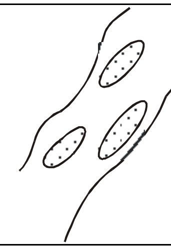
B9	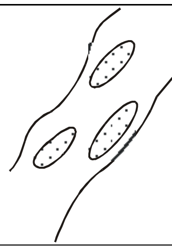	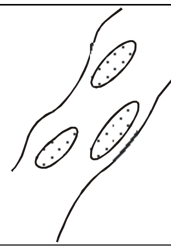	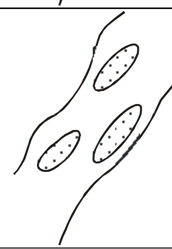	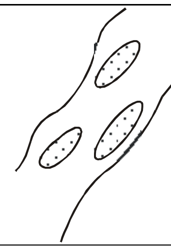	disappear	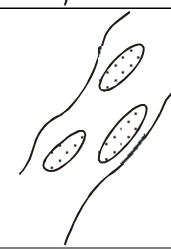
C1		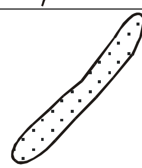	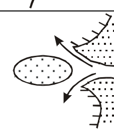	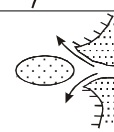		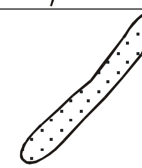

C2	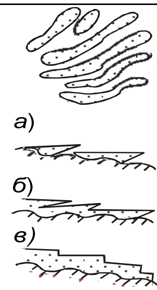	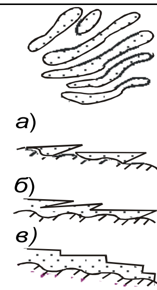		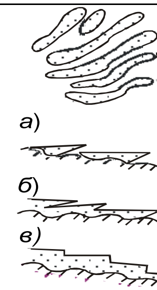	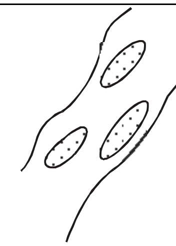	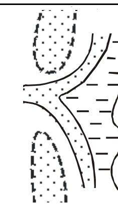
C4	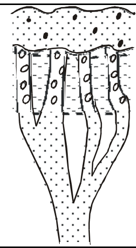	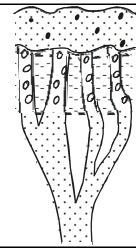	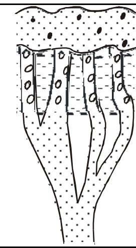			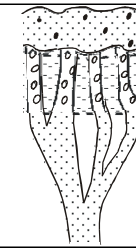
C5	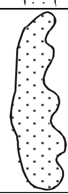	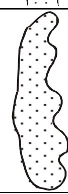	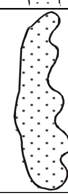			
C6	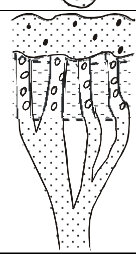	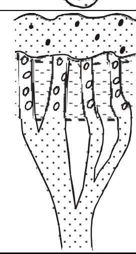	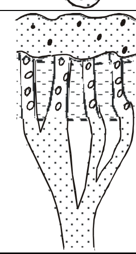	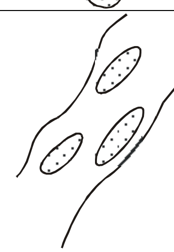	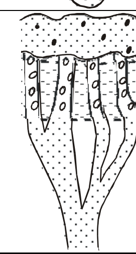	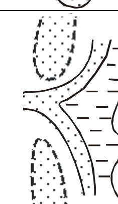

C7	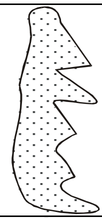	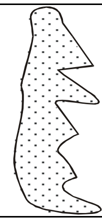	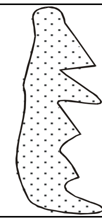	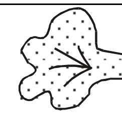	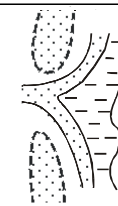	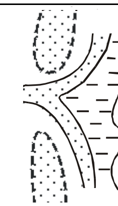
C8	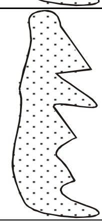	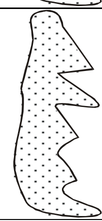	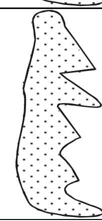			
C9	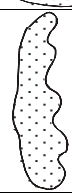	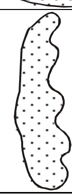	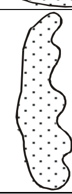		No info	

6.4.1 Description

This analysis takes place from the greatest depth to the shallowest, ie from layer C9, moving upwards to layer A1.

C9: This has very clear regressive bars. As mentioned before, there is coarsening upwards, giving the triangular shape of the SP log as shown in number 16 of App. B. The well information for Well 338R is missing, however the same facies shape can be seen for the remaining wells.

C8: As it is known that the sea water is always flowing, it is possible for there to be changes in the movement of the sea. Here, the first three wells form transgressive bars, whilst the last three retain the regressive bars from the lower layer.

C7: Bars form along the shoreline. If these bars are strong and stable, it is possible for lagoons to form between the shore and the bar. However, if this bar is not particularly stable, as seems to be the case in this layer, it is possible for the water currents from the river to break through, forming the head parts of breaking currents. The last two wells have the washouts of breaking currents as the river breaks through the bar and begins to spread. The first three wells still remain transgressive bars as before.

C6: Since there has been transgression of the sea, water comes further onto the shore, which may lead to waterflooding and cause some bars to be underwater. This is what gives rise to the underwater slope of the delta. As rivers flow and come into contact with the sea, their momentum is lost and they begin to deposit sediment. The various river channels spread out as ‘sleeves’ and this is the case for the first three wells, as well as well 338R. From layer C7 to this layer, it is possible that the angle of flow of the river has changed, to the west, seeing that the head part of breaking current in well 313R becomes the washouts of breaking currents in well 312R. When water from the river and water from the sea collides and interacts, it is possible for a change in direction of the water to occur.

C5: Once again, as with flow and movement of the sea water, there is regression, forming these regressive bars. The sleeves of the deltas carry a lot of sand. This is eventually deposited and accumulated, also leading to the formation of regressive bars.

C4: Underwater slope of deltas are formed in most of these wells. In wells 313R and 338R, it can be seen that transgressive bars are formed.

C2: If these stable bars do not exist, instead of lagoons, it is possible for shelves to form, as is the case with wells 335R, 360R and 313R. The sleeves of the delta do not only carry sand, but may also carry shale. Here, sedimentary rock of shallow shelves is found.

C1: Mouth bars are formed at wells 333R and 313R. It is possible for beach ridges to form on the sides of these mouth bars since as water flows to and fro it may push sand up in a certain area, forming these ridges. The beach ridges are formed at wells 360R and 312R as it can be seen there is a change from transgressive to regressive bars at wells 335R and 338R.

B9: Shallow river beds of shallow rivers appear for all wells except 338R. There may be more sandy conditions here, with a possible extension of the shoreline. There is a loss of the sandstone layer for well 338R. This layer can be considered an intermediate layer, or a region of stability. This explains why it is mainly shallow beds that occur here, since there is not any major movement of water here.

B8: Transgressive bars are formed for wells 335R, 360R, 313R and 338R. This is therefore where the sea water is flowing onto the shore. Where the shallow beds are maintained, for wells 333R and 312R, this can be considered to be washouts of these transgressive bars.

B7: The first three wells (335R, 360R, 333R) are very thin layers, which form transgressive bars. This layer gets thicker in wells 313R and 338R and becomes more of a shallow river bed in well 338R. The layer becomes slightly thinner again in well 312R and again forms the transgressive bar. From the previous layer to this one, there is a continued change in the direction of the river water. There is again movement to the west.

B6: Again there is movement of sea water, transgression, forming the underwater slope of the delta in well 335R. Transgression of the river is seen in the remaining wells.

B5: The underwater slope of the delta is formed in these wells. It seems that for well 313R, it is possible that a valley of a deltaic complex is formed.

B4: Again, there is further transgression of the river.

B2: Continuous transgression of the river.

B1: Now, there is regression as the movement of the river changes.

A9: Again, a change to transgression. Usually the periods of regression and transgression are long. It is, however, possible that there are temporary periods of regression and transgression. For regression, for example, this may arise if there are sudden periods of hot weather where there will be loss of water close to the shore (as opposed to the ocean pulling back the water)

A8: Shallow beds are formed as further transgression occurs.

A5: Transgressive bars are continued to be formed.

A3: There is only information for wells 313R and 338R for this layer. Transgression bars are formed here from transgression of the river further onto the shore.

A2: Again only wells 313R and 338R have log information. As there is no information for the other wells, it is possible to assume that there is the head part of breaking currents forming in another well forming the washouts of these breaking currents for well 313R. Regressive bars form for well 338R.

A1: Here also, there is only information for wells 313R and 338R for this layer. This is a very shaly layer and represents open sea and large sea gulfs.

It can be seen that there is a cycle of regression of the sea water between layers C9 – C5, where regressive bars are formed. This is followed by a cycle of transgression from layer C4 to C2, with transgressive bars. Regressive bars are again formed in layer C1. Layer B9 has a period of stability, or can be considered an intermediate stage and then another cycle of transgression occurs, between layers B9 and B2. In this cycle, there are some periods of waterflooding, but the major occurrence here is transgression and the formation of transgressive bars. B1 has regression of the seawater and regressive bar formation and from A9 to A1 has regular flow of the sea water, onto the shore and back into the sea with transgression being the dominant process. These trends are also evident in Fig. 23, described further below.

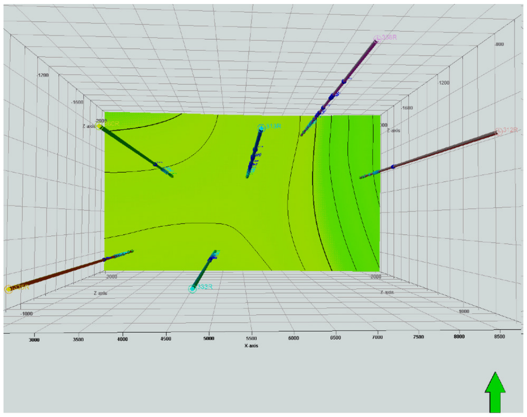
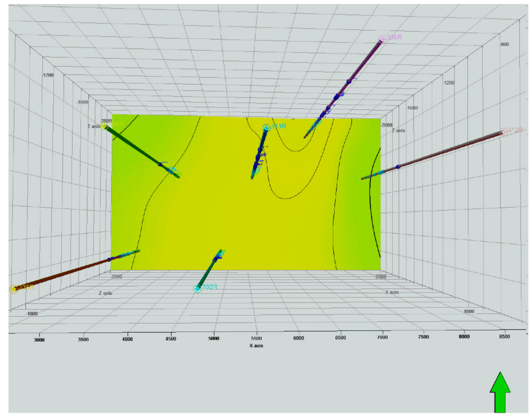

Top (a) Base

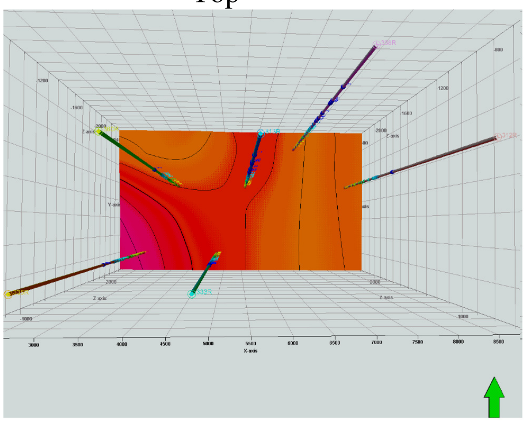
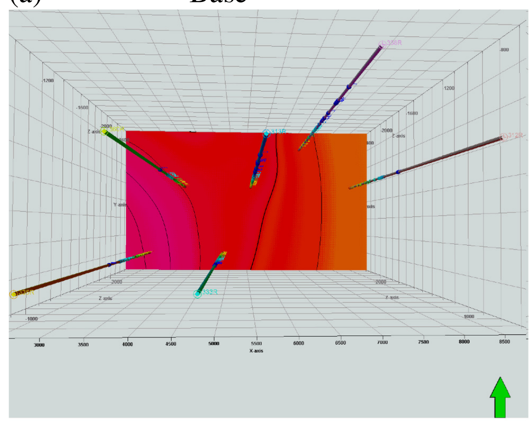

Top (b) Base

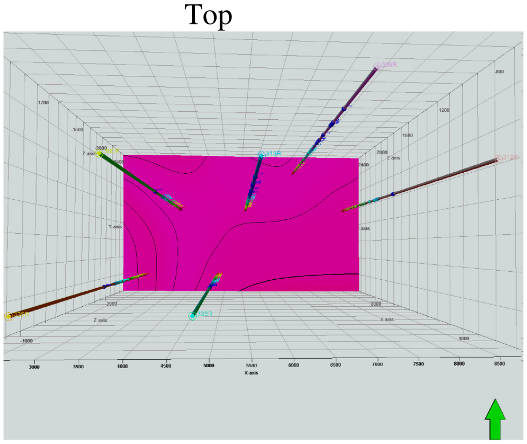
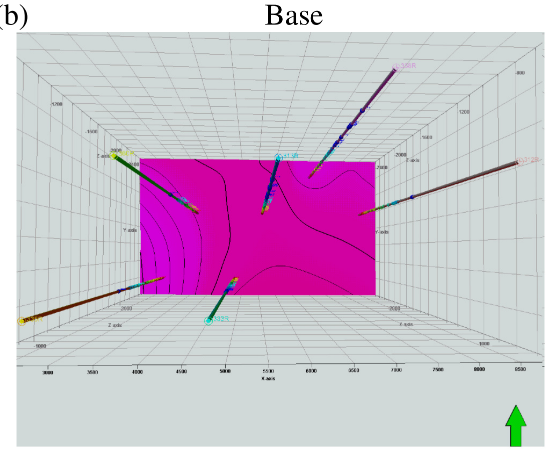

Top (c) Base

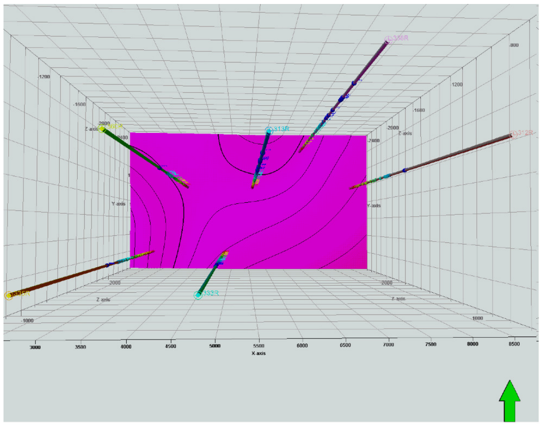
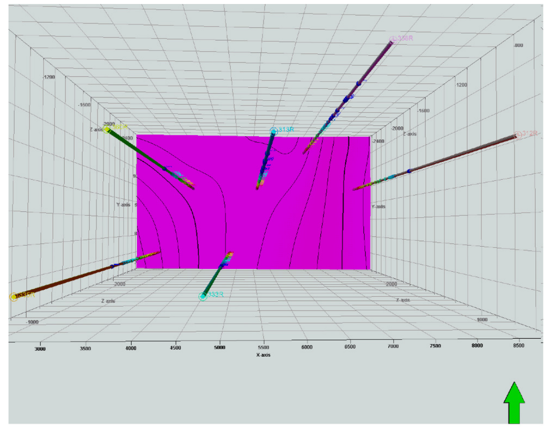

Top (d) Base

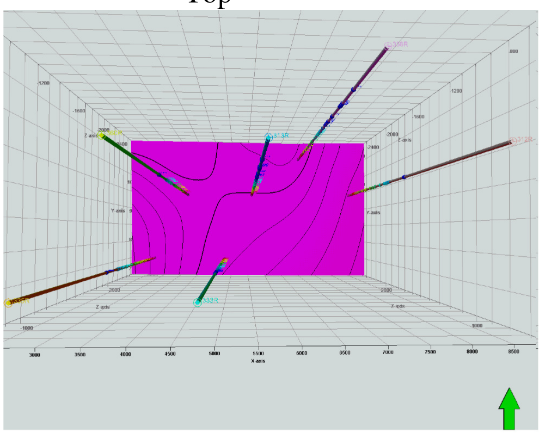
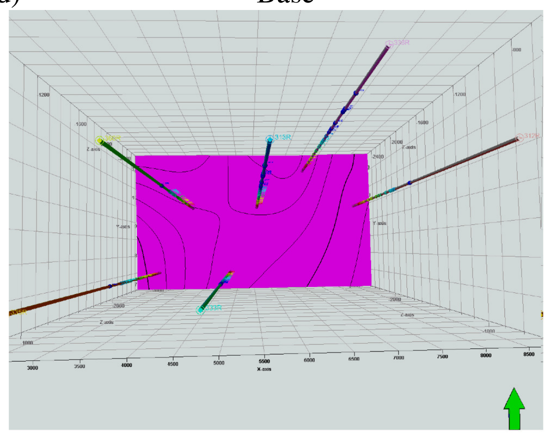

Top (e) Base

Fig. 22 Top and base contour lines for layers B5 (a), C1 (b), C4 (c), C6 (d) & C7 (e)

The contour lines here show the top and base description for select layers. These are layers where significant changes in the movement of the sea occurred, leading to the formation of distinct facies.

For example, with layer C7, the head parts of breaking currents are formed here, where unstable bars are present, and then the washouts of breaking currents. This is depicted in the top and base contour layers as there is a change in the region, seemingly a breakthrough, surrounding the first four wells.

6.5 Clay Volume

The SP log in *IP* was used to determine the clay volume. Even though it gives small deflections for thin layers, it is insensitive to other surrounding factors. Clay volume is important to calculate seeing that it takes up some of the pore space within rocks.

Table 11 Minimum, maximum and reference depth SP values for clay volume calculation

	335				360				333				313				338				312			
	SP				SP				SP				SP				SP				SP			
	Min	Max	Log	Ref. depth	Min	Max	Log	Ref. depth	Min	Max	Log	Ref. depth	Min	Max	Log	Ref. depth	Min	Max	Log	Ref. depth	Min	Max	Log	Ref. depth
A2	–	–	–	–	–	–	–	–	–	–	–	–	17	61	19	1150.6	27	71	29	1156.8	–	–	–	–
A3	–	–	–	–	–	–	–	–	–	–	–	–	26	66	27	1183.0	26	71	29	1178.6	–	–	–	–
A4	–	–	–	–	–	–	–	–	–	–	–	–	27	68	33	1333.0	19	71	24	1345.0	–	–	–	–
A5	44	89	49	1429.0	19	79	25	1414.4	12	65	26	1404.4	14	67	18	1429.4	16	75	19	1422.2	41	65	47	1407.2
A6	–	–	–	–	–	–	–	–	10	62	19	1456.4	17	68	18	1478.0	19	74	34	1478.6	–	–	–	–
A7	–	–	–	–	–	–	–	–	5	63	13	1542.0	17	68	22	1569.0	16	76	21	1546.2	–	–	–	–
A8	29	87	30	1625.4	6	81	15	1614.8	5	66	13	1606.0	15	67	20	1630.2	14	76	21	1617.9	52	67	56	1622.6
A9	44	89	63	1672.8	12	79	28	1641.0	5	65	11	1641.8	18	66	19	1669.0	23	76	25	1654.6	43	69	51	1657.0
B1	46	84	55	1722.8	14	83	31	1695.4	2	64	7	1693.0	16	67	21	1695.4	13	75	17	1692.0	35	70	49	1679.0
B2	25	89	33	1763.2	14	79	21	1765.2	2	64	19	1764.4	5	65	12	1756.2	6	79	15	1764.0	16	67	35	1745.2
B4	8	91	19	1910.0	24	87	28	1901.0	-2	68	13	1882.0	6	68	13	1879.0	4	79	11	1882.2	20	75	45	1857.0
B5	7	90	10	1984.4	-5	88	2	1982.6	-10	68	2	1996.2	2	71	9	2000.4	-6	81	-1	1976.3	13	78	21	1958.8
B6	7	89	9	2080.8	1	87	5	2047.0	-5	72	15	2043.8	-2	69	10	2049.0	4	84	7	2046.9	17	76	33	2025.4
B7	19	93	26	2123.0	-3	85	9	2089.2	14	71	20	2085.8	1	69	8	2114.6	-3	86	3	2113.8	17	76	27	2092.6
B8	2	91	11	2215.0	-3	87	14	2193.2	-15	74	-1	2176.4	-2	68	2	2188.2	-12	83	-7	2199.0	0	74	2	2184.8
B9	2	90	6	2271.4	-16	85	-10	2238.6	-13	74	-7	2228.0	-11	63	-7	2253.4	–	–	–	–	10	83	17	2233.6
C1	20	94	34	2319.8	-3	85	5	2287.0	-7	75	4	2296.0	-3	67	4	2295.0	-1	85	5	2291.5	19	84	14	2263.0
C2	1	93	5	2346.2	2	88	11	2312.8	-4	75	6	2328.2	-7	69	1	2333.4	-14	86	-9	2334.5	17	86	27	2314.0
C4	1	95	10	2402.0	-10	84	-1	2371.2	-12	76	1	2366.4	-5	69	1	2387.0	-14	86	-7	2400.0	9	87	16	2403.2
C5	22	93	30	2462.8	-2	59	2	2428.8	7	76	15	2429.8	2	71	17	2435.4	-11	89	2	2440.0	35	85	44	2417.6
C6	-9	80	3	2485.4	-12	84	3	2464.6	-8	76	1	2441.6	-12	56	-4	2474.6	-16	83	-1	2466.7	12	83	20	2439.8
C7	-6	84	8	2546.6	-5	82	1	2505.0	-3	76	2	2514.4	-6	71	14	2523.0	-15	88	3	2519.9	25	95	31	2491.4
C8	-7	94	24	2592.0	-8	87	2	2540.4	1	75	4	2551.4	3	72	4	2556.4	-18	57	-1	2556.8	25	94	40	2524.4
C9	-10	92	10	2622.4	-11	94	2	2580.2	-9	74	-1	2585.2	-3	70	4	2588.6	–	–	–	–	34	94	46	2598.0

Clay volume = $[SP_{clean} – SP_{log}] / [SP_{clean} – SP_{shale}]$ or [Min – log] / [Min – Max]
; where
Min = SP_{clean} (clean sandstone)
Max = SP_{shale}
log = Sp_{log}

Table 12 Clay and sand volumes for each layer of each well

Layer	335	360	333	313	338	312	Mean V_{sh}	Mean V_{sand} (1 – Mean V_{sh})
A2	–	–	–	0.045	0.045	–	0.045	0.955
A3	–	–	–	0.025	0.067	–	0.046	0.954
A4	–	–	–	0.146	0.096	–	0.121	0.879
A5	0.111	0.100	0.264	0.075	0.051	0.250	0.142	0.858
A6	–	–	0.173	0.020	0.273	–	0.155	0.845
A7	–	–	0.138	0.098	0.083	–	0.106	0.894
A8	0.017	0.120	0.131	0.096	0.113	0.267	0.124	0.876
A9	0.422	0.239	0.100	0.021	0.038	0.308	0.188	0.812
B1	0.237	0.246	0.081	0.098	0.065	0.400	0.188	0.812
B2	0.125	0.108	0.274	0.117	0.123	0.373	0.187	0.813
B4	0.133	0.063	0.214	0.113	0.093	0.455	0.179	0.822
B5	0.036	0.075	0.154	0.101	0.057	0.123	0.091	0.909
B6	0.024	0.047	0.260	0.169	0.038	0.271	0.135	0.865
B7	0.095	0.136	0.105	0.103	0.067	0.169	0.113	0.888
B8	0.101	0.189	0.157	0.057	0.053	0.027	0.097	0.903
B9	0.045	0.059	0.069	0.054	–	0.096	0.065	0.935
C1	0.189	0.091	0.134	0.100	0.070	0.071	0.085	0.916
C2	0.043	0.105	0.127	0.105	0.050	0.145	0.096	0.904
C4	0.096	0.096	0.148	0.081	0.070	0.090	0.097	0.903
C5	0.113	0.000	0.116	0.217	0.130	0.180	0.137	0.863
C6	0.135	0.156	0.107	0.118	0.152	0.113	0.130	0.870
C7	0.156	0.069	0.063	0.260	0.175	0.086	0.135	0.865
C8	0.307	0.105	0.041	0.014	0.227	0.217	0.152	0.848
C9	0.196	0.124	0.096	0.096	–	0.200	0.142	0.858

Clay volume can also be read from the *IP* program. The plot is generated from Interpretation – Clay Volume in *IP* and the clay volume values found at the same reference depth chosen for the log value of the SP for each layer of each well. There may be slight differences between the manual and *IP* clay volume values. This is because in general the manual calculation is an over estimation (assumes there is less clay volume than there really is) since it is based on the SSP, which is an estimated value. In addition to this, the calculation of clay volume from the equation uses one reference point depth whilst the calculation from IP uses the entire SP curve, consisting of several points, to obtain the clay volume. In this report, the manual calculation is used. Though not shown here, the values of clay volume from *IP* corroborated those obtained from the manual calculation.

6.5.1 Sand, Shale distribution of Facies Models

A2 resulting facies fractions:

Sand: 93.96 %
Shale: 6.04 %

A3 resulting facies fractions:

Sand: 95.19 %
Shale: 4.81 %

A4 resulting facies fractions:

Sand: 89.89 %
Shale: 10.11 %

A5 resulting facies fractions:

Sand: 82.58 %
Shale: 17.42 %

A6 resulting facies fractions:

Sand: 82.43 %
Shale: 17.57 %

A7 resulting facies fractions:

Sand: 83.92 %
Shale: 16.08 %

A8 resulting facies fractions:

Sand: 76.98 %
Shale: 23.02 %

A9 resulting facies fractions:

Sand: 77.41 %
Shale: 22.59 %

B1 resulting facies fractions:

Sand: 85.02 %
Shale: 14.98 %

B2 resulting facies fractions:

Sand: 79.01 %
Shale: 20.99 %

B4 resulting facies fractions:

Sand: 84.92 %
Shale: 15.08 %

B5 resulting facies fractions:

Sand: 89.71 %
Shale: 10.29 %

B6 resulting facies fractions:

Sand: 94.13 %
Shale: 5.87 %

B7 resulting facies fractions:

Sand: 84.76 %
Shale: 15.24 %

B8 resulting facies fractions:

Sand: 91.77 %
Shale: 8.23 %

B9 resulting facies fractions:

Sand: 97.35 %
Shale: 2.65 %

C1 resulting facies fractions:

Sand: 93.16 %
Shale: 6.84 %

C2 resulting facies fractions:

Sand: 85.65 %
Shale: 14.35 %

C4 resulting facies fractions:

Sand: 95.05 %
Shale: 4.95 %

C5 resulting facies fractions:

Sand: 93.76 %
Shale: 6.24 %

C6 resulting facies fractions:

Sand: 86.36 %
Shale: 13.64 %

C7 resulting facies fractions:

Sand: 79.71 %
Shale: 20.29 %

C8 resulting facies fractions:

Sand: 88.21 %
Shale: 11.79 %

C9 resulting facies fractions:

Sand: 84.29 %
Shale: 15.71 %

Above shows the sand-to-shale ratios for each layer, used to determine the facies models.

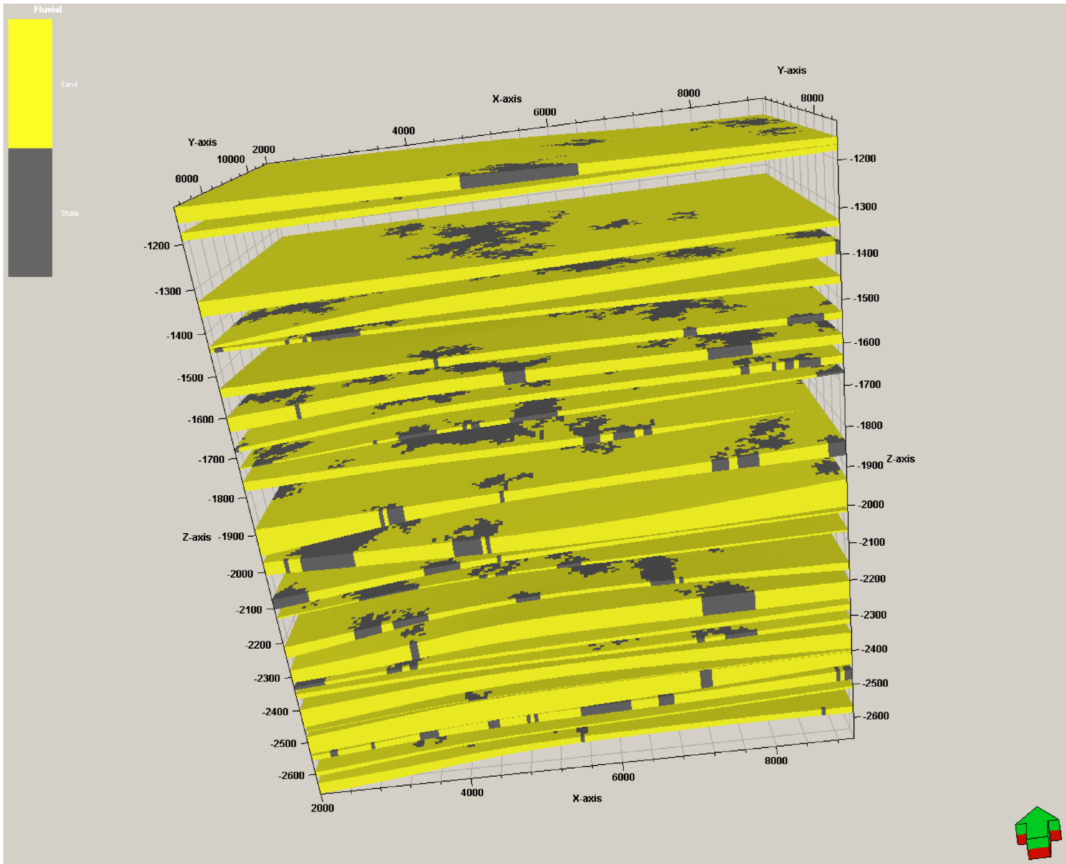

Fig. 23 Facies model of all sandstone units across the six wells

The figure above depicts each of the layers and their sand-shale distributions.

It shows the separation of sandstone bodies by shale. Shale located at depth of 2200m is moving west until about 2000m. In the next layer there seems to be some interruption where it disappears and reappears at about 1900m. There is again a repetition of this westward movement of shale up to about 1500m. These depictions, in general, match the trend of the facies analysis in Table 10.

Five representative layers are shown below to see how these facies models were determined separately.

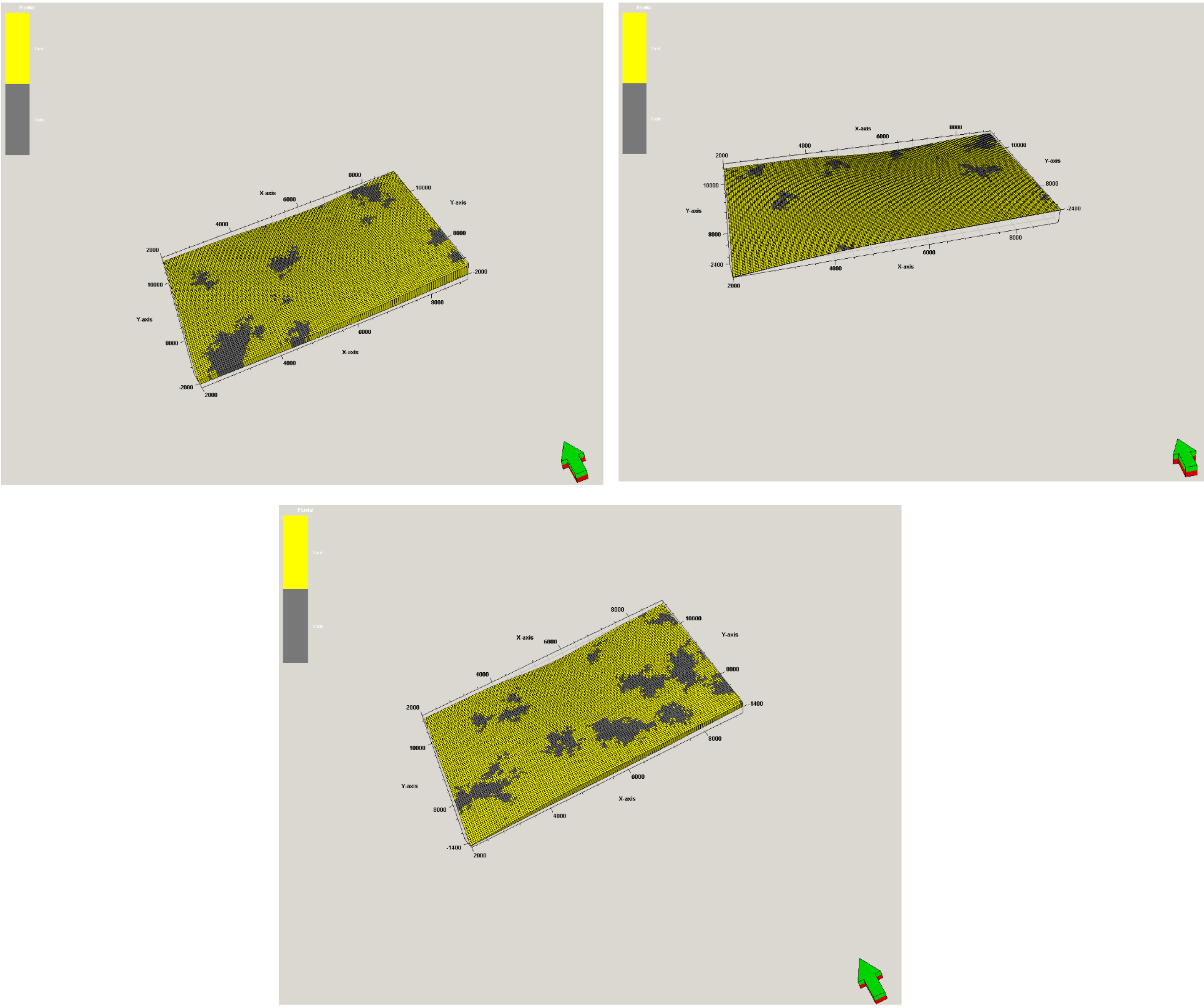

Fig. 24 Facies model representation of three layers (layers A5, B5 & C5)

7 Calculation of Petrophysical Parameters

7.1 Formation Water Resistivity & Salinity

These parameters were found using various Schlumberger charts as well as the SP log. Well 312R, in Table 13, will be used as an example in this chapter, with the information on the remaining five wells found in App. C

R_{xo} and R_t were found from the GZ2 and GZ4 resistivity plots in *IP* respectively.

After finding Essp from the SP log in IP, Schlumberger chart SP-1 is used to find R_{mfeq} and R_{weq} [see Fig. 25]

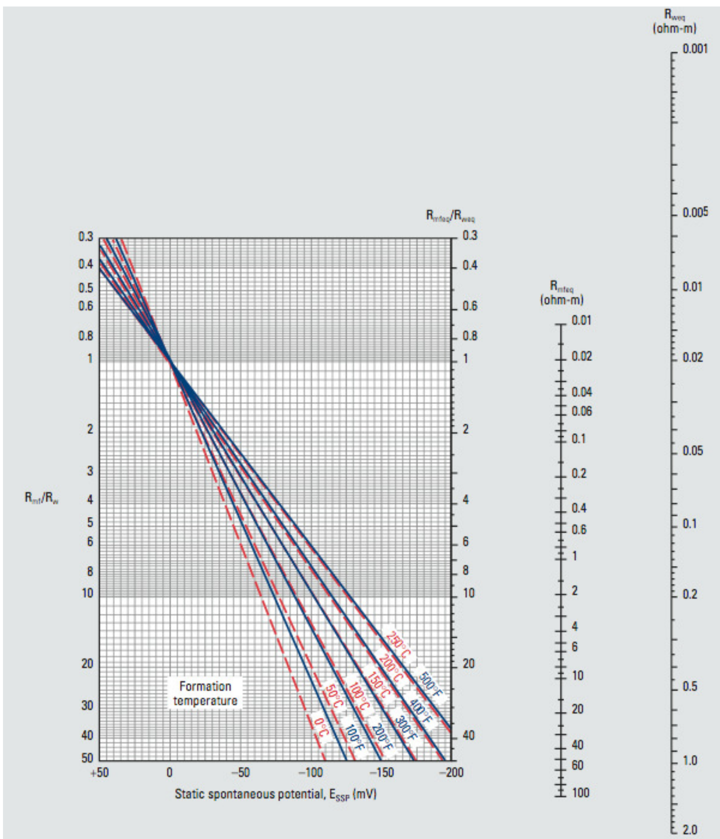

Fig. 25 R_{weq} and R_{mfeq} determination from E_{ssp} [42]

R_w is then found from R_{weq} using Schlumberger chart SP-3 below.

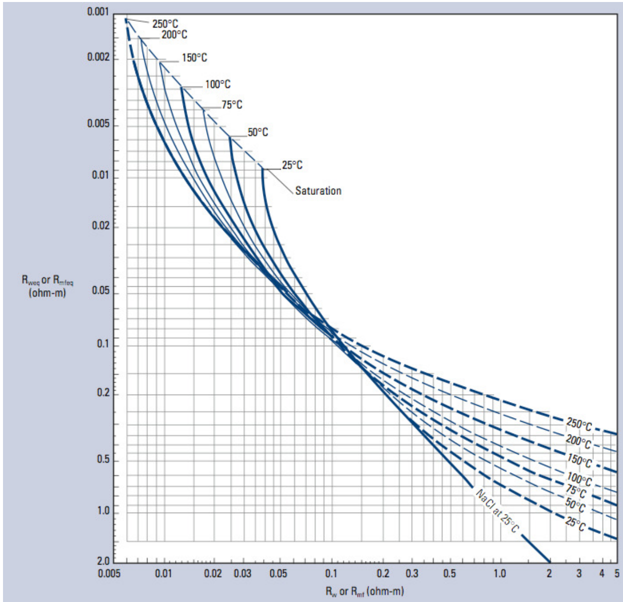

Fig. 26 R_{weq} vs R_w and formation temperature[42]

Using this value of R_w and Schlumberger Chart Gen-6, the salinity can be determined.

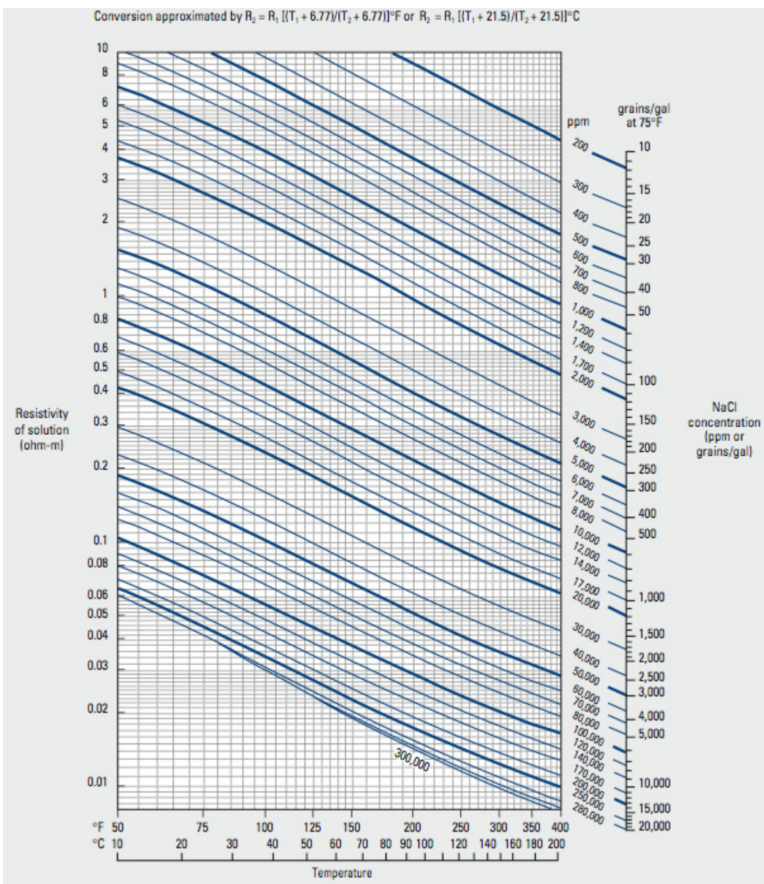

Fig. 27 Salinity determination from R_w and formation temperature[42]

Table 13 Resistivity and salinity information for Well 312R

Layer	ΔU_{sp} (mV)	Ref. depth	R_t (Ω-m)	R_m (Ω-m)	R_{mf} (Ω-m)	V_{sp}	$E_{ssp} = \Delta U_{sp}/V_{sp}$ (mV)	R_{mfeq}/R_{weq}	R_{mfeq} (Ω-m)	R_{weq} (Ω-m)	R_w (Ω-m)	Salinity (g/L)
A2	–	–	–	–	–	–	–	–	–	–	–	–
A3	–	–	–	–	–	–	–	–	–	–	–	–
A4	–	–	–	–	–	–	–	–	–	–	–	–
A5	-24	1407.2	4.78	3.0	2.4	1	-24	2.0	0.08	0.040	0.0475	65.0
A6	–	–	–	–	–	–	–	–	–	–	–	–
A7	–	–	–	–	–	–	–	–	–	–	–	–
A8	-15	1622.6	6.11	3.0	2.4	1	-15	1.6	0.06	0.034	0.0425	80.0
A9	-26	1657.0	6.64	3.0	2.4	1	-26	2.0	0.08	0.040	0.0475	65.0
B1	-35	1679.0	6.07	3.0	2.4	1	-35	2.6	0.15	0.058	0.0700	45.0
B2	-51	1745.2	13.3	3.0	2.4	1	-51	4.0	0.35	0.088	0.1000	30.0
B4	-55	1857.0	10.3	3.0	2.4	1	-55	4.6	0.50	0.109	0.1200	25.0
B5	-65	1958.8	3.47	3.0	2.4	1	-65	6.0	0.80	0.133	0.1400	20.0
B6	-59	2025.4	9.57	3.0	2.4	1	-59	5.2	0.60	0.115	0.1300	22.0
B7	-59	2092.6	10.1	3.0	2.4	1	-59	5.2	0.60	0.115	0.1300	22.0
B8	-74	2184.8	7.53	3.0	2.4	1	-74	8.0	1.36	0.170	0.2000	14.0
B9	-73	2233.6	4.43	3.0	2.4	1	-73	8.0	1.36	0.170	0.2000	14.0
C1	-65	2263.0	2.98	3.0	2.4	1	-65	6.0	0.80	0.133	0.1400	20.0
C2	-69	2314.0	3.76	3.0	2.4	1	-69	7.0	1.00	0.143	0.1500	18.5
C4	-78	2403.2	3.35	3.0	2.4	1	-78	9.0	1.62	0.180	0.2100	13.0
C5	-50	2417.6	4.3	3.0	2.4	1	-50	4.0	0.35	0.088	0.1000	30.0
C6	-71	2439.8	4.0	3.0	2.4	1	-71	7.0	1.00	0.143	0.1500	18.5
C7	-70	2491.4	9.02	3.0	2.4	1	-70	7.0	1.00	0.143	0.1500	18.5
C8	-69	2524.4	5.42	3.0	2.4	1	-69	7.0	1.00	0.143	0.1500	18.5
C9	-60	2598.0	11.0	3.0	2.4	1	-60	5.2	0.60	0.115	0.1300	22.0

7.2 Permeability

Permeability was found using porosity values, with the equation:

$k^{1/2} = (250 * \phi^3) / S_{wi}$

; where S_{wi} is the irreducible water saturation, here assumed to be the minimum value of 0.1

Table 14 Permeability information for Well 312R

312	Layer	ϕ	k
	A2	–	–
	A3	–	–
	A4	–	–
	A5	0.399	12.602
	A6	–	–
	A7	–	–
	A8	0.451	15.144
	A9	0.420	13.610
	B1	0.311	8.672
	B2	0.161	3.230
	B4	0.123	2.157
	B5	0.132	2.398
	B6	0.239	5.842
	B7	0.191	4.174
	B8	0.208	4.743
	B9	0.206	4.675
	C1	0.203	4.573
	C2	0.136	2.508
	C4	0.147	2.818
	C5	0.350	10.353
	C6	0.170	3.505
	C7	0.234	5.660
	C8	0.234	5.660
	C9	0.191	4.174

7.3 Porosity & Water Saturation

The Archie formulae were used to find porosity and water saturation, shown below.

Porosity, $\phi = [(a*R_{mf})/R_{xo}]^{1/m}$

Water Saturation, $S_w = [(a/\phi^m)*(R_w/R_t)]^{1/m}$

; where a=0.64 and m=1.74, which are the standard Schlumberger values used for porosity calculation.

Table 15 Porosity and water saturation information for Well 312R

Layer	Ref. depth	R_{mf} (Ω-m)	R_{xo} (Ω-m)	R_t (Ω-m)	R_w (Ω-m)	a	m	ϕ	S_w	$S_{hc} = 1-S_w$
A2	–	–	–	–	–	–	–	–	–	–
A3	–	–	–	–	–	–	–	–	–	–
A4	–	–	–	–	–	–	–	–	–	–
A5	1407.2	2.4	7.6	4.78	0.0475	0.64	1.74	0.399	0.137	0.863
A6	–	–	–	–	–	–	–	–	–	–
A7	–	–	–	–	–	–	–	–	–	–
A8	1622.6	2.4	6.15	6.11	0.0425	0.64	1.74	0.451	0.099	0.901
A9	1657.0	2.4	6.96	6.64	0.0475	0.64	1.74	0.420	0.108	0.892
B1	1679.0	2.4	11.7	6.07	0.0700	0.64	1.74	0.311	0.191	0.809
B2	1745.2	2.4	36.7	13.3	0.1000	0.64	1.74	0.161	0.288	0.712
B4	1857.0	2.4	58.6	10.3	0.1200	0.64	1.74	0.123	0.486	0.514
B5	1958.8	2.4	51.8	3.47	0.1400	0.64	1.74	0.132	0.924	0.076
B6	2025.4	2.4	18.5	9.57	0.1300	0.64	1.74	0.239	0.273	0.727
B7	2092.6	2.4	27.4	10.1	0.1300	0.64	1.74	0.191	0.332	0.668
B8	2184.8	2.4	23.7	7.53	0.2000	0.64	1.74	0.208	0.463	0.537
B9	2233.6	2.4	24.1	4.43	0.2000	0.64	1.74	0.206	0.635	0.365
C1	2263.0	2.4	24.7	2.98	0.1400	0.64	1.74	0.203	0.659	0.341
C2	2314.0	2.4	49.6	3.76	0.1500	0.64	1.74	0.136	0.895	0.105
C4	2403.2	2.4	43.4	3.35	0.2100	0.64	1.74	0.147	1.075	-0.075
C5	2417.6	2.4	9.56	4.3	0.1000	0.64	1.74	0.350	0.255	0.745
C6	2439.8	2.4	33.4	4.0	0.1500	0.64	1.74	0.170	0.688	0.312
C7	2491.4	2.4	19.2	9.02	0.1500	0.64	1.74	0.234	0.314	0.686
C8	2524.4	2.4	19.2	5.42	0.1500	0.64	1.74	0.234	0.420	0.580
C9	2598.0	2.4	27.3	11.0	0.1300	0.64	1.74	0.191	0.316	0.684

8 Discussion

8.1 Formation water resistivity

The formation water resistivity was calculated for each sandstone unit in each of the six wells using Schlumberger charts. [Figs. 25, 26] The values, in general, ranged between 0.1 and 0.2ohm-m. In addition Schlumberger Chart Gen-6 [Fig. 27] was used to find the corresponding salinities, which had quite a large range for Well 312R, between 13-80g/L.

R_w can be hard to determine due to several factors such as imperfect cationic membranes, R_w changes occurring below the oil-water contact, and long vertical transitions from fresh to salt water. For example, in some special areas, notably in Algeria and Nigeria and in mountainous areas, large variations in R_w from one bed to another, or even across oil-water contacts, result in SP anomalies and baseline shifts that make interpretation difficult.[4] This may therefore account for the difference in R_w values obtained between the sandstone units over the six wells.

8.2 Porosity

As stated, seeing that there was no available well log data for porosity determination – acoustic, sonic, neutronlogs – the Archie equation was used. The range of porosity values lay between 0.059 and 0.516. The overestimation of some of the higher values of porosity may have come from the sandstone layers chosen. The ‘a’ and ‘m’ values must also be carefully chosen, as these may drastically alter the porosity results. The values of 0.64 and 1.74 respectively were selected as the values that gave the best results for the porosity values. Clay volume was found to be less than 0.2 through all the sandstone units and this suggests that for the layers chosen, about 80% or more of the pore space was occupied by hydrocarbons. In Table 15 it is seen that for Well 312R, the average porosity value is about 0.24.

8.3 Permeability

Permeability ranged between 1 and 15mD for Well 312R. An average permeability value of 5.7mD was found across the six wells. As permeability is a measure of the interconnectedness of pore spaces, it is important to have a relatively good permeability to ensure the flow of hydrocarbons from areas around the injection wells towards the production wells. This value must be good regardless or whether or not a high porosity is found. The average permeability value here is quite good and can ensure the flow of hydrocarbons in at least some of the layers.

8.4 Water Saturation

The Archie formula, which utilises the porosity, was used to find S_w and eventually S_{hc}. The results suggested that majority of the layers contained some amounts of hydrocarbons, with most of the sandstone units having S_w less than 0.45, ie S_{hc} greater than 0.55. Some of the layers can be seen to have S_w greater than 1, thereby giving a negative S_{hc} value, which is not possible. Seeing that the water saturation calculation is directly related to the porosity for the Archie formula, the same overestimation found there can be explained here.

From Well 312R, shown in Table 15, it can be seen that only layers B5, B9, C1, C2, C4 and C6 are water-bearing, suggesting that the remaining 13 sandstone layers have some amounts of hydrocarbons within them.

Some of the sandstone units selected were not as clear and obvious throughout the six wells as others were. These were mainly located in the middle areas of the length of the well. Therefore the selection of these sandstone units may not have been as accurate as other units, and this may have been what caused certain overestimations in porosity and water saturation.

8.5 IP & Petrel

The map of the six wells, as mentioned, was created based on arbitrary co-ordinates. The placing of each of the wells was determined from the multi-well correlation plot in *IP*. The trace of the sandstone units through each of the wells gave an idea of their position relative to one another. Seeing that sandstone units were being analysed, the reference depths, as seen in Table 11, for each of the zone regions were chosen very carefully. They were selected as close as possible to the sandstone line of the SP log. This was analysed together with the resistivity curves. As it is known that a reservoir region most likely occurs where all the resistivity curves have a high value, as compared with other regions of the well, these were the areas considered for reference depth selection.

The facies models in *Petrel* give an idea of the amount of shale and sand there is distributed over each layer selected.

From Table 10, it can be seen that there are certain points at which there is a significant change in the movement of the sea that gives rise to the various facies that are obtained. These are also expressed in the contour slices, which reflect these changes. The facies give information about the type of rock present and this is invaluable information that can tell about where the potential hydrocarbon sites may be.

9 Conclusion

- The aim of this research was to analyse the six wells chosen from the Komso field and identify sandstone units for each well over each of their whole depths.
- Zonation was first done which isolated about 25 sandstone layers across the depths of the six fields
- Multi-well correlation between these six wells was then performed to link these layers and determine trends between the wells
- Mapping of the wells was done in addition to determining the tops and bases of each of the layers. These had shale bodies serving as a ‘barrier’ between them, as shown in Fig. 20
- 3D modelling was performed in *Petrel* and facies analysis carried out. 3 cycles can be identified in Fig. 23 as shale body movement, with the movement of sandstone between them. The first cycle moved from a depth of 2600m to 2000m, the next ranging from 1900m to 1500m and the last from 1400m to 1200m. There were mainly transgressive and regressive bars formed over the sandstone units, with some changes occurring at a few points – giving mouth bars, breaking currents and deltas. This strongly denotes the ever-changing movement of the seas and rivers.
- Formation water resistivity, R_w was calculated utilising Schlumberger charts. R_{mfeq} and R_{weq} needed to be found first, before finally determining R_w. This ranged in general between 0.04 and 0.25ohm-m, with some outliers and a salinity range of 10-30g/L, also with some outliers
- The Spontaneous Potential (SP) well log plots were used, together with reference depths, to determine the clay volume, which helped both in the facies analysis, and determination of the amount of pore space available for hydrocarbons. The resistivity curves were used in conjunction with SP, as seen in Fig. 19, in order to determine the reference depths used for this calculation
- Porosity was calculated using the Archie formula, with R_{mf} value 2.4ohm-m. This value, knowing the formation temperature of 75^{o}C, was found from the Fig. A1 in App. A. R_{xo} and R_t were determined from well logs and a reference depth – the GZ2 and GZ4 resistivity logs respectively. *a* and *m* were carefully selected, using Schlumberger standards. *a* was chosen as 0.64 and *m* chosen as 1.74. Porosity had an average value over all the layers and across the six wells of about 22%

- Permeability was calculated using and equation based on the porosity. This required a S_{wi} value, which was taken to be the minimum value of 0.1. The average permeability over all the layers and across all the wells was given to be about 5.7mD
- Water saturation was also determined using the Archie formula. This also utilised the porosity values, as well as formation water resistivity. A large number of each of the sandstone units for the six wells had hydrocarbon saturation larger than 55%, or a water saturation of less than 45%, which is a good estimation for the presence of oil and gas in the majority of the layers, suggesting that the Komso field is oil-saturated. Together with a true map of the field, and determination of the gross reservoir volume, the actual amount of oil in each well could be found and labelled as either an oil and gas field suited for commercial use or not.

10 References

1 Hearst JR, Nelson PH, Paillett FL. Well Logging for Physical Properties: A Handbook for Geophysicists, Geologists and Engineers. 2nd ed. New York: John Wiley & Sons Inc.; 2000

2 Glover P. *Petrophysique et Analyse géologique des diagraphies (Petrophysical and geological analysis of logs).* Petrophysics MSc. Course Notes. Département de Géologie et de Génie Géologique (Department of Geology and Geological Engineering), Université Laval, Canada; 2000

3 Natural Resources Canada. Borehole Geophysics and Petrophysics – Acoustic Logging. 2007. Geological Survey of Canada. Available from: http://gsc.nrcan.gc.ca/borehole/acoustic_e.php

4 Schlumberger. Log Interpretation Principles/Applications. Sugarland, Texas: Schlumberger Wireline & Testing; 1989

5 Geology Course Notes, Rudyk SN. Spring 2010

6 Schlumberger. The oilfield glossary: where the oil field meets the dictionary. Schlumberger Limited; 2011. Available from: http://www.glossary.oilfield.slb.com/

7 Serra O. Fundamentals of Well-Log Interpretation - The Acquisition of Logging Data. Volume 15, Part 1. Elsevier Inc.; 1984: 51-76

8 Henderson Petrophysics. Calculating formation water resistivity from the SP Log. 2009. Available from: http://www.hendersonpetrophysics.com/RW_SP.html

9 Henderson Petrophysics. Formation water resistivity (R_w) from resistivity ratio. 2009. Available from: http://www.hendersonpetrophysics.com/R_Ratio.html

10 Talash AW, Crawford PB. An improved method for calculating water resistivities from chemical analyses. J. Pet. Technol. 1965; 17 (12): 1396–1406

11 Patnode HW. Relationship of drilling mud resistivity to mud filtrate resistivity. J. Pet. Technol. 1949; 1 (1): 14–16

12 Archie GE. The electrical resistivity log as an aid in determining some reservoir characteristics. Trans. AIME. 1942; 31: 350–366

13 Moore EJ, Szaez SE and Whitney BC. Determining formation water resistivity from chemical analysis. J. Pet. Technol. 1966; 18 (3): 373–376.

14 Lyons WC, Plisga GJ. Standard Handbook of Petroleum and Natural Gas Engineering. 2nd Edition. UK: Elsevier Inc.; 2005: 1-225

15 MacLeod N. Stratigraphic principles, in Selley, R. C., Cocks, L. R. M., and Plimer, I. R., eds., Encyclopedia of geology: London, Academic Press, p. 295–307; 2005

16 Emery D, Myers K, Bertram GT. Seismic Stratigraphy, Chapter 3. MA, USA: Blackwell Science Ltd; 1996

17 "Chronostratigraphy." World of Earth Science. Ed. K. Lee Lerner and Brenda Wilmoth Lerner. Gale Cengage, 2003. eNotes.com. 2006. 3 Jun, 2011 http://www.enotes.com/earth-science/chronostratigraphy

18 Simmons MD, Berggren WA, Koshkarly RO, O'Neill BJ, Scott RW, Ziegler W. Biostratigraphy and Geochronology in the 21st Century. Paleo21. 1997

19 Reynolds JH. Magnetostratigraphy Adds a Temporal Dimension to Basin Analysis. Search and Discovery Article #40050 (2002)

20 Ramsayer GR. Seismic Stratigraphy, A Fundamental Exploration Tool. Offshore Technology Conference. 1979, Houston, Texas

21 Reading HG. Clastic facies models, a personal perspective. Bulletin of the Geological Society of Denmark Vol. 48, pp. 101–115. Copenhagen; 2001

22 Blick NC and Driscoll NW. Sequence Stratigraphy. Annual Review of Earth and Planetary Sciences, Vol. 23: 451-478; 1995

23 Everett L. Chronostratigraphy, Biochronology, Datum Events, Land Mammal Ages, Stage of Evolution, and Appearance Event Ordination. Bulletin of the American Museum of Natural History Number 279 :212-230; 2003

24 Norton M. Schematic diagram showing types of depositional environment. 2008. Available from: http://commons.wikimedia.org/wiki/File:SedimentaryEnvironment.jpg. Accessed on 04/06/2011

25 "Depositional Environments." World of Earth Science. Ed. K. Lee Lerner and Brenda Wilmoth Lerner. Gale Cengage, 2003. eNotes.com. 2006. 3 Jun, 2011 <http://www.enotes.com/earth-science/□depositional-environments>

26 Gore PJW. Sedimentary Environments Classification Charts. Georgia Perimeter College Copyright 1982-2004
Available from: http://facstaff.gpc.edu/~pgore/geology/historical_lab/environmentchart.htm. Accessed on 04/06/2011

27 American Geological Institute. *Dictionary of Geological Terms*. New York: Dolphin Books, 1962

28 NASA/GSFC/METI/ERSDAC/JAROS & U.S./Japan ASTER Science Team. Available from: http://asterweb.jpl.nasa.gov/gallery-detail.asp?name=fan. Accessed on 04/06/2011

29 "Delta." World of Earth Science. Ed. K. Lee Lerner and Brenda Wilmoth Lerner. Gale Cengage, 2003. eNotes.com. 2006. 4 Jun, 2011 <http://www.enotes.com/earth-science/delta>

30 Science Buzz, National Science Foundation. 2004-2011. Available from: http://www.sciencebuzz.org/blog/people-and-coastlines-cant-we-all-just-get-along. Accessed on 04/06/2011

31 "Continental Shelf." World of Earth Science. Ed. K. Lee Lerner and Brenda Wilmoth Lerner. Gale Cengage, 2003. eNotes.com. 2006. 4 Jun, 2011 <http://www.enotes.com/earth-science/continental-shelf>

32 Gross G M. Oceanography: A View of the Earth. Englewood Cliffs: Prentice-Hall, Inc., 1972

33 Biyokulule online. 2009. Available from: http://www.biyokulule.com/view_content.php?articleid=1871. Accessed on 04/06/2011

34 Perrodon A. Dynamics of Oil & Gas Accumulations. Elf Aquitaine et Masson. France; 1983

35 Pacific Gas and Electric Company. Science and Safety of Electricity & Natural Gas. Culverco, LLC; 2002. Available from: http://www.pgesafetyeducation.com/school/sseng/gas/index.html

36 Cosse R. Oil and gas field development techniques: Basics of reservoir engineering. Paris: Editions Technip; 1993

37 Schön JH, Georgi DT, Fanini ON. Deriving directional permeability. E&P. 2002

38 Iverson WP, Dunn TL, Ajdari I. Relative Permeability Anisotropy Measurements in Tensleep Sandstones. OnePetro. 1996

39 Report on Komso field

40 Gregory AP. Coal: Breaking oil’s chokehold. University of Kentucky Odyssey. 2007

41 Gore PJW. Sedimentary rocks, facies, transgressions and regressions, Walther’s law. Georgia Perimeter College. 1995-2009

42 Schlumberger. Log Interpretation Charts. 2009 Edition. Texas

43 Album of templates & graphs for well logging data interpretation. Voronovskaya. Moskow; 1994

11 Appendices

11.1 App. A

11.1.1 Determination of mudcake (R_{mc}) and mud filtrate (R_{mf}) resistivity

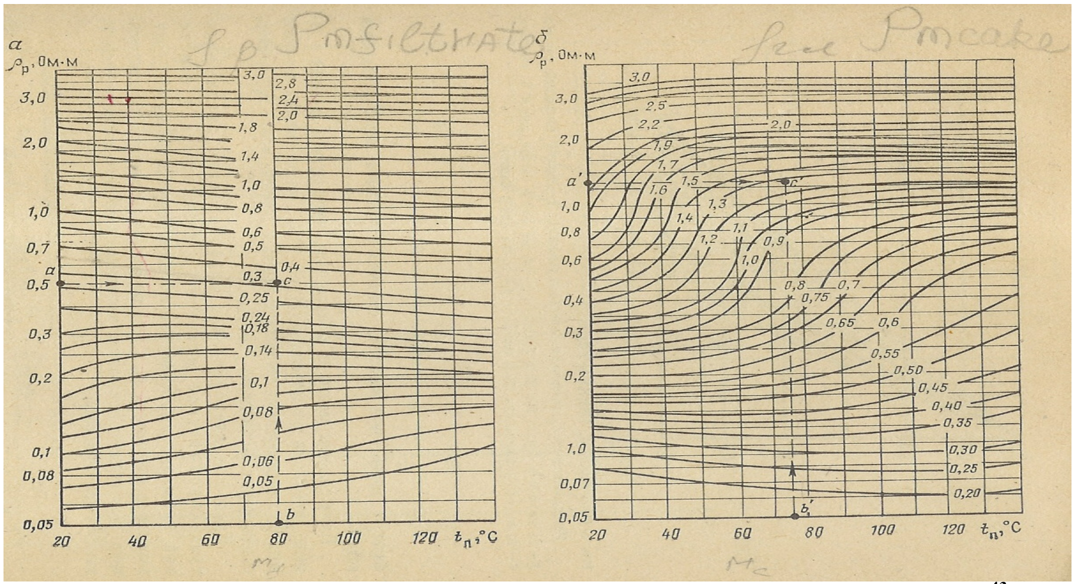

Fig. A 1 Graph for determination of R_{mf} (left) and R_{mc} (right) from formation temp. and R_{dm}[43]

11.1.2 Determination of resistivity of flushed zone, R_{xo}

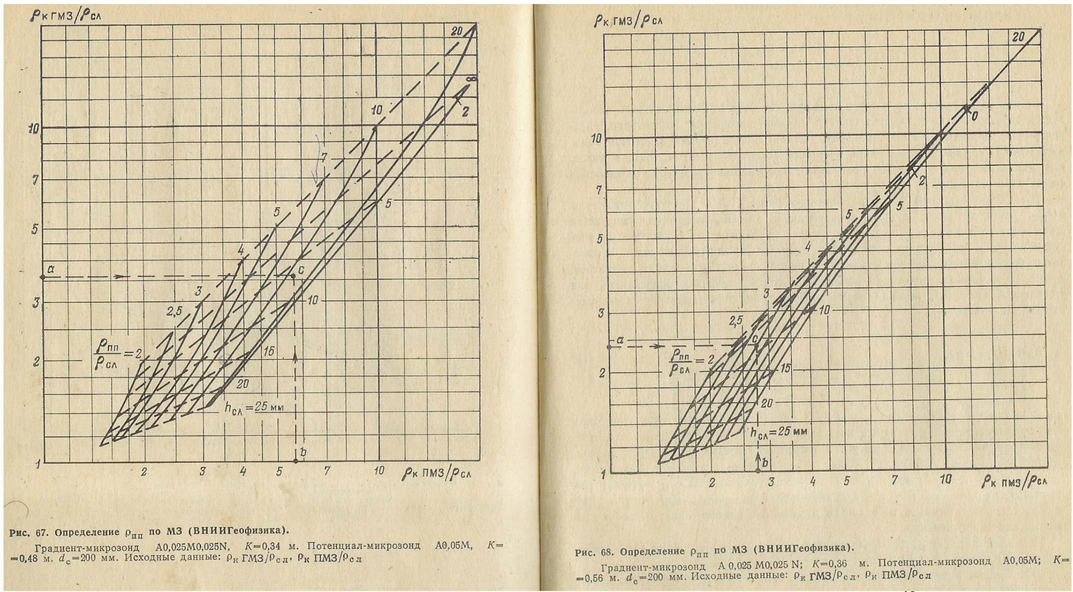

Fig. A 2 Graph of microsondes (microlateral vs micronormal) for R_{xo} determination[43]

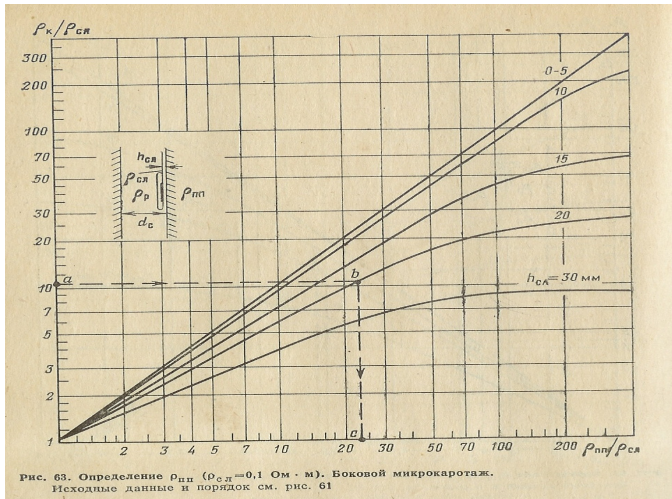

Fig. A 3 Graph of the shallow microlateral log for R_{xo} determination[43]

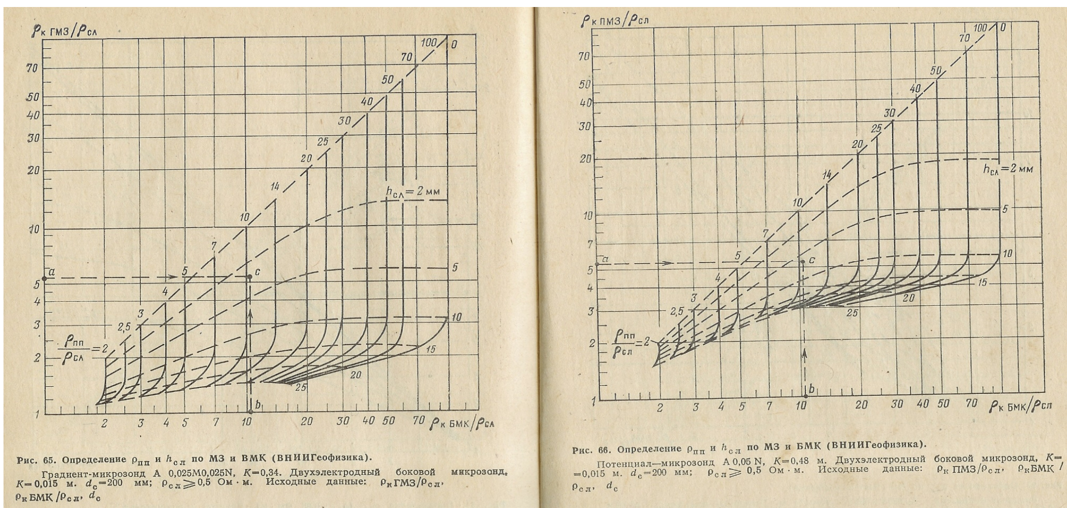

Fig. A 4 Graph of each microsonde vs the shallow microlateral log for R_{xo} determination[43]

For Fig A 2 to A 4, depending upon the design that is used, these graphs may differ slightly. This is seen from their *K* values, which indicate the design, and differ slightly between graphs.

11.2 App. B

11.2.1Facies

Table B 1 Various facies with accompanying vertical, horizontal and SP images

	Face	Vertical image	Horizontal image	SP image
1	Temporary flows (Proluvial)	The width of tens meters, thickness is 2-5 m. 	Area is hundreds of km^2. 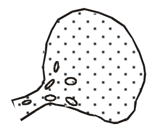	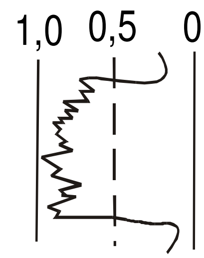
2	Shallow river bed of the straight rivers	Width is hundreds of meters, the thickness in axial part is up to 10 m. 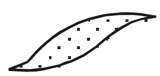	The length is tens km. 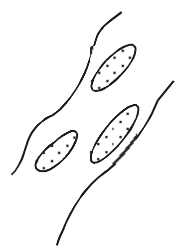	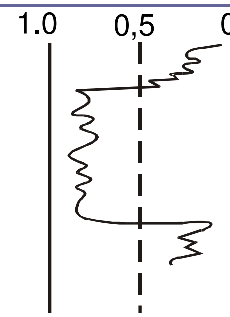
3	Shallow river bed of the branching rivers	Width is hundreds of meters, thickness is 3-10 m. 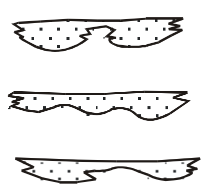	Length in hundreds and thousands km. 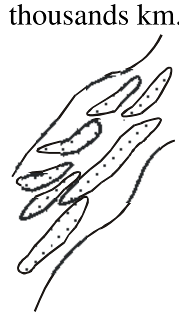	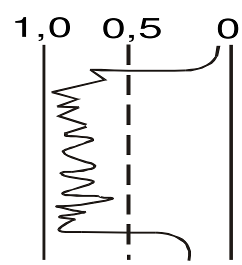
4	Shallow river bed of meandering rivers	Width is a few km. 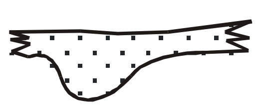	Length in hundreds and thousands km. 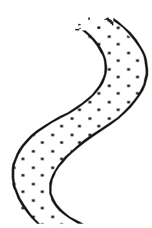	. 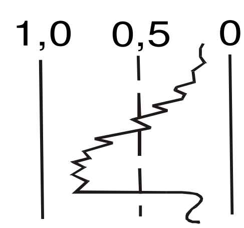

5	Shallow river bed of intensively meandering rivers	Width to tens of km. Thickness is 8-12 m. 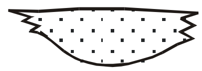	Stripes in hundreds of m or wide zones with the area of hundreds and thousands of km^2. 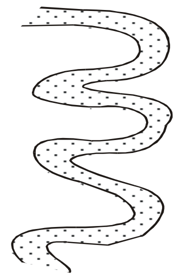	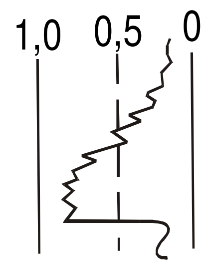
6	Beach ridges	Width 3-25 m. Thickness is 0,5-2,5 m. 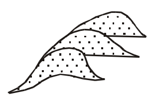	Length of tens of m and m. 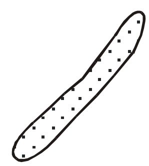	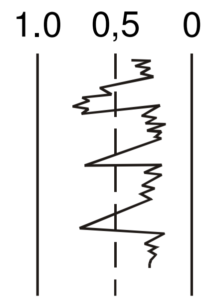
7		Width tens of m. Thickness is 5-6 m. 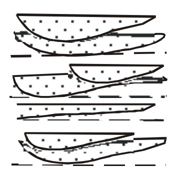	Hundreds of m. 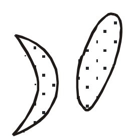	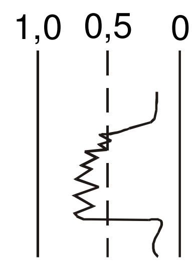
8		Width is:hundreds of m, tens of km. 	Area of hundreds and thousands of km^2 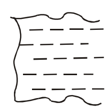	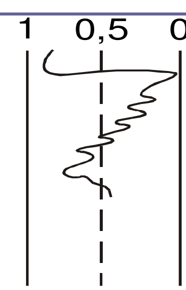

9	Floodplain rivers and lakes	Clays with sublayers of coal. Width is a few km. 	Tens of km. 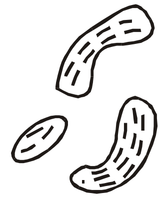	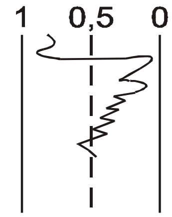
10	Underwater slope of delta	Width is from tens of m to km. Thickness is 40-70 m. 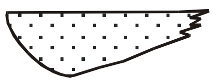	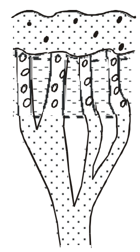	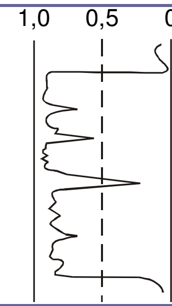
11	River dunes (eolian)	Width is 8-15m, height is 2-3 m. 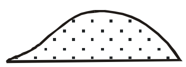	Length is tens and hundreds of m. 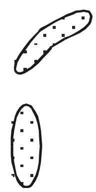	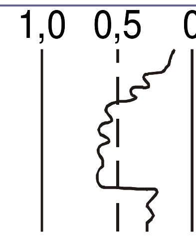
12	Mouth bar	Width is m and tens of km. Thickness is up to 10 m. 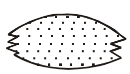	Area of tens and hundreds of km^2. 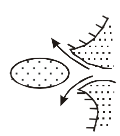	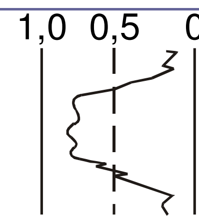
13	Beaches	Width is from m to km. Height is about 2 m. 	Length of tens of km 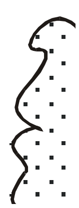	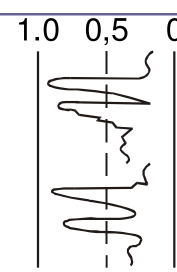

14	Along beach of transgressive bars and near-shore bank	Width is hundreds m, km. Height is up to 10m. 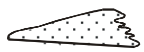	Length is tens and hundreds of km. 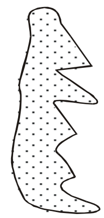	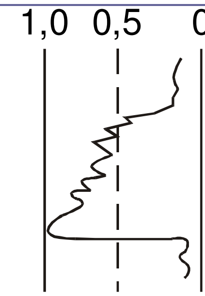
15	Near sea swamps, and marshes.	Width is km and tens of km. Thickness is 1-2 m. 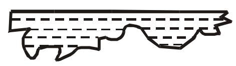	Coaly clay bodies. Area of tens and hundreds of km^2. 	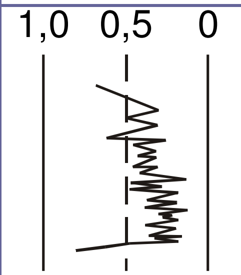
16	Along –beach regressive bars and near-shore banks.	Width is hundreds m, km. Height is up to 10m. 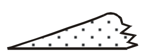	Length is tens and hundreds of km. 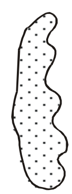	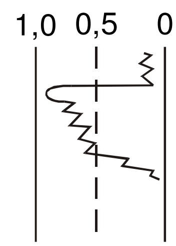
17	Barrier islands	Width m and tens of m, height is up to 10 m.	Length is tens and hundreds of km. 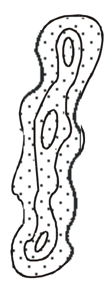	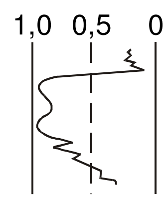

18	Lagoons behind bars during regression of marine basin	Width is tens of km. Thickness is up to 4 m. 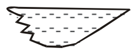	Area is tens and hundreds of km^2. 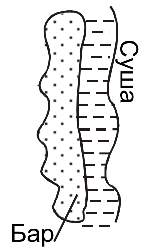	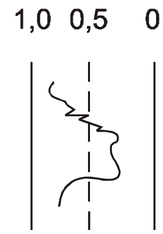
19	Lagoons behind bars during transgression of marine basin	Width is tens of km. Thickness is up to 4 m. 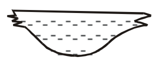	Area is tens and hundreds of km^2. 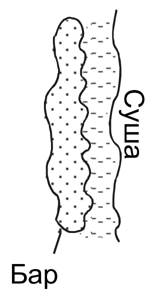	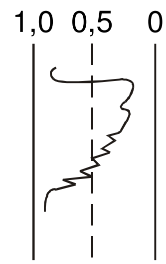
20	Gully riptide Washouts of breaking currents	Width is hundreds of m. Thickness is 1-2 m. 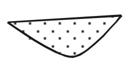	Area is tens of km^2. 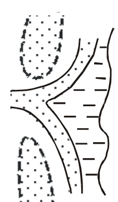	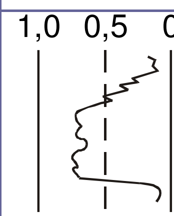
21	Head parts of breaking currents	Width is km and tens of km. Thickness is 2-5 m. 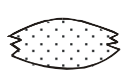	Area is hundreds of km^2. 	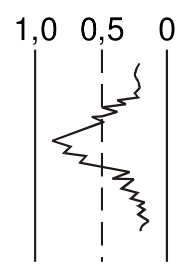

22	Valley of deltaic complex	Width is tens and hundreds of m. Thickness is 0,5-3,0 м. 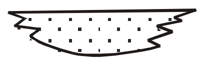	Area is tens and hundreds of km^2. 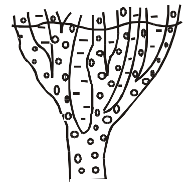	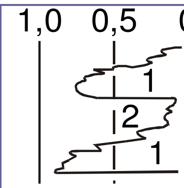
23	Sedimentary rocks of shallow shelf	Width is hundreds of m and km. Height is 10-40 m. Formed on the depth of 10-100 m. 	Area is tens of km^2. 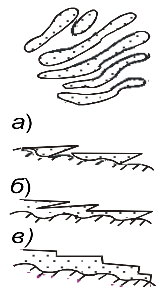	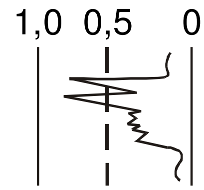
24	Open sea and large sea gulfs	Grey and green montmorillonite. Width is hundreds and thousands of km.Thickness is 50-200 m. 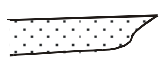	Hundreds and thousands of km^2 on the sea bottom. 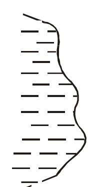	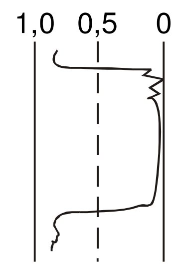

11.3 App. C

11.3.1 Formation Water Resistivity & Salinity data

Table C 1 Resistivity & Salinity data for Well 335R

Layer	ΔU_{sp} (mV)	Ref. depth	R_t (Ω-m)	R_m (Ω-m)	R_{mf} (Ω-m)	V_{sp}	$E_{ssp} = \Delta U_{sp}/V_{sp}$ (mV)	R_{mfeq}/R_{weq}	R_{mfeq} (Ω-m)	R_{weq} (Ω-m)	R_w (Ω-m)	Salinity (g/L)
A2	–	–	–	–	–	–	–	–	–	–	–	–
A3	–	–	–	–	–	–	–	–	–	–	–	–
A4	–	–	–	–	–	–	–	–	–	–	–	–
A5	-45	1429.0	2.76	3.0	2.4	1	-45	3.5	0.25	0.071	0.0850	37.0
A6	–	–	–	–	–	–	–	–	–	–	–	–
A7	–	–	–	–	–	–	–	–	–	–	–	–
A8	-58	1625.4	14.8	3.0	2.4	1	-58	5.2	0.60	0.115	0.1300	22.0
A9	-45	1672.8	14.8	3.0	2.4	1	-45	3.5	0.25	0.071	0.0850	37.0
B1	-38	1722.8	14.0	3.0	2.4	1	-38	3.0	0.20	0.067	0.0750	40.0
B2	-64	1763.2	5.23	3.0	2.4	1	-64	6.0	0.80	0.133	0.1400	20.0
B4	-83	1910.0	4.25	3.0	2.4	1	-83	11.0	2.50	0.227	0.3000	9.0
B5	-83	1984.4	12.1	3.0	2.4	1	-83	11.0	2.50	0.227	0.3000	9.0
B6	-82	2080.8	6.34	3.0	2.4	1	-82	9.0	1.62	0.180	0.2111	13.0
B7	-74	2123.0	2.93	3.0	2.4	1	-74	8.0	1.36	0.170	0.2000	14.0
B8	-89	2215.0	5.53	3.0	2.4	1	-89	12.0	3.00	0.250	0.3500	7.5
B9	-88	2271.4	6.76	3.0	2.4	1	-88	12.0	3.00	0.250	0.3500	7.5
C1	-74	2319.8	7.23	3.0	2.4	1	-74	8.0	1.36	0.170	0.2000	14.0
C2	-92	2346.2	1.31	3.0	2.4	1	-92	12.0	3.00	0.250	0.3500	7.5
C4	-94	2402.0	5.27	3.0	2.4	1	-94	14.0	4.00	0.289	0.4000	6.5
C5	-71	2462.8	11.4	3.0	2.4	1	-71	7.0	1.00	0.143	0.1500	18.5
C6	-89	2485.4	7.44	3.0	2.4	1	-89	12.0	3.00	0.250	0.3500	7.5
C7	-90	2546.6	8.00	3.0	2.4	1	-90	12.0	3.00	0.250	0.3500	7.5
C8	-101	2592.0	3.19	3.0	2.4	1	-101	17.0	6.00	0.353	0.6000	4.0
C9	-102	2622.4	9.1	3.0	2.4	1	-102	17.0	6.00	0.353	0.6000	4.0

Table C 2 Resistivity & Salinity data for Well 360R

Layer	ΔU_{sp} (mV)	Ref. depth	R_t (Ω-m)	R_m (Ω-m)	R_{mf} (Ω-m)	V_{sp}	$E_{ssp} = \Delta U_{sp}/V_{sp}$ (mV)	R_{mfeq}/R_{weq}	R_{mfeq} (Ω-m)	R_{weq} (Ω-m)	R_w (Ω-m)	Salinity (g/L)
A2	–	–	–	–	–	–	–	–	–	–	–	–
A3	–	–	–	–	–	–	–	–	–	–	–	–
A4	–	–	–	–	–	–	–	–	–	–	–	–
A5	-60	1414.4	6.73	3.0	2.4	1	-60	5.2	0.60	0.115	0.1300	22.0
A6	–	–	–	–	–	–	–	–	–	–	–	–
A7	–	–	–	–	–	–	–	–	–	–	–	–
A8	-75	1614.8	12.1	3.0	2.4	1	-75	8.0	1.36	0.170	0.2000	14.0
A9	-67	1641.0	11.4	3.0	2.4	1	-67	6.0	0.80	0.133	0.1400	20.0
B1	-69	1695.4	94.5	3.0	2.4	1	-69	7.0	1.00	0.143	0.1500	18.5
B2	-65	1765.2	15.9	3.0	2.4	1	-65	6.0	0.80	0.133	0.1400	20.0
B4	-63	1901.0	2.33	3.0	2.4	1	-63	6.0	0.80	0.133	0.1400	20.0
B5	-93	1982.6	10.7	3.0	2.4	1	-93	14.0	4.00	0.289	0.4000	6.5
B6	-86	2047.0	3.94	3.0	2.4	1	-86	11.0	2.50	0.227	0.3000	9.0
B7	-88	2089.2	2.96	3.0	2.4	1	-88	12.0	3.00	0.250	0.3500	7.5
B8	-90	2193.2	2.23	3.0	2.4	1	-90	12.0	3.00	0.250	0.3500	7.5
B9	-101	2238.6	5.11	3.0	2.4	1	-101	17.0	6.00	0.353	0.6000	4.0
C1	-88	2287.0	3.76	3.0	2.4	1	-88	12.0	3.00	0.250	0.3500	7.5
C2	-86	2312.8	1.12	3.0	2.4	1	-86	11.0	2.50	0.227	0.3000	9.0
C4	-94	2371.2	5.48	3.0	2.4	1	-94	14.0	4.00	0.289	0.4000	6.5
C5	-57	2428.8	7.26	3.0	2.4	1	-57	4.6	0.50	0.109	0.1200	25.0
C6	-96	2464.6	3.41	3.0	2.4	1	-96	14.0	4.00	0.289	0.4000	6.5
C7	-87	2505.0	9.95	3.0	2.4	1	-87	11.0	2.50	0.227	0.3000	9.0
C8	-95	2540.4	4.44	3.0	2.4	1	-95	14.0	4.00	0.289	0.4000	6.5
C9	-105	2580.2	4.69	3.0	2.4	1	-105	18.00	7.00	0.389	0.8000	3.0

Table C 3 Resistivity & Salinity data for Well 333R

Layer	ΔU_{sp} (mV)	Ref. depth	R_t (Ω-m)	R_m (Ω-m)	R_{mf} (Ω-m)	V_{sp}	$E_{ssp} = \Delta U_{sp}/V_{sp}$ (mV)	R_{mfeq}/R_{weq}	R_{mfeq} (Ω-m)	R_{weq} (Ω-m)	R_w (Ω-m)	Salinity (g/L)
A2	–	–	–	–	–	–	–	–	–	–	–	–
A3	–	–	–	–	–	–	–	–	–	–	–	–
A4	–	–	–	–	–	–	–	–	–	–	–	–
A5	-53	1404.4	13.9	3.0	2.4	1	-53	4.6	0.50	0.109	0.1200	25.0
A6	-52	1456.4	4.00	3.0	2.4	1	-52	4.0	0.35	0.088	0.1000	30.0
A7	-58	1542.0	6.5	3.0	2.4	1	-58	5.2	0.60	0.115	0.1300	22.0
A8	-61	1606.0	5.83	3.0	2.4	1	-61	5.2	0.60	0.115	0.1300	22.0
A9	-60	1641.8	8.71	3.0	2.4	1	-60	5.2	0.60	0.115	0.1300	22.0
B1	-62	1693.0	3.41	3.0	2.4	1	-62	5.2	0.60	0.115	0.1300	22.0
B2	-62	1764.4	12.0	3.0	2.4	1	-62	5.2	0.60	0.115	0.1300	22.0
B4	-70	1882.0	9.04	3.0	2.4	1	-70	7.0	1.00	0.143	0.1500	18.5
B5	-78	1996.2	24.5	3.0	2.4	1	-78	9.0	1.62	0.180	0.2100	13.0
B6	-77	2043.8	7.92	3.0	2.4	1	-77	8.0	1.36	0.170	0.2000	14.0
B7	-57	2085.8	5.58	3.0	2.4	1	-57	4.6	0.50	0.109	0.1200	25.0
B8	-89	2176.4	3.83	3.0	2.4	1	-89	12.0	3.00	0.250	0.3500	7.5
B9	-87	2228.0	10.7	3.0	2.4	1	-87	11.0	2.50	0.227	0.3000	9.0
C1	-82	2296.0	3.21	3.0	2.4	1	-82	9.0	1.62	0.180	0.2100	13.0
C2	-79	2328.2	4.0	3.0	2.4	1	-79	9.0	1.62	0.180	0.2100	13.0
C4	-88	2366.4	7.17	3.0	2.4	1	-88	12.0	3.00	0.250	0.3500	7.5
C5	-69	2429.8	4.46	3.0	2.4	1	-69	7.0	1.00	0.143	0.1500	18.5
C6	-84	2441.6	3.21	3.0	2.4	1	-84	11.0	2.50	0.227	0.3000	9.0
C7	-79	2514.4	9.5	3.0	2.4	1	-79	9.0	1.62	0.180	0.2100	13.0
C8	-74	2551.4	8.29	3.0	2.4	1	-74	8.0	1.36	0.170	0.2000	14.0
C9	-83	2585.2	6.0	3.0	2.4	1	-83	11.0	2.50	0.227	0.3000	9.0

Table C 4 Resistivity & Salinity data for Well 313R

Layer	ΔU_{sp} (mV)	Ref. depth	R_t (Ω-m)	R_m (Ω-m)	R_{mf} (Ω-m)	V_{sp}	$E_{ssp} = \Delta U_{sp}/V_{sp}$ (mV)	R_{mfeq}/R_{weq}	R_{mfeq} (Ω-m)	R_{weq} (Ω-m)	R_w (Ω-m)	Salinity (g/L)
A2	-44	1150.6	2.38	3.0	2.4	1	-44	3.5	0.25	0.071	0.0850	37.0
A3	-40	1183.0	2.57	3.0	2.4	1	-40	3.0	0.20	0.067	0.0750	40.0
A4	-41	1333.0	2.22	3.0	2.4	1	-41	3.0	0.20	0.067	0.0750	40.0
A5	-53	1429.4	4.19	3.0	2.4	1	-53	4.6	0.50	0.109	0.1200	25.0
A6	-51	1478.0	2.36	3.0	2.4	1	-51	4.0	0.35	0.088	0.1000	30.0
A7	-51	1569.0	2.22	3.0	2.4	1	-51	4.0	0.35	0.088	0.1000	30.0
A8	-52	1630.2	2.92	3.0	2.4	1	-52	4.0	0.35	0.088	0.1000	30.0
A9	-48	1669.0	3.56	3.0	2.4	1	-48	4.0	0.35	0.088	0.1000	30.0
B1	-51	1695.4	2.36	3.0	2.4	1	-51	4.0	0.35	0.088	0.1000	30.0
B2	-60	1756.2	10.8	3.0	2.4	1	-60	5.2	0.60	0.115	0.1300	22.0
B4	-62	1879.0	10.7	3.0	2.4	1	-62	5.2	0.60	0.115	0.1300	22.0
B5	-69	2000.4	1.71	3.0	2.4	1	-69	7.0	1.00	0.143	0.1500	18.5
B6	-71	2049.0	4.0	3.0	2.4	1	-71	7.0	1.00	0.143	0.1500	18.5
B7	-68	2114.6	4.35	3.0	2.4	1	-68	7.0	1.00	0.143	0.1500	18.5
B8	-70	2188.2	4.67	3.0	2.4	1	-70	7.0	1.00	0.143	0.1500	18.5
B9	-74	2253.4	4.5	3.0	2.4	1	-74	8.0	1.36	0.170	0.2000	14.0
C1	-70	2295.0	1.12	3.0	2.4	1	-70	7.0	1.00	0.143	0.1500	18.5
C2	-76	2333.4	3.94	3.0	2.4	1	-76	8.0	1.36	0.170	0.2000	14.0
C4	-74	2387.0	5.19	3.0	2.4	1	-74	8.0	1.36	0.170	0.2000	14.0
C5	-69	2435.4	4.46	3.0	2.4	1	-69	7.0	1.00	0.143	0.1500	18.5
C6	-68	2474.6	7.71	3.0	2.4	1	-68	7.0	1.00	0.143	0.1500	18.5
C7	-77	2523.0	9.99	3.0	2.4	1	-77	8.0	1.36	0.170	0.2000	14.0
C8	-69	2556.4	9.71	3.0	2.4	1	-69	7.0	1.00	0.143	0.1500	18.5
C9	-73	2588.6	16.8	3.0	2.4	1	-73	8.0	1.36	0.170	0.2000	14.0

Table C 5 Resistivity & Salinity data for Well 338R

Layer	ΔU_{sp} (mV)	Ref. depth	R_t (Ω-m)	R_m (Ω-m)	R_{mf} (Ω-m)	V_{sp}	$E_{ssp} = \Delta U_{sp}/V_{sp}$ (mV)	R_{mfeq}/R_{weq}	R_{mfeq} (Ω-m)	R_{weq} (Ω-m)	R_w (Ω-m)	Salinity (g/L)
A2	-44	1156.8	3.82	3.0	2.4	1	-44	3.5	0.25	0.071	0.0850	37.0
A3	-45	1178.6	3.02	3.0	2.4	1	-45	3.5	0.25	0.071	0.0850	37.0
A4	-52	1345.0	3.06	3.0	2.4	1	-52	4.0	0.35	0.088	0.1000	30.0
A5	-59	1422.2	4.44	3.0	2.4	1	-59	5.2	0.60	0.115	0.1300	22.0
A6	-55	1478.6	3.56*	3.0	2.4	1	-55	4.6	0.50	0.109	0.1200	25.0
A7	-60	1546.2	2.68*	3.0	2.4	1	-60	5.2	0.60	0.115	0.1300	22.0
A8	-62	1617.9	4.78	3.0	2.4	1	-62	5.2	0.60	0.115	0.1300	22.0
A9	-53	1654.6	3.02	3.0	2.4	1	-53	4.6	0.50	0.109	0.1200	25.0
B1	-62	1692.0	3.44	3.0	2.4	1	-62	5.2	0.60	0.115	0.1300	22.0
B2	-73	1764.0	1.8	3.0	2.4	1	-73	8.0	1.36	0.170	0.2000	14.0
B4	-75	1882.2	9.27	3.0	2.4	1	-75	8.0	1.36	0.170	0.2000	14.0
B5	-87	1976.3	11.3/.8	3.0	2.4	1	-87	11.0	2.50	0.227	0.3000	9.0
B6	-80	2046.9	8.43	3.0	2.4	1	-80	9.0	1.62	0.180	0.2100	13.0
B7	-89	2113.8	2.72	3.0	2.4	1	-89	12.0	3.00	0.250	0.3500	7.5
B8	-95	2199.0	3.52	3.0	2.4	1	-95	14.0	4.00	0.289	0.4000	6.5
B9	–	–	–	–	–	–	–	–	–	–	–	–
C1	-86	2291.5	3.35	3.0	2.4	1	-86	11.0	2.50	0.227	0.3000	9.0
C2	-100	2334.5	4.02	3.0	2.4	1	-100	17.0	6.00	0.353	0.6000	4.0
C4	-100	2400.0	0.504	3.0	2.4	1	-100	17.0	6.00	0.353	0.6000	4.0
C5	-100	2440.0	1.84	3.0	2.4	1	-100	17.0	6.00	0.353	0.6000	4.0
C6	-99	2466.7	3.23	3.0	2.4	1	-99	17.0	6.00	0.353	0.6000	4.0
C7	-103	2519.9	4.19	3.0	2.4	1	-103	18.00	7.00	0.389	0.8000	3.0
C8	-75	2556.8	8.22	3.0	2.4	1	-75	8.0	1.36	0.170	0.2000	14.0
C9	–	–	–	–	–	–	–	–	–	–	–	–

11.4 App. D

11.4.1 Permeability data

Table D 1 Permeability data for wells 335R, 360R, 333R, 313R and 338R

335R	Layer	ϕ	k
	A2	–	–
	A3	–	–
	A4	–	–
	A5	0.448	14.993
	A6	–	–
	A7	–	–
	A8	0.093	1.418
	A9	0.288	7.728
	B1	0.323	9.179
	B2	0.168	3.443
	B4	0.095	1.464
	B5	0.092	1.395
	B6	0.091	1.373
	B7	0.238	5.805
	B8	0.093	1.418
	B9	0.092	1.395
	C1	0.397	12.507
	C2	0.134	2.453
	C4	0.092	1.395
	C5	0.159	3.170
	C6	0.093	1.418
	C7	0.140	2.619
	C8	0.185	3.979
	C9	0.094	1.441

360R	Layer	ϕ	k
	A2	–	–
	A3	–	–
	A4	–	–
	A5	0.117	2.001
	A6	–	–
	A7	–	–
	A8	0.075	1.027
	A9	0.108	1.775
	B1	0.070	0.926
	B2	0.101	1.605
	B4	0.248	6.175
	B5	0.060	0.735
	B6	0.205	4.641
	B7	0.219	5.124
	B8	0.234	5.660
	B9	0.118	2.027
	C1	0.218	5.089
	C2	0.229	5.479
	C4	0.141	2.647
	C5	0.168	3.443
	C6	0.219	5.124
	C7	0.101	1.605
	C8	0.292	7.889
	C9	0.121	2.104

333R	Layer	ϕ	k
	A2	–	–
	A3	–	–
	A4	–	–
	A5	0.102	1.629
	A6	0.152	2.963
	A7	0.062	0.772
	A8	0.183	3.914
	A9	0.171	3.536
	B1	0.250	6.250
	B2	0.121	2.104
	B4	0.211	4.846
	B5	0.064	0.810
	B6	0.126	2.236
	B7	0.227	5.408
	B8	0.208	4.743
	B9	0.073	0.986
	C1	0.208	4.743
	C2	0.246	6.101
	C4	0.154	3.022
	C5	0.218	5.089
	C6	0.261	6.667
	C7	0.111	1.849
	C8	0.140	2.619
	C9	0.119	2.053

313R	Layer	ϕ	k
	A2	0.328	9.392
	A3	0.318	8.966
	A4	0.304	8.381
	A5	0.173	3.598
	A6	0.244	6.026
	A7	0.217	5.054
	A8	0.283	7.527
	A9	0.292	7.889
	B1	0.218	5.089
	B2	0.168	3.443
	B4	0.070	0.926
	B5	0.213	4.915
	B6	0.132	2.398
	B7	0.264	6.782
	B8	0.119	2.053
	B9	0.051	0.576
	C1	0.141	2.647
	C2	0.116	1.975
	C4	0.128	2.290
	C5	0.429	14.049
	C6	0.125	2.210
	C7	0.076	1.048
	C8	0.149	2.876
	C9	0.100	1.581

338R	Layer	ϕ	k
	A2	0.465	15.854
	A3	0.516	18.533
	A4	0.492	17.255
	A5	0.193	4.239
	A6	0.454	15.295
	A7	0.382	11.805
	A8	0.347	10.220
	A9	0.330	9.479
	B1	0.275	7.211
	B2	0.296	8.052
	B4	0.081	1.153
	B5	0.059	0.717
	B6	0.095	1.464
	B7	0.279	7.368
	B8	0.203	4.573
	B9	–	–
	C1	0.192	4.207
	C2	0.175	3.660
	C4	0.284	7.567
	C5	0.293	7.930
	C6	0.258	6.552
	C7	0.254	6.401
	C8	0.136	2.508
	C9	–	–

11.5 App. E

11.5.1 Porosity & Water Saturation data

Table E 1 Porosity & Water Saturation data for Well 335R

Layer	Ref. depth	R_{mf} (Ω-m)	R_{xo} (Ω-m)	R_t (Ω-m)	R_w (Ω-m)	a	m	ϕ	S_w	$S_{hc} = 1-S_w$
A2	–	–	–	–	–	–	–	–	–	–
A3	–	–	–	–	–	–	–	–	–	–
A4	–	–	–	–	–	–	–	–	–	–
A5	1429.0	2.4	6.21	2.76	0.0850	0.64	1.74	0.448	0.234	0.766
A6	–	–	–	–	–	–	–	–	–	–
A7	–	–	–	–	–	–	–	–	–	–
A8	1625.4	2.4	96.3	14.8	0.1300	0.64	1.74	0.093	0.549	0.451
A9	1672.8	2.4	13.4	14.8	0.0850	0.64	1.74	0.288	0.138	0.862
B1	1722.8	2.4	11.0	14.0	0.0750	0.64	1.74	0.323	0.119	0.881
B2	1763.2	2.4	34.2	5.23	0.1400	0.64	1.74	0.168	0.575	0.425
B4	1910.0	2.4	91.5	4.25	0.3000	0.64	1.74	0.095	1.766	-0.766
B5	1984.4	2.4	97.4	12.1	0.3000	0.64	1.74	0.092	1.004	-0.004
B6	2080.8	2.4	98.7	6.34	0.2111	0.64	1.74	0.091	1.198	-0.198
B7	2123.0	2.4	18.7	2.93	0.2000	0.64	1.74	0.238	0.696	0.304
B8	2215.0	2.4	96.1	5.53	0.3500	0.64	1.74	0.093	1.706	-0.706
B9	2271.4	2.4	98.5	6.76	0.3500	0.64	1.74	0.092	1.542	-0.542
C1	2319.8	2.4	7.66	7.23	0.2000	0.64	1.74	0.397	0.248	0.752
C2	2346.2	2.4	50.8	1.31	0.3500	0.64	1.74	0.134	2.707	-1.707
C4	2402.0	2.4	98.1	5.27	0.4000	0.64	1.74	0.092	1.917	-0.917
C5	2462.8	2.4	37.8	11.4	0.1500	0.64	1.74	0.159	0.405	0.595
C6	2485.4	2.4	96.1	7.44	0.3500	0.64	1.74	0.093	1.439	-0.439
C7	2546.6	2.4	47.0	8.00	0.3500	0.64	1.74	0.140	0.915	0.085
C8	2592.0	2.4	28.9	3.19	0.6000	0.64	1.74	0.185	1.600	-0.600
C9	2622.4	2.4	93.2	9.1	0.6000	0.64	1.74	0.094	1.717	-0.717

Table E 2 Porosity & Water Saturation data for Well 360R

Layer	Ref. depth	R_{mf} (Ω-m)	R_{xo} (Ω-m)	R_t (Ω-m)	R_w (Ω-m)	a	m	ϕ	S_w	$S_{hc} = 1-S_w$
A2	–	–	–	–	–	–	–	–	–	–
A3	–	–	–	–	–	–	–	–	–	–
A4	–	–	–	–	–	–	–	–	–	–
A5	1414.4	2.4	64.2	6.73	0.1300	0.64	1.74	0.117	0.684	0.316
A6	–	–	–	–	–	–	–	–	–	–
A7	–	–	–	–	–	–	–	–	–	–
A8	1614.8	2.4	138	12.1	0.2000	0.64	1.74	0.075	0.971	0.029
A9	1641.0	2.4	74.1	11.4	0.1400	0.64	1.74	0.108	0.573	0.427
B1	1695.4	2.4	158	94.5	0.150	0.64	1.74	0.070	0.273	0.727
B2	1765.2	2.4	82.6	15.9	0.1400	0.64	1.74	0.101	0.504	0.496
B4	1901.0	2.4	17.4	2.33	0.1400	0.64	1.74	0.248	0.620	0.380
B5	1982.6	2.4	207	10.7	0.4000	0.64	1.74	0.060	1.960	-0.960
B6	2047.0	2.4	24.3	3.94	0.3000	0.64	1.74	0.205	0.861	0.139
B7	2089.2	2.4	21.6	2.96	0.3500	0.64	1.74	0.219	1.036	-0.036
B8	2193.2	2.4	19.3	2.23	0.3500	0.64	1.74	0.234	1.143	-0.143
B9	2238.6	2.4	63.1	5.11	0.6000	0.64	1.74	0.118	1.911	-0.911
C1	2287.0	2.4	21.8	3.76	0.3500	0.64	1.74	0.218	0.908	0.092
C2	2312.8	2.4	19.9	1.12	0.3000	0.64	1.74	0.229	1.582	-0.582
C4	2371.2	2.4	46.6	5.48	0.4000	0.64	1.74	0.141	1.222	-0.222
C5	2428.8	2.4	34.1	7.26	0.1200	0.64	1.74	0.168	0.435	0.565
C6	2464.6	2.4	21.5	3.41	0.4000	0.64	1.74	0.219	1.029	-0.029
C7	2505.0	2.4	82.3	9.95	0.3000	0.64	1.74	0.101	1.019	-0.019
C8	2540.4	2.4	13.1	4.44	0.4000	0.64	1.74	0.292	0.665	0.335
C9	2580.2	2.4	61.0	4.69	0.8000	0.64	1.74	0.121	2.323	-1.323

Table E 3 Porosity & Water Saturation data for Well 333R

Layer	Ref. depth	R_{mf} (Ω-m)	R_{xo} (Ω-m)	R_t (Ω-m)	R_w (Ω-m)	a	m	ϕ	S_w	$S_{hc} = 1-S_w$
A2	–	–	–	–	–	–	–	–	–	–
A3	–	–	–	–	–	–	–	–	–	–
A4	–	–	–	–	–	–	–	–	–	–
A5	1404.4	2.4	81.8	13.9	0.1200	0.64	1.74	0.102	0.495	0.505
A6	1456.4	2.4	40.9	4.00	0.1000	0.64	1.74	0.152	0.612	0.388
A7	1542.0	2.4	196	6.5	0.1300	0.64	1.74	0.062	1.326	-0.326
A8	1606.0	2.4	29.5	5.83	0.1300	0.64	1.74	0.183	0.475	0.525
A9	1641.8	2.4	33.3	8.71	0.1300	0.64	1.74	0.171	0.405	0.595
B1	1693.0	2.4	17.1	3.41	0.1300	0.64	1.74	0.250	0.473	0.527
B2	1764.4	2.4	60.4	12.0	0.1300	0.64	1.74	0.121	0.474	0.526
B4	1882.0	2.4	23	9.04	0.1500	0.64	1.74	0.211	0.348	0.652
B5	1996.2	2.4	183	24.5	0.2100	0.64	1.74	0.064	0.783	0.217
B6	2043.8	2.4	56.2	7.92	0.2000	0.64	1.74	0.126	0.739	0.261
B7	2085.8	2.4	20.3	5.58	0.1200	0.64	1.74	0.227	0.376	0.624
B8	2176.4	2.4	23.7	3.83	0.3500	0.64	1.74	0.208	0.943	0.057
B9	2228.0	2.4	145	10.7	0.3000	0.64	1.74	0.073	1.354	-0.354
C1	2296.0	2.4	23.7	3.21	0.2100	0.64	1.74	0.208	0.778	0.222
C2	2328.2	2.4	17.6	4.0	0.2100	0.64	1.74	0.246	0.578	0.422
C4	2366.4	2.4	39.8	7.17	0.3500	0.64	1.74	0.154	0.886	0.114
C5	2429.8	2.4	21.8	4.46	0.1500	0.64	1.74	0.218	0.506	0.494
C6	2441.6	2.4	15.9	3.21	0.3000	0.64	1.74	0.261	0.759	0.241
C7	2514.4	2.4	70.3	9.5	0.2100	0.64	1.74	0.111	0.779	0.221
C8	2551.4	2.4	47.2	8.29	0.2000	0.64	1.74	0.140	0.651	0.349
C9	2585.2	2.4	62.5	6.0	0.3000	0.64	1.74	0.119	1.164	-0.164

Table E 4 Porosity & Water Saturation data for Well 313R

Layer	Ref. depth	R_{mf} (Ω-m)	R_{xo} (Ω-m)	R_t (Ω-m)	R_w (Ω-m)	a	m	ϕ	S_w	$S_{hc} = 1\text{-}S_w$
A2	1150.6	2.4	10.7	2.38	0.0850	0.64	1.74	0.328	0.348	0.652
A3	1183.0	2.4	11.3	2.57	0.0750	0.64	1.74	0.318	0.320	0.680
A4	1333.0	2.4	12.2	2.22	0.0750	0.64	1.74	0.304	0.363	0.637
A5	1429.4	2.4	32.4	4.19	0.1200	0.64	1.74	0.173	0.579	0.421
A6	1478.0	2.4	17.9	2.36	0.1000	0.64	1.74	0.244	0.516	0.484
A7	1569.0	2.4	22	2.22	0.1000	0.64	1.74	0.217	0.601	0.399
A8	1630.2	2.4	13.8	2.92	0.1000	0.64	1.74	0.283	0.393	0.607
A9	1669.0	2.4	13.1	3.56	0.1000	0.64	1.74	0.292	0.340	0.660
B1	1695.4	2.4	21.8	2.36	0.1000	0.64	1.74	0.218	0.578	0.422
B2	1756.2	2.4	34.4	10.8	0.1300	0.64	1.74	0.168	0.364	0.636
B4	1879.0	2.4	157	10.7	0.1300	0.64	1.74	0.070	0.876	0.124
B5	2000.4	2.4	22.7	1.71	0.1500	0.64	1.74	0.213	0.898	0.102
B6	2049.0	2.4	52.1	4.0	0.1500	0.64	1.74	0.132	0.888	0.112
B7	2114.6	2.4	15.6	4.35	0.1500	0.64	1.74	0.264	0.423	0.577
B8	2188.2	2.4	62.2	4.67	0.1500	0.64	1.74	0.119	0.900	0.100
B9	2253.4	2.4	273	4.5	0.2000	0.64	1.74	0.051	2.538	-1.538
C1	2295.0	2.4	46.7	1.12	0.1500	0.64	1.74	0.141	1.734	-0.734
C2	2333.4	2.4	65.4	3.94	0.2000	0.64	1.74	0.116	1.205	-0.205
C4	2387.0	2.4	55	5.19	0.2000	0.64	1.74	0.128	0.931	0.069
C5	2435.4	2.4	6.71	4.46	0.1500	0.64	1.74	0.429	0.257	0.743
C6	2474.6	2.4	57.6	7.71	0.1500	0.64	1.74	0.125	0.646	0.354
C7	2523.0	2.4	135	9.99	0.2000	0.64	1.74	0.076	1.071	-0.071
C8	2556.4	2.4	42.3	9.71	0.1500	0.64	1.74	0.149	0.473	0.527
C9	2588.6	2.4	85	16.8	0.2000	0.64	1.74	0.100	0.609	0.391

Table E 5 Porosity & Water Saturation data for Well 338R

Layer	Ref. depth	R_{mf} (Ω-m)	R_{xo} (Ω-m)	R_t (Ω-m)	R_w (Ω-m)	a	m	ϕ	S_w	$S_{hc} = 1\text{-}S_w$
A2	1156.8	2.4	5.83	3.82	0.0850	0.64	1.74	0.465	0.187	0.813
A3	1178.6	2.4	4.85	3.02	0.0850	0.64	1.74	0.516	0.193	0.807
A4	1345.0	2.4	5.27	3.06	0.1000	0.64	1.74	0.492	0.220	0.780
A5	1422.2	2.4	27	4.44	0.1300	0.64	1.74	0.193	0.528	0.472
A6	1478.6	2.4	6.08	3.56*	0.1200	0.64	1.74	0.454	0.243	0.757
A7	1546.2	2.4	8.21	2.68*	0.1300	0.64	1.74	0.382	0.356	0.644
A8	1617.9	2.4	9.7	4.78	0.1300	0.64	1.74	0.347	0.281	0.719
A9	1654.6	2.4	10.6	3.02	0.1200	0.64	1.74	0.330	0.368	0.632
B1	1692.0	2.4	14.5	3.44	0.1300	0.64	1.74	0.275	0.428	0.572
B2	1764.0	2.4	12.8	1.8	0.2000	0.64	1.74	0.296	0.740	0.260
B4	1882.2	2.4	122	9.27	0.2000	0.64	1.74	0.081	1.054	-0.054
B5	1976.3	2.4	213/268	11.3/.8	0.3000	0.64	1.74	0.059	1.636	-0.636
B6	2046.9	2.4	92.5	8.43	0.2100	0.64	1.74	0.095	0.977	0.023
B7	2113.8	2.4	14.2	2.72	0.3500	0.64	1.74	0.279	0.855	0.145
B8	2199.0	2.4	24.6	3.52	0.4000	0.64	1.74	0.203	1.092	-0.092
B9	–	–	–	–	–	–	–	–	–	–
C1	2291.5	2.4	27.2	3.35	0.3000	0.64	1.74	0.192	1.009	-0.009
C2	2334.5	2.4	31.9	4.02	0.6000	0.64	1.74	0.175	1.482	-0.482
C4	2400.0	2.4	13.7	0.504	0.6000	0.64	1.74	0.284	3.008	-2.008
C5	2440.0	2.4	13	1.84	0.6000	0.64	1.74	0.293	1.387	-0.387
C6	2466.7	2.4	16.2	3.23	0.6000	0.64	1.74	0.258	1.139	-0.139
C7	2519.9	2.4	16.7	4.19	0.8000	0.64	1.74	0.254	1.177	-0.177
C8	2556.8	2.4	49.7	8.22	0.2000	0.64	1.74	0.136	0.674	0.326
C9	–	–	–	–	–	–	–	–	–	–